

# Natural parameter conditions for singular perturbations of chemical and biochemical reaction networks

Justin Eilertsen  
Mathematical Reviews  
American Mathematical Society  
416 4th Street  
Ann Arbor, MI, 48103  
e-mail: [jse@ams.org](mailto:jse@ams.org)

Santiago Schnell  
Department of Biological Sciences and  
Department of Applied and Computational Mathematics and Statistics  
University of Notre Dame  
Notre Dame, IN 46556  
e-mail: [santiago.schnell@nd.edu](mailto:santiago.schnell@nd.edu)

Sebastian Walcher  
Mathematik A, RWTH Aachen  
D-52056 Aachen, Germany  
e-mail: [walcher@matha.rwth-aachen.de](mailto:walcher@matha.rwth-aachen.de)

November 22, 2022

## Abstract

We consider reaction networks that admit a singular perturbation reduction in a certain parameter range. The focus of this paper is on deriving “small parameters” (briefly for small perturbation parameters), to gauge the accuracy of the reduction, in a manner that is consistent, amenable to computation and permits an interpretation in chemical or biochemical terms. Our work is based on local timescale estimates via ratios of the real parts of eigenvalues of the Jacobian near critical manifolds; this approach is familiar from computational singular perturbation theory. While parameters derived by this method cannot provide universal estimates for the accuracy of a reduction, they represent a critical first step toward this end. Working directly with eigenvalues is generally unfeasible, and at best cumbersome. Therefore we focus on the coefficients of the characteristic polynomial to derive parameters, and relate them to timescales. Thus we obtain distinguished parameters for systems of arbitrary dimension, with particular emphasis on reduction to dimension one. As a first application, we discuss the Michaelis–Menten reaction mechanism system in various settings, with new and perhaps surprising results. We proceed to investigate more complex enzyme catalyzed reaction mechanisms (uncompetitive, competitive inhibition and cooperativity) of dimension three, with reductions to dimension one and two. The distinguished parameters we derive for these three-dimensional systems are new; in fact no rigorous derivation of small parameters seems to exist in the literature so far. Numerical simulations are included to illustrate the efficacy of the parameters obtained, but also to show that certain limitations must be observed.

**Keywords:** Reaction network, dimension reduction, perturbation parameter, timescale, eigenvalue, symmetric polynomial, quasi-steady-state approximation, Lyapunov function, singular perturbation  
**MSC (2020):** 92C45, 34D15, 80A30, 13P10

# 1 Introduction

Reducing the dimension of chemical and biochemical reaction networks is of great relevance both for theoretical considerations and for laboratory practice. For instance, the fundamental structure of a reaction network is frequently known, or assumed from educated guesswork, but reaction rate constants remain to be determined. Therefore it is important to identify scenarios and parameter regions that guarantee accuracy of a suitably chosen reduction. Singular perturbations frequently appear here<sup>1</sup>, and the fundamental theorems by Tikhonov [43] and Fenichel [17] provide a reliable theoretical foundation, including a procedure to determine a reduced equation, and convergence results. These theorems require the a priori identification of a perturbation parameter (called “small parameter” from here on), which we denote by  $\varepsilon_S$  for the moment. More to the point, one should consider a critical manifold together with an associated small parameter, and the corresponding slow invariant manifold. In contrast to the critical manifold, the parameter is far from unique.<sup>2</sup> Singular perturbation theory provides strong qualitative statements, such as convergence of a solution to a corresponding solution of the reduced equation as  $\varepsilon_S \rightarrow 0$  (which is frequently phrased as  $\varepsilon_S \ll 1$ ). However, additional information is desirable: Ideally, from a quantitative perspective,  $\varepsilon_S$  should provide an upper estimate for the discrepancy between the exact and approximate solutions over the whole course of the slow dynamics; and from a qualitative biochemical perspective it should reflect the influence of reaction parameters.

In many application-oriented publications, the authors assume (explicitly or implicitly) that certain parameters provide a quantitative estimate for the approximation [23, 38, 42, 37, 8]. However, while heuristical arguments may support such assumptions, no mathematical proof is given [12]. In fact, there seem to be no rigorous results on quantitative error estimates for reductions of biochemical reaction networks, and there exists no general methodology even for an initial step towards this goal.

From a general perspective, one could say that finding ideal small parameters, for a given singular perturbation scenario, requires a three-step procedure:

1. In a first step, estimate the approach of a particular solution to the slow manifold: A common method employs Lyapunov functions. Thus one obtains a parameter that measures the discrepancy between the right hand sides of the full system and the reduced equation, following a short initial transient.
2. In a second step, estimate a suitable critical time at which the slow dynamics sets in, and estimate the solution at this critical time. This is needed to guarantee that the transient phase is indeed short, and to obtain a suitable initial value for the reduced equation.
3. In a third step, estimate the approximation of the exact solution by the corresponding solution of the reduced equation. (Note: The proximity of the phase-space trajectory to the slow manifold does not ensure that the time evolutions of the approximate solution and the true solution are close; see e.g. Eilertsen et al. [12, FIG. 4].)

From a theoretical perspective, this procedure poses no problems; in theory the feasibility of the steps outlined above is guaranteed by standard results about ordinary differential equations. But the hard part lies in their practical implementation for a given parameter-dependent system: Generally it is not easy to obtain meaningful and reasonably sharp estimates. A case-by-case discussion seems to be necessary [36, 13, 10, 11, 14, for a few examples], for each given system.

With these three steps as a background, our goal is to make a significant contribution toward the first step, via linear timescale arguments. We will both expand and improve existing results, and moreover obtain perturbation parameters for higher-dimensional systems for which no rigorous results have previously been reported. From a local perspective, we consider (real parts of) eigenvalue ratios, based on the idea that underlies computational singular perturbation theory going back to Lam and Goussis [27]. Our emphasis is on parameters that are workable for application-oriented readers in mathematical enzymology, and admit an interpretation in biochemical terms.

---

<sup>1</sup>Other types of reduction scenarios do occur, but we will not discuss these in the present work.

<sup>2</sup>Even for the familiar Michaelis–Menten system there are several parameters in use.

## 1.1 Background

A solid mathematical foundation for qualitative viability of most reduction procedures in chemistry and biochemistry is provided by singular perturbation theory (Tikhonov [43], Fenichel [17]). This was first clearly stated and utilized in Heineken, Tsuchiya and Aris [23].

For illustrative purposes, and as further motivation, we consider a familiar system from biochemistry, viz. the (irreversible) Michaelis–Menten reaction mechanism or network [28], which is modelled by the two-dimensional differential equation

$$\begin{aligned} \dot{s} &= -k_1 e_0 s + (k_1 s + k_{-1})c, \\ \dot{c} &= k_1 e_0 s - (k_1 s + k_{-1} + k_2)c. \end{aligned} \tag{1}$$

For small initial enzyme concentration with respect to the initial substrate concentration, Briggs and Haldane [4] assumed quasi-steady state (QSS) for complex concentration, thus obtaining the QSS manifold given by

$$c = \frac{k_1 e_0 s}{k_{-1} + k_2 + k_1 s}; \tag{2}$$

and reduction to the Michaelis–Menten equation

$$\dot{s} = -\frac{k_1 k_2 e_0 s}{k_{-1} + k_2 + k_1 s}. \tag{3}$$

To quantify the notion of smallness for enzyme concentration, they introduced the dimensionless parameter

$$\varepsilon_{BH} := \frac{e_0}{s_0} \tag{4}$$

(later utilized by Heineken et al. [23] in the first application of singular perturbation theory to this network), and required  $\varepsilon_{BH} \ll 1$  as a necessary condition for accuracy of the reduction. Further parameters to ensure accuracy of approximation by the Michaelis–Menten equation were introduced later on. Reich and Selkov [35] introduced

$$\varepsilon_{RS} := k_1 e_0 / (k_{-1} + k_2), \tag{5}$$

for which Palsson and Lightfoot [33] later gave a justification based on linearization at the stationary point 0.<sup>3</sup> Moreover, Segel and Slemrod [39] derived

$$\varepsilon_{SSI} := \frac{k_1 e_0}{k_{-1} + k_2 + k_1 s_0}. \tag{6}$$

The fundamental approach by Segel and Slemrod [39], obtaining perturbation parameters by comparing suitable timescales has been used widely in the literature ever since.<sup>4</sup>

For Michaelis–Menten reaction mechanism, singular perturbation theory shows convergence of solutions of (1) to corresponding solutions of the reduced equation as  $e_0 \rightarrow 0$ , in which case all of the parameters  $\varepsilon_{BH}$ ,  $\varepsilon_{RS}$ ,  $\varepsilon_{SSI}$  approach zero. But on the other hand, it is *not* generally true that  $\varepsilon_{BH} \rightarrow 0$ , or  $\varepsilon_{RS} \rightarrow 0$ , or  $\varepsilon_{SSI} \rightarrow 0$ , implies convergence to the solution of the reduced system. This, as well as related matters, was discussed in detail in Eilertsen et al. [12], with a presentation of counterexamples. We also invite the readers to see other examples in Section 4.

These facts illustrate that considering a single parameter – without context and without a clearly defined notion of the limiting process – will generally not be sufficient to ensure the validity of some particular reduction. In a singular perturbation setting the critical manifold is the basic object, and one generally needs to specify the way in which corresponding small parameters approach zero.

With regard to the procedure outlined in Steps 1 to 3 above, a wish list for small parameters includes the following physically motivated conditions:

- $\varepsilon_S$  is dimensionless;

<sup>3</sup>In a recent paper, Patsatzis and Goussis [34] suggested a parameter involving  $s$  and  $c$  along a trajectory; taking the maximum over  $s$  and  $c$  yields  $\varepsilon_{RS}$ .

<sup>4</sup>The particular argument in [39] is somewhat problematic since the notion of timescale is ambiguous for nonlinear systems.

- $\varepsilon_S$  is composed of reaction rates and initial values (admitting an interpretation in physical terms);
- $\varepsilon_S$  is controllable in experiments.

These requirements will be taken into account as well.

Our vantage point is work by Goeke et al. [21, 22], which provides an algorithmic approach to determine critical parameter values (Tikhonov-Fenichel parameter values, TFPV), and their critical manifolds: Choosing a curve in parameter space (with curve parameter  $\varepsilon$ ) that starts at a TFPV gives rise to a singularly perturbed system, based on a clearly defined approach of the small parameter to zero.

Pursuing a less ambitious goal than the one outlined in Steps 1 to 3 above, we will utilize the separation of timescales on the slow manifold, adapting work by Lam and Goussis [27] on computational singular perturbation theory. We focus attention on local considerations. Timescales are identified as inverse absolute real parts of eigenvalues of the linearization of a vector field, near stationary points. Restriction to the vicinity of stationary points is an essential condition here. Given a singular perturbation setting, Zagaris et al. [47] proved that the approach via “small eigenvalue ratios” is consistent. Unless some eigenvalues of large modulus are purely imaginary, the eigenvalue approach provides a small parameter that satisfies the requirement in Step 1 above, up to a multiplicative constant that remains to be determined.<sup>5</sup> But dealing directly with eigenvalues (even in the rare case when they are explicitly known) is generally too cumbersome to allow productive work and concrete conclusions.

The emphasis of the present paper lies on local (linear) timescale estimates and comparisons, using a mix of algebraic and analytic tools. We will obtain parameters that are palatable to application-oriented readers and allow for interpretation in a biochemical context. Most of the parameters obtained have not appeared in the literature before, and some perhaps are unexpected.

## 1.2 Overview of results

Given a chemical or biochemical reaction network, we will present a method to obtain distinguished dimensionless parameters. These parameters are directly related to the local fast-slow dynamics of the singularly perturbed system. In contrast to many existing timescale estimates in the literature, the one employed here is conceptually consistent: timescale considerations mutate from artwork to a relatively routine procedure, and we establish necessary conditions for timescale separation and singular perturbation reductions.

In the preparatory Section 2 we collect some notions and results related to singular perturbation theory; in particular, we recall Tikhonov-Fenichel parameter values (TFPV). We also note properties of the Jacobian and its characteristic polynomial on the critical manifold. It should be emphasized that our search always begins with identifying a TFPV and its associated critical manifold; all our small parameter estimates are rooted in this scenario. We establish a repository of dimensionless parameters from coefficients of the characteristic polynomial, and we recall the relation between these coefficients and the eigenvalues of the Jacobian. Finally, we fix some notation and establish some blanket nondegeneracy conditions that are assumed throughout the paper.

Section 3 is devoted to one-dimensional critical manifolds, which are of considerable relevance to experimentalists: Generally, the timecourse of a single product or substrate is measured in an experiment. Specific kinetic parameters (such as the Michaelis constant) are estimated via nonlinear regression, in which the recorded timecourse data is fitted to a one-dimensional and autonomous QSS model that approximates substrate depletion (or product formation) of the reaction on the slow timescale; see, for example, Stroberg and Schnell [41] and Choi et al. [8]. In the one-dimensional setting, near the critical manifold there is one and only one eigenvalue of the Jacobian with small absolute real part. From the characteristic polynomial we obtain distinguished small parameters, and we establish their correspondence to timescales. The parameters thus obtained admit an interpretation in terms of reaction parameters, so they satisfy a crucial practical requirement. They measure the ratio of the slow to the fastest timescale, and thus provide a necessary condition for timescale separation. But in dimension greater than two, this condition is not strong enough when there are large discrepancies within the fast timescales. According to the Appendix, subsection 9.1, the ratio of the slow to the “slowest of the fast” timescales is the relevant quantity. To estimate this ratio,

---

<sup>5</sup>A proof of this fact is sketched in Appendix 9.1, which also indicates that eigenvalue ratios are relevant for Step 3. The multiplicative constant reflects the effect of a coordinate transformation.

we introduce another type of parameter that yields sharp estimates whenever all eigenvalues are “essentially real” (borrowing terminology of Lam and Goussis [27]). We then specialize our results to systems of dimensions two and three.

In Section 4, we apply the results from Section 3 to the (reversible and irreversible) Michaelis–Menten system in various circumstances. We obtain a distinguished parameter for the reversible system with small enzyme concentration, and we show that the Reich-Selkov parameter  $\varepsilon_{RS}$  is the most suitable among the standard parameters in the irreversible system. Moreover we obtain a rather surprising distinguished parameter for the partial equilibrium approximation with slow product formation. To support the claim that this is indeed an appropriate parameter for step 1, as stated above, we determine relevant Lyapunov estimates, and we add some observations with regard to step 3. To illustrate the necessity of some technical restrictions in our results, we close this section by discussing a degenerate scenario with a singular critical variety.

In Section 5 we turn to critical manifolds of dimension greater than one. Imitating the approach for one-dimensional critical manifolds and invoking results from local analytic geometry, we obtain distinguished parameters that measure the ratio of the fastest timescale to the “fastest of the slow” timescales. We provide a detailed analysis for three dimensional systems with two dimensional critical manifold.

In Section 6 we apply our theory to some familiar three-dimensional systems from biochemistry, viz. cooperative systems with two complexes, and competitive as well as uncompetitive inhibition, for low enzyme concentration. For these systems the only available perturbation parameters in common use seem to be  $\varepsilon_{BH} = e_0/s_0$ ,  $\varepsilon_{SSI}$  and ad-hoc variants of these. There seems to exist no derivation of small parameters via timescale arguments (in the spirit of Segel and Slemrod) in the literature. We thus break new ground, and we obtain meaningful and useful distinguished parameters. We illustrate our results with several numerical examples, to verify the efficacy of the parameters. But we also include simulations to show their limited applicability in certain regions of parameter space. Such limitations were to be expected, since steps 2 and 3 are needed for a complete analysis. These examples also illustrate the necessity of additional hypotheses imposed in the derivation of the distinguished parameters.

In Section 7 we consider some reductions of three dimensional systems obtained via projection onto two-dimensional critical manifolds. Specifically, we compute some two-dimensional reductions of the competitive and uncompetitive inhibitory reaction mechanisms, and we derive distinguished parameters that are relevant for the accuracy of these reductions. Again we illustrate our results by numerical simulations. To finish, we discuss a three timescale scenario that leads to a hierarchical structure in which the two-dimensional slow manifold contains an embedded one-dimensional “very slow” manifold.

An Appendix contains a recapitulation of the Lyapunov function method for singularly perturbed systems, also outlining the relevance of the eigenvalue ratios for step 1, and some observations on steps 2 and 3. Moreover the Appendix contains a summary of some facts from the literature, and proofs for some technical results.

Sections 2, 3 and 5 as well as the Appendix are mostly technical. Readers primarily interested in applications may want to skim these only, and focus on the applications in sections 4, 6 and 7.

## 2 Preliminaries

We will discuss parameter-dependent ordinary differential equations

$$\dot{x} = h(x, \pi), \quad x \in \mathbb{R}^n, \quad \pi \in \Pi, \quad \Pi \subseteq \mathbb{R}^m \text{ closed}, \quad (7)$$

with the right-hand side a polynomial in  $x$  and  $\pi$ . Our main motivation is the study of chemical mass action reaction networks and their singular perturbation reductions.

### 2.1 Tikhonov-Fenichel parameter values (a review)

We consider singular perturbation reductions that are based on the classical work by Tikhonov [43] and Fenichel [17]. Frequently the pertinent theorems are stated for systems in slow-fast standard form

$$\begin{aligned} \dot{u}_1 &= \varepsilon f_1(u_1, u_2, \varepsilon), \\ \dot{u}_2 &= f_2(u_1, u_2, \varepsilon), \end{aligned} \quad (8)$$

with a small parameter  $\varepsilon$ , subject to certain additional conditions. In slow time  $\tau = \varepsilon t$ , the reduced system takes the form

$$\begin{aligned}\frac{du_1}{d\tau} &= f_1(u_1, u_2, \varepsilon), \\ 0 &= f_2(u_1, u_2, \varepsilon),\end{aligned}$$

and the above mentioned conditions ensure that the second equation admits a local resolution for  $u_2$  as a function of  $u_1$  and  $\varepsilon$ . For general parameter dependent systems (7) one first needs to identify the parameter values from which such reductions emanate. We recall some notions and results (slightly modified from Goeke et al. [21]):

1. A parameter  $\hat{\pi} \in \Pi$  is called a *Tikhonov-Fenichel parameter value (TFPV) for dimension  $s$*  ( $1 \leq s \leq n - 1$ ) of system (7) whenever the following hold:

- (i) An irreducible component of the critical variety, i.e., of the zero set  $\mathcal{V}(h(\cdot, \hat{\pi}))$  of  $x \mapsto h(x, \hat{\pi})$ , contains a (Zariski dense) local submanifold  $\tilde{Y}$  of dimension  $s$ , which is called the critical manifold.
- (ii) For all  $x \in \tilde{Y}$  one has  $\text{rank } D_1 h(x, \hat{\pi}) = n - s$  and

$$\mathbb{R}^n = \text{Ker } D_1 h(x, \hat{\pi}) \oplus \text{Im } D_1 h(x, \hat{\pi}).$$

Here  $D_1$  denotes the partial derivative with respect to  $x$ .

- (iii) For all  $x \in \tilde{Y}$  the nonzero eigenvalues of  $D_1 h(x, \hat{\pi})$  have real parts  $< 0$ .

2. Given a TFPV, for any smooth curve  $\varepsilon \mapsto \hat{\pi} + \varepsilon \rho + \dots$  in parameter space  $\Pi$ , the system

$$\dot{x} = h(x, \hat{\pi} + \varepsilon \rho + \dots) = h(x, \hat{\pi}) + \varepsilon D_2 h(x, \hat{\pi}) \rho + \dots =: h^{(0)}(x) + \varepsilon h^{(1)}(x) + \dots,$$

with  $D_2$  denoting the partial derivative with respect to  $\pi$ , admits a singular perturbation (Tikhonov-Fenichel) reduction.

A standard method is to fix a parameter direction and a “ray”  $\varepsilon \mapsto \hat{\pi} + \varepsilon \rho$  in parameter space. In a chemical interpretation this may correspond to a gradual increase of some parameters, such as initial concentrations. Our work will always be based on this procedure; by this specification we avoid ambiguities about the range of parameters.

3. The computation of a reduction in the coordinate-free setting is described in Goeke and Walcher [20]: Assuming the TFPV conditions in item 1, there exist rational functions  $P$ , with values in  $\mathbb{R}^{n \times (n-s)}$ , and  $\mu$ , with values in  $\mathbb{R}^{n-s}$ , such that

$$h^{(0)}(x) = P(x)\mu(x) \text{ on } \tilde{Y},$$

and  $P(x)$  as well as  $D\mu(x)$  have full rank on  $\tilde{Y}$ . The reduced equation on  $\tilde{Y}$  then has the representation

$$\dot{x} = \varepsilon \left( I - P(x) (D\mu(x)P(x))^{-1} D\mu(x) \right) h^{(1)}(x), \quad (9)$$

which is correct up to  $O(\varepsilon^2)$ . By Tikhonov and Fenichel, solutions of (7) that start near  $\tilde{Y}$  will converge to solutions of the reduced system as  $\varepsilon \rightarrow 0$ . But some caveats are in order:

- The reduction is guaranteed only locally, for neighborhoods of compact subsets of the critical manifold and for sufficiently small  $\varepsilon$ . Determining a neighborhood explicitly for which the reduction is valid poses an individual problem for each system. <sup>6</sup>
- In particular, the distance of the initial value of (7) from the slow manifold (not only from the critical manifold) is relevant for the reduction. In general an approximate initial value for the reduced equation on the slow manifold must be determined.

---

<sup>6</sup>A similar problem is familiar from linearly stable stationary points.

- If the transversality condition in (ii) above breaks down, standard singular perturbation theory is no longer applicable. But even when it is satisfied, the range of validity for the reduction may be quite small. This reflects the effect of a local transformation to Tikhonov standard form.
- Finally, the reduced equation may be trivial, in which case higher order terms in  $\varepsilon$  are dominant and no conclusion can be drawn from the first order reduction. By the same token, if the term following  $\varepsilon$  in (9) is small then the quality of the reduction may be poor.

4. Turning to computational matters, consider the characteristic polynomial

$$\chi(\tau, x, \pi) = \tau^n + \sigma_1(x, \pi)\tau^{n-1} + \cdots + \sigma_{n-1}(x, \pi)\tau + \sigma_n(x, \pi) \quad (10)$$

of the Jacobian  $D_1h(x, \pi)$ . Then, given  $0 < s < n$ , a parameter value  $\hat{\pi}$  is a TFPV with locally exponentially attracting critical manifold  $\tilde{Y}$  of dimension  $s$ , and  $x_0 \in \tilde{Y}$ , only if the following hold:

- $h(x_0, \hat{\pi}) = 0$ .
- The characteristic polynomial  $\chi(\tau, x, \pi)$  satisfies
  - $\sigma_n(x_0, \hat{\pi}) = \cdots = \sigma_{n-s+1}(x_0, \hat{\pi}) = 0$ ;
  - all roots of  $\chi(\tau, x_0, \hat{\pi})/\tau^s$  have negative real parts.

This characterization shows that  $x_0$  satisfies an overdetermined system of equations (more than  $n$  equations in  $n$  variables), which in turn allows to algorithmically determine conditions on  $\hat{\pi}$  by way of elimination theory; see Goeke et al. [21].

Due to the Hurwitz-Routh theorem (see e.g. Gantmacher [18]),

$$\sigma_k(x_0, \hat{\pi}) > 0 \text{ for } x_0 \in \tilde{Y}, 1 \leq k \leq n - s$$

is a necessary consequence of condition (ii). Necessary and sufficient conditions for TFPV are stated in [21], but we will not need them here.

## 2.2 Dimensionless parameters

From Goeke et al. [21] one finds critical parameter values and corresponding critical manifolds, but there remains to specify the notion of “small perturbation”, and to relate it to reaction parameters. Singular perturbation theory guarantees convergence in the limit  $\varepsilon \rightarrow 0$ , but for a given system estimates for the rate of convergence are desirable.

To be physically meaningful, relevant small parameters should be dimensionless. The only dimensions appearing in reaction network parameters are time and concentration, thus by dimensional analysis (Buckingham Pi Theorem; see e.g. Wan [46]) there exist  $\geq m - 2$ <sup>7</sup> independent dimensionless Laurent monomials in the parameters, such that every dimensionless analytic function of the reaction parameters can locally be expressed as a function of these. This collection may be quite large; we impose the additional requirement that parameters should correspond to timescales. In a preliminary step we therefore list an inventory of rational dimensionless quantities for the network.

**Lemma 1.** *Let (7) correspond to a CRN with mass action kinetics, and  $\chi$  as in (10). Then:*

- The coefficient  $\sigma_k$  of  $\chi$  has dimension (Time)<sup>-k</sup>.*
- Whenever  $i_1, \dots, i_p \geq 1$  and  $j_1, \dots, j_q \geq 1$  are integers such that  $i_1 + \cdots + i_p = j_1 + \cdots + j_q$ , the expression*

$$\frac{\sigma_{i_1} \cdots \sigma_{i_p}}{\sigma_{j_1} \cdots \sigma_{j_q}}$$

*(when defined) is dimensionless.*

*Proof.* Every monomial on the right-hand side of (7) has dimension (Concentration)/(Time), since this holds for the left-hand side. The entries of the Jacobian  $D_1h$  are obtained via differentiation with respect to some  $x_i$ , hence have dimension (Time)<sup>-1</sup>. Since  $\sigma_i$  is a polynomial in the matrix entries of degree  $i$ , part (a) follows. Part (b) is an immediate consequence.  $\square$

<sup>7</sup>Generically there are exactly  $m - 2$ .

## 2.3 Timescales

There exist various notions of timescale in the literature, and in some cases this ambiguity influences the derivation of small parameters. (For a case in point see Segel and Slemrod [39], who use different notions of timescale for the fast and slow dynamics.) But for systems that decay or grow exponentially, and by extension for linear and approximately linear systems, there exists a well-defined notion:

**Definition 1.** *Let  $A : \mathbb{R}^n \rightarrow \mathbb{R}^n$  be a linear map, and consider the linear differential equation  $\dot{x} = Ax$ . For  $\lambda$  an eigenvalue of  $A$ , with nonzero real part, we call  $|\operatorname{Re} \lambda|^{-1}$  the timescale corresponding to  $\lambda$ . The timescale of an invariant subspace  $V \subseteq \mathbb{R}^n$  (which is a subspace of a sum of generalized eigenspaces) is defined as the slowest timescale of the eigenvalues involved.*

For a single eigenvalue, the timescale characterizes the speed of growth or decay of solutions along the generalized eigenspace of  $\lambda$ . For an invariant subspace it characterizes the speed for generic initial values.

We will work with this consistent notion of linear timescale, and its extension to linearizations of nonlinear systems near stationary points, throughout the paper. Thus we adopt the perspective taken in Lam and Goussis [27], which is justified by Fenichel's local characterization of the dynamics near the critical manifold  $\tilde{Y}$  ([17], Section V), as proven by Zagaris, Kaper and Kaper [47]. Indeed, the time evolution near  $\tilde{Y}$  is governed by the linearization  $D_1 h(x, \hat{\pi} + \varepsilon \rho)$ , with  $\pi = \hat{\pi} + \varepsilon \rho$  close to a TFPV  $\hat{\pi}$ , and  $x \in \tilde{Y}$ . For  $\pi = \hat{\pi}$  the Jacobian has vanishing eigenvalues, hence for  $\pi$  near  $\hat{\pi}$  one will have eigenvalues of small modulus, while all nonzero eigenvalues of  $D_1 h(x, \hat{\pi})$  have negative real parts.

From a practical perspective, eigenvalues are at best inconvenient to work with. Moreover, in our context, resorting to numerical approximations is not a viable option. To obtain more palatable parameters, we recall the correspondence between the eigenvalues  $\lambda_1, \dots, \lambda_n$  of  $D_1 h(x, \hat{\pi} + \varepsilon \rho)$  and the coefficients  $\sigma_k$  of the characteristic polynomial: One has

$$\sigma_k = (-1)^k \sum \lambda_{i_1} \cdots \lambda_{i_k}$$

with the summation extending over all tuples  $i_1, \dots, i_k$  such that  $1 \leq i_1 < \cdots < i_k \leq n$ . In particular

$$\begin{aligned} -\sigma_1 &= \lambda_1 + \cdots + \lambda_n; \\ (-1)^{n-1} \sigma_{n-1} &= \sum_{i=1}^n \prod_{j \neq i} \lambda_j; \\ (-1)^n \sigma_n &= \lambda_1 \cdots \lambda_n; \\ \frac{\sigma_{n-1}}{\sigma_n} &= -\sum \frac{1}{\lambda_j}. \end{aligned} \tag{11}$$

## 2.4 Blanket assumptions

The principal goal of the present paper is to provide consistent and workable local timescale estimates in terms of the reaction parameters. Throughout the remainder of the paper the following notions will be used and the following assumptions will be understood:

1. We consider a polynomial parameter dependent system (7), and a TFPV  $\hat{\pi}$  for dimension  $s \geq 1$ , with critical manifold  $\tilde{Y}$ . The entries of  $\hat{\pi}$  are not uniquely determined by the critical manifold. We allow these entries to range in a suitable compact subset of parameter space (to be restricted by requirements in the following items).
2. We fix  $\rho$  in the parameter space, and consider the singularly perturbed system for the ray in parameter space  $\hat{\pi} + \varepsilon \rho$ , with  $0 \leq \varepsilon \leq \varepsilon_{\max}$ , and restrictions on  $\varepsilon_{\max} > 0$  to be specified.
3. Moreover we let  $K \subset \mathbb{R}^n$  be a compact set with nonempty interior, such that  $\tilde{Y} \cap K$  is also compact.  $K$  should contain the initial values for all relevant solutions of (7).<sup>8</sup>
4. Since  $\hat{\pi}$  is a TFPV, we have  $\sigma_k(x, \hat{\pi}) > 0$  for all  $x \in \tilde{Y} \cap K$ ,  $1 \leq k \leq n - s$ . We choose  $\varepsilon_{\max}$  so that  $\sigma_k(x, \hat{\pi} + \varepsilon \rho)$  is defined and bounded above and below by positive constants on

$$K^* = K^*(\varepsilon_{\max}) = \left( \tilde{Y} \cap K \right) \times [0, \varepsilon_{\max}], \tag{12}$$

---

<sup>8</sup>In many applications it will be possible to choose a positively invariant compact neighborhood, but this will not be required a priori.

for  $1 \leq k \leq n - s$ . (Such a choice is possible by compactness and continuity, given a suitable compact set in parameter space.)

5. As a crucial basic condition we require that Tikhonov-Fenichel reduction is accurate up to order  $\varepsilon^2$  in a compact neighborhood  $\tilde{K}$  of  $\tilde{Y} \cap K$ , with  $\varepsilon \leq \varepsilon_{\max}$ . See Appendix, subsection 9.1, to verify that this requirement can be satisfied.

We emphasize that the present paper focuses on *asymptotic timescale estimates* near the critical manifold, which are based on Fenichel's local theory. The determination of  $\varepsilon_{\max}$  (and by extension, the range of applicability) will not be addressed in general. Moreover, in applications we may replace sharp estimates by weaker ones that permit an interpretation in biochemical terms.

### 3 Critical manifolds of dimension one

In this technical section we consider system (7) in  $\mathbb{R}^n$ ,  $n \geq 2$  with a critical manifold of dimension  $s = 1$ . We will derive two types of distinguished parameters that characterize timescale discrepancies, and discuss systems of dimensions 2 and 3 in some detail.

We have  $\sigma_n(x, \hat{\pi}) = 0$  on  $\tilde{Y}$ , and  $\sigma_k(x, \hat{\pi} + \varepsilon\rho) > 0$  for  $1 \leq k \leq n - 1$ ,  $x \in \tilde{Y} \cap K$  and  $0 \leq \varepsilon \leq \varepsilon_{\max}$ . Moreover

$$\sigma_n(x, \hat{\pi} + \varepsilon\rho) = \varepsilon \hat{\sigma}_n(x, \hat{\pi}, \rho, \varepsilon) \quad (13)$$

with a polynomial  $\hat{\sigma}_n$ . We require the *nondegeneracy condition*

$$\hat{\sigma}_n(x, \hat{\pi}, \rho, 0) \neq 0 \text{ for all } x \in \tilde{Y} \cap K. \quad (14)$$

Denote by  $\lambda_1, \dots, \lambda_n$  the eigenvalues of  $D_1 h(x, \pi)$ , choosing the labels so that  $\lambda_n(x, \hat{\pi}) = 0$  for all  $x \in \tilde{Y} \cap K$ .

The following facts are known. We recall some proofs in the Appendix, for the reader's convenience.

**Lemma 2.** (a) *One has*

$$\lambda_n(x, \hat{\pi} + \varepsilon\rho) = \varepsilon \hat{\lambda}_n(x, \hat{\pi}, \rho, \varepsilon),$$

with  $\hat{\lambda}_n$  analytic, and  $\hat{\lambda}_n(x, \hat{\pi}, \rho, 0) \neq 0$  on  $K$ .

- (b) *Given  $\beta > 1$  there exist  $\Theta > 0$ ,  $\theta > 0$  such that  $-\Theta/\beta \leq \operatorname{Re} \lambda_i(x, \hat{\pi}) \leq -\beta\theta$  for all  $x \in \tilde{Y} \cap K$ ,  $1 \leq i \leq n - 1$ .*

- (c) *For suitably small  $\varepsilon_{\max}$  one has*

$$-\Theta \leq \operatorname{Re} \lambda_i(x, \hat{\pi} + \varepsilon\rho) \leq -\theta$$

for all  $(x, \varepsilon) \in K^*$ ,  $1 \leq i \leq n - 1$ .

#### 3.1 Distinguished small parameters

We turn to the construction of small parameters from the repository in Lemma 1. Consider the rational function

$$(x, \varepsilon) \mapsto \frac{\sigma_n(x, \hat{\pi} + \varepsilon\rho)}{\sigma_1(x, \hat{\pi} + \varepsilon\rho) \cdot \sigma_{n-1}(x, \hat{\pi} + \varepsilon\rho)}, \quad x \in \tilde{Y} \cap K, \varepsilon \in [0, \varepsilon_{\max}]. \quad (15)$$

**Definition 2.** (i) Let

$$\begin{aligned} L(\hat{\pi}, \rho) &:= \inf_{x \in \tilde{Y} \cap K} \left| \frac{\hat{\sigma}_n(x, \hat{\pi}, \rho, 0)}{\sigma_1(x, \hat{\pi}) \cdot \sigma_{n-1}(x, \hat{\pi})} \right|, \\ U(\hat{\pi}, \rho) &:= \sup_{x \in \tilde{Y} \cap K} \left| \frac{\hat{\sigma}_n(x, \hat{\pi}, \rho, 0)}{\sigma_1(x, \hat{\pi}) \cdot \sigma_{n-1}(x, \hat{\pi})} \right|. \end{aligned} \quad (16)$$

- (ii) We call

$$\varepsilon^*(\hat{\pi}, \rho, \varepsilon) := \varepsilon \cdot U(\hat{\pi}, \rho) \quad (17)$$

the *distinguished upper bound for the TFPV  $\hat{\pi}$  with parameter direction  $\rho$* , of system (7), and we call

$$\varepsilon_*(\hat{\pi}, \rho, \varepsilon) := \varepsilon \cdot L(\hat{\pi}, \rho) \quad (18)$$

the *distinguished lower bound for the TFPV  $\hat{\pi}$  with parameter direction  $\rho$* .

By the nondegeneracy condition one has  $U(\widehat{\pi}, \rho) \geq L(\widehat{\pi}, \rho) > 0$ . We obtain the following asymptotic inequalities:

**Proposition 1.** *Given  $\alpha > 0$ , for sufficiently small  $\varepsilon_{\max}$  the inequalities*

$$\frac{1}{(1+\alpha)}L(\widehat{\pi}, \rho) \leq \left| \frac{\widehat{\sigma}_n(x, \widehat{\pi}, \rho, \varepsilon)}{\sigma_1(x, \widehat{\pi} + \varepsilon\rho) \cdot \sigma_{n-1}(x, \widehat{\pi} + \varepsilon\rho)} \right| \leq (1+\alpha)U(\widehat{\pi}, \rho) \quad (19)$$

hold on  $K^*$ .

*Proof.* By analyticity in  $\varepsilon$  one has, for  $\varepsilon_{\max}$  sufficiently small:

$$\left| \frac{\widehat{\sigma}_n(x, \widehat{\pi}, \rho, \varepsilon)}{\sigma_1(x, \widehat{\pi} + \varepsilon\rho) \cdot \sigma_{n-1}(x, \widehat{\pi} + \varepsilon\rho)} - \frac{\widehat{\sigma}_n(x, \widehat{\pi}, \rho, 0)}{\sigma_1(x, \widehat{\pi}) \cdot \sigma_{n-1}(x, \widehat{\pi})} \right| \leq \text{const.} \cdot \varepsilon$$

for all  $(x, \varepsilon) \in K^*$ . The assertion follows.  $\square$

**Remark 1.** • *By definition, determining the distinguished upper and lower bounds amounts to determining the maximum and minimum of a rational function on a compact set. It may not be possible (or not advisable) to determine  $\varepsilon^*$  or  $\varepsilon_*$  exactly, and one may have to content with sufficiently tight upper resp. lower estimates.*

- *The derivation of the small parameters involves the critical manifold and the TFPV  $\widehat{\pi}$ , hence they depend on these choices. Moreover there is some freedom of choice for the parameter direction  $\rho$ , which also influences the bounds. For these reasons one should not assume universal efficacy of any small parameter without further context.*

### 3.2 The correspondence to timescales

We now discuss the correspondence between timescales and the parameters determined from (15). By direct verification, via (11) one finds for the eigenvalues  $\lambda_1, \dots, \lambda_n$  of  $D_1h(x, \pi)$ :

**Lemma 3.** (a) *The identity*

$$\sum_{i \neq j} \frac{\lambda_i}{\lambda_j} = \frac{\sigma_1 \sigma_{n-1}}{\sigma_n} - n \quad (20)$$

holds whenever all  $\lambda_i \neq 0$ .

(b) *With  $(x, \varepsilon) \in K^*$ , for  $\varepsilon \neq 0$  one has*

$$\frac{1}{\varepsilon} \sum_{i < n} \lambda_i / \widehat{\lambda}_n + \sum_{i \neq j; i, j < n} \lambda_i / \lambda_j + \varepsilon \sum_{i < n} \widehat{\lambda}_n / \lambda_i = \frac{1}{\varepsilon} \frac{\sigma_1 \sigma_{n-1}}{\widehat{\sigma}_n} - n.$$

This gives rise to further asymptotic inequalities:

**Proposition 2.** *Let  $\beta$ ,  $\theta$  and  $\Theta$  be as in Lemma 2, and  $\alpha > 0$ . Then for sufficiently small  $\varepsilon_{\max} > 0$  the following hold:*

(a) *For all  $(x, \varepsilon) \in K^*$ ,*

$$\frac{1}{(1+\alpha)}\varepsilon_*(\widehat{\pi}, \rho, \varepsilon) \leq \left| \frac{\lambda_n(x, \widehat{\pi} + \varepsilon\rho)}{\sum_{i < n} \lambda_i(x, \widehat{\pi} + \varepsilon\rho)} \right| \leq (1+\alpha)\varepsilon^*(\widehat{\pi}, \rho, \varepsilon). \quad (21)$$

*In particular there exist constants  $C_1, C_2$  such that*

$$C_1\varepsilon \leq \left| \frac{\lambda_n(x, \widehat{\pi} + \varepsilon\rho)}{\sum_{i < n} \lambda_i(x, \widehat{\pi} + \varepsilon\rho)} \right| \leq C_2\varepsilon.$$

(b) *The global estimates*

$$\frac{1}{(1+\alpha)\varepsilon^*} \leq \frac{\inf |\lambda_n|}{(n-1)\Theta} \leq \frac{\sup |\lambda_n|}{(n-1)\theta} \leq (1+\alpha)\varepsilon^* \quad (22)$$

hold, with infimum and supremum being taken over all  $(x, \varepsilon) \in K^*$ .

*Proof.* From Lemma 3 one obtains that

$$\frac{|\widehat{\lambda}_n(x, \widehat{\pi}, \rho, \varepsilon)|}{|\sum_{i=1}^{n-1} \lambda_i(x, \widehat{\pi} + \varepsilon\rho)|} = \left| \frac{\widehat{\sigma}_n(x, \widehat{\pi}, \rho, \varepsilon)}{\sigma_1(x, \widehat{\pi} + \varepsilon\rho)\sigma_{n-1}(x, \widehat{\pi} + \varepsilon\rho)} \right| + \varepsilon\eta(x, \widehat{\pi}, \rho, \varepsilon)$$

for all  $(x, \varepsilon) \in K^*$ , with bounded  $\eta$ . Combining this with Proposition 1 yields the assertions of part (a), and also

$$\frac{1}{(1+\alpha)}L(\widehat{\pi}, \rho) \leq \left| \frac{\widehat{\lambda}_n(x, \widehat{\pi}, \rho, \varepsilon)}{\sum_{i < n} \lambda_i(x, \widehat{\pi} + \varepsilon\rho)} \right| \leq (1+\alpha)U(\widehat{\pi}, \rho)$$

for all  $(x, \varepsilon) \in K^*$ , provided  $\varepsilon_{\max}$  is sufficiently small. Noting

$$\left| \sum_{i=1}^{n-1} \lambda_i(x, \pi) \right| = \left| \sum_{i=1}^{n-1} \operatorname{Re} \lambda_i(x, \pi) \right| = \sum_{i=1}^{n-1} |\operatorname{Re} \lambda_i(x, \pi)|,$$

the second statement follows by standard estimates.  $\square$

Informally speaking, Proposition 2 provides estimates for the ratio of the slowest to the fastest timescale, with  $\sum_{i < n} \lambda_i$  being dominated by the real part with largest modulus. Thus for dimension  $n > 2$  the estimates may be unsatisfactory whenever  $\Theta \gg \theta$ . For applications the second estimate in (22) is more relevant, since the fast dynamics will be governed by the smallest absolute real part of  $\lambda_1, \dots, \lambda_{n-1}$ ; see Appendix, subsection 9.1. The parameter  $\varepsilon^*$  by itself does not completely characterize the timescale discrepancies, as should be expected: If there is more than one eigenvalue ratio to consider then a single quantity cannot measure all of them.

However, in the following – specialized but relevant – setting a general estimate can be obtained from the coefficients of the characteristic polynomial.

**Proposition 3.** *Let  $\beta$ ,  $\theta$  and  $\Theta$  be as in Lemma 2, and  $\alpha > 0$ . Moreover assume that the eigenvalues  $\lambda_1, \dots, \lambda_{n-1}$  satisfy  $|\operatorname{Re} \lambda_j| > |\operatorname{Im} \lambda_j|$ , and let  $|\operatorname{Re} \lambda_1| \geq \dots \geq |\operatorname{Re} \lambda_{n-1}|$ . Define*

$$\mu^* := \varepsilon \cdot \sup_{x \in \widetilde{Y} \cap K} \left| \frac{\widehat{\sigma}_n(x, \widehat{\pi}, \rho, 0) \cdot \sigma_{n-2}(x, \widehat{\pi})}{\sigma_{n-1}(x, \widehat{\pi})^2} \right|. \quad (23)$$

Then for sufficiently small  $\varepsilon_{\max} > 0$  one has

$$\sup_{(x, \varepsilon) \in K^*} \left| \frac{\lambda_n}{\operatorname{Re} \lambda_{n-1}} \right| \leq \sqrt{2}(1+\alpha) \mu^*. \quad (24)$$

Whenever  $\lambda_{n-1} \in \mathbb{R}$  then the estimate can be sharpened to

$$\sup_{(x, \varepsilon) \in K^*} \left| \frac{\lambda_n}{\operatorname{Re} \lambda_{n-1}} \right| \leq (1+\alpha) \mu^*. \quad (25)$$

*Proof.* (i) Preliminary observation: Let  $k \geq 2$  and  $\beta_1, \dots, \beta_k \in \mathbb{C}$  with negative real parts, and  $|\operatorname{Re} \beta_1| \geq \dots \geq |\operatorname{Re} \beta_k|$ . Moreover denote by  $(-1)^\ell \tau_\ell$  the  $\ell^{\text{th}}$  elementary symmetric polynomial in the  $\beta_j$ . If  $|\operatorname{Re} \beta_j| > |\operatorname{Im} \beta_j|$  for  $j = 1, \dots, k$ , then

$$|\operatorname{Re} \beta_k| \geq \frac{\tau_k}{\sqrt{2}\tau_{k-1}}, \text{ and } |\beta_k| \geq \frac{\tau_k}{\tau_{k-1}} \text{ when } \beta_k \in \mathbb{R}.$$

To verify this, recall

$$\sum_{i \neq j} \frac{\beta_i}{\beta_j} = \frac{\tau_1 \tau_{k-1}}{\tau_k} - k \leq \frac{\tau_1 \tau_{k-1}}{\tau_k} - 1.$$

Now, for complex numbers  $z, w$  with negative real parts and  $|\operatorname{Re} z| > |\operatorname{Im} z|$ ,  $|\operatorname{Re} w| > |\operatorname{Im} w|$ , one has  $\operatorname{Re} \frac{z}{w} > 0$ . Therefore, all  $\operatorname{Re} \beta_i/\beta_j > 0$ ,  $1 \leq i, j \leq k-1$ , and since their sum is real we obtain the estimate

$$\frac{\tau_1}{|\beta_k|} = \sum_{i=1}^k \frac{\beta_i}{\beta_k} = 1 + \sum_{i=1}^{k-1} \frac{\beta_i}{\beta_k} \leq \frac{\tau_1 \tau_{k-1}}{\tau_k}.$$

With  $|\operatorname{Re} \beta_k| \geq |\beta_k|/\sqrt{2}$  the assertion follows. For real  $\beta_k$  the factor  $\sqrt{2}$  may be discarded.

(ii) We apply the above to the  $\lambda_i(x, \hat{\pi})$  and  $\sigma_j(x, \hat{\pi})$ ,  $1 \leq i \leq n-1$ , obtaining

$$\sigma_1 \leq \sqrt{2} |\operatorname{Re} \lambda_{n-1}| \frac{\sigma_1 \sigma_{n-2}}{\sigma_{n-1}}.$$

By Lemma 3 we have (with arguments  $x \in \tilde{Y} \cap K$ ,  $\hat{\pi}$  and  $\rho$  suppressed)

$$\left| \frac{\sigma_1 \sigma_{n-1}}{\hat{\sigma}_n} \right| = \left| \frac{\lambda_1 + \dots + \lambda_{n-1}}{\hat{\lambda}_n} \right| = \left| \frac{\sigma_1}{\hat{\lambda}_n} \right| \leq \sqrt{2} \left| \frac{\operatorname{Re} \lambda_{n-1}}{\hat{\lambda}_n} \right| \cdot \left| \frac{\sigma_1 \sigma_{n-2}}{\sigma_{n-1}} \right|,$$

and in turn

$$\left| \frac{\hat{\lambda}_n(x, \hat{\pi}, \rho, 0)}{\operatorname{Re} \lambda_{n-1}(x, \hat{\pi})} \right| \leq \sqrt{2} \frac{\hat{\sigma}_n(x, \hat{\pi}, \rho, 0) \sigma_{n-2}(x, \hat{\pi})}{\sigma_{n-1}(x, \hat{\pi})^2}.$$

By continuity and compactness the assertion readily follows when  $\varepsilon_{\max}$  is sufficiently small. As in (i) the factor  $\sqrt{2}$  may be discarded for real  $\lambda_{n-1}$ . □

**Remark 2.** • As with the distinguished upper bound, determining  $\mu^*$  amounts to finding the maximum of a rational function on a compact set.

- The proofs of Propositions 2 and 3 implicitly impose further restrictions on  $\varepsilon_{\max}$ .
- Proposition 3 holds in particular in settings when all eigenvalues are “essentially real”, meaning small  $|\operatorname{Im} \lambda|/|\operatorname{Re} \lambda|$ . This is frequently the case for chemical reaction networks.
- One can obviously derive analogous but weaker estimates whenever the ratios  $|\operatorname{Im} \lambda|/|\operatorname{Re} \lambda|$  are bounded above by some constant. Likewise, the estimates underlying part (i) of the proof could be sharpened.

### 3.3 Two-dimensional systems

We turn to systems of dimension two, where a TFPV necessarily refers to a critical manifold of dimension  $s = 1$ . We keep the notation and conventions from subsection 2.4. Rather than specializing the asymptotic results from Propositions 2 and 3, we will retrace their derivation and obtain slightly sharper estimates.

First and foremost, the TFPV conditions imply that  $\sigma_1$  must be bounded above and below by positive constants. The accuracy of the reduction is reflected in the ratio of the eigenvalues  $\lambda_1, \lambda_2$  of  $D_1 h(x, \hat{\pi} + \varepsilon \rho)$  with  $x$  in the critical manifold, and  $\lambda_2 = 0$  at  $\hat{\pi}$ . Then

$$\sigma_1 = -(\lambda_1 + \lambda_2), \quad \sigma_2 = \lambda_1 \lambda_2$$

and moreover  $\lambda_2 = \varepsilon \hat{\lambda}_2$  and  $\sigma_2 = \varepsilon \hat{\sigma}_2$ . For  $n = 2$  the familiar identity

$$\frac{\lambda_2}{\lambda_1} + \frac{\lambda_1}{\lambda_2} = \frac{\lambda_1^2 + \lambda_2^2}{\lambda_1 \lambda_2} = \frac{\sigma_1^2 - 2\sigma_2}{\sigma_2} = \frac{\sigma_1^2}{\sigma_2} - 2 \tag{26}$$

for  $\lambda_1 \neq 0, \lambda_2 \neq 0$  yields sharper estimates than Proposition 2. (Similar estimates were also used in Eilertsen et al. [12].)

**Lemma 4.** (a) For all  $M > 1$ ,  $\widetilde{M} > 2$ ,  $M^* > 3$  the implications

$$\begin{aligned} |\lambda_1/\lambda_2| > M &\Rightarrow |\sigma_1^2/\sigma_2| > \widetilde{M} + 2; \\ |\sigma_1^2/\sigma_2| \leq \widetilde{M} &\Rightarrow |\lambda_1/\lambda_2| \leq \widetilde{M} - 2; \\ |\sigma_1^2/\sigma_2| > M^* &\Rightarrow |\lambda_1/\lambda_2| > M^* - 3, \end{aligned}$$

hold whenever  $|\lambda_2/\lambda_1| < 1$ .

(b) In the TFPV case,

$$\frac{1}{\varepsilon} \cdot \frac{\sigma_1^2}{\widehat{\sigma}_2} = 2 + \varepsilon \frac{\widehat{\lambda}_2}{\lambda_1} + \frac{1}{\varepsilon} \frac{\lambda_1}{\widehat{\lambda}_2}$$

and with  $\varepsilon \rightarrow 0$

$$\frac{\widehat{\sigma}_2(x, \widehat{\pi}, \rho, 0)}{\sigma_1^2(x, \widehat{\pi})} = \frac{\widehat{\lambda}_2(x, \widehat{\pi}, \rho, 0)}{\lambda_1(x, \widehat{\pi})}.$$

(c) For given  $\alpha > 0$ , suitable choice of  $\varepsilon_{\max}$  yields

$$\frac{1}{(1+\alpha)} \varepsilon_* \leq \inf \frac{|\lambda_2|}{|\lambda_1|} \leq \sup \frac{|\lambda_2|}{|\lambda_1|} \leq (1+\alpha) \varepsilon_*, \quad (27)$$

with infimum and supremum taken over all  $(x, \varepsilon) \in K^*$ .

Lemma 4 shows that  $\varepsilon^*$  provides a tight global upper estimate for the eigenvalue ratio (and thus for the timescale ratio) as  $\varepsilon \rightarrow 0$ , with  $x$  running through  $\widetilde{Y} \cap K$ . Moreover, in the analysis of particular systems one may retrace the arguments leading to the lemma, and determine estimates for  $\varepsilon_{\max}$  e.g. from higher order Taylor expansions.

### 3.4 Three-dimensional systems

We specialize the general results to dimension three. Given the blanket assumptions from subsection 2.4, we denote by  $\lambda_1, \lambda_2$ , and  $\lambda_3 = \varepsilon \widehat{\lambda}_3$  the eigenvalues of the linearization. We have

$$U(\widehat{\pi}, \rho) = \sup_{x \in \widetilde{Y} \cap K} \left| \frac{\widehat{\sigma}_3(x, \widehat{\pi}, \rho, 0)}{\sigma_1(x, \widehat{\pi}) \cdot \sigma_2(x, \widehat{\pi})} \right|, \quad \varepsilon^*(\widehat{\pi}, \rho, \varepsilon) = \varepsilon U(\widehat{\pi}, \rho), \quad (28)$$

and similar expressions for  $L$  and  $\varepsilon_*$ . As for applicability of the parameter  $\mu^*$ , one has:

**Proposition 4.** (a) • The eigenvalues  $\lambda_1$  and  $\lambda_2$  are real if and only if  $\sigma_1^2 - 4\sigma_2 \geq 0$ .

• Given that  $\lambda_1 \notin \mathbb{R}$  and  $\lambda_2 = \bar{\lambda}_1$ , one has  $|\operatorname{Re} \lambda_1| > |\operatorname{Im} \lambda_1|$  if and only if  $\sigma_1^2 - 2\sigma_2 > 0$ .

(b) Assume that one of the conditions in part (a) holds. Then, given  $\alpha > 0$ , for sufficiently small  $\varepsilon_{\max}$  one has

$$\sup_{(x, \varepsilon) \in K^*} \left| \frac{\lambda_3}{\operatorname{Re} \lambda_2} \right| \leq \sqrt{2}(1+\alpha) \mu^*,$$

resp.

$$\sup_{(x, \varepsilon) \in K^*} \left| \frac{\lambda_3}{\lambda_2} \right| \leq (1+\alpha) \mu^* \text{ whenever } \lambda_2 \in \mathbb{R};$$

with

$$\mu^* = \varepsilon \cdot \sup_{x \in \widetilde{Y} \cap K} \left| \frac{\widehat{\sigma}_3(x, \widehat{\pi}, \rho, 0) \cdot \sigma_1(x, \widehat{\pi})}{\sigma_2(x, \widehat{\pi})^2} \right|.$$

*Proof.* To determine the nature of the eigenvalues on the critical manifold, use the identity

$$\left( \frac{\lambda_1 - \lambda_2}{\lambda_1 + \lambda_2} \right)^2 = 1 - 4 \frac{\sigma_2}{\sigma_1^2} \text{ on } \widetilde{Y}. \quad (29)$$

This implies the (of course well known) first statement of part (a). The second statement follows from

$$-\left(\frac{\operatorname{Im} \lambda_1}{\operatorname{Re} \lambda_1}\right)^2 = 1 - 4\frac{\sigma_2}{\sigma_1^2}.$$

The rest is straightforward with Proposition 3.  $\square$

**Remark 3.** • For  $\lambda_1$  and  $\lambda_2$  real and negative, one obtains a lower estimate from

$$\left|\frac{2\lambda_2}{\widehat{\lambda}_3}\right| \leq \left|\frac{\lambda_1 + \lambda_2}{\widehat{\lambda}_3}\right| = \left|\frac{\sigma_1\sigma_2}{\widehat{\sigma}_3}\right| \implies 2\left|\frac{\widehat{\sigma}_3}{\sigma_1\sigma_2}\right| \leq \left|\frac{\widehat{\lambda}_3}{\lambda_2}\right| \text{ on } \widetilde{Y} \cap K.$$

- If  $\lambda_1$  is not real and  $\lambda_2 = \bar{\lambda}_1$ , with negative real parts, then the specialization of (20), viz.

$$\frac{\lambda_1 + \lambda_2}{\lambda_3} + \left(\frac{\lambda_1}{\lambda_2} + \frac{\lambda_2}{\lambda_1}\right) + \left(\frac{\lambda_3}{\lambda_1} + \frac{\lambda_3}{\lambda_2}\right) = \frac{\sigma_1\sigma_2}{\sigma_3} - 3,$$

for real  $\lambda_3$ ,  $|\lambda_3| < |\operatorname{Re} \lambda_1|$ , shows that both the second term and the third term on the left hand side are bounded below by  $-2$  and above by  $2$ , and we obtain

$$\frac{\sigma_1\sigma_2}{\sigma_3} - 7 \leq \frac{2\operatorname{Re} \lambda_1}{\lambda_3} \leq \frac{\sigma_1\sigma_2}{\sigma_3} + 1.$$

In particular this yields an asymptotic timescale estimate

$$\left|\frac{\widehat{\lambda}_3}{\operatorname{Re} \lambda_1}\right| \rightarrow 2\left|\frac{\widehat{\sigma}_3}{\sigma_1\sigma_2}\right| \text{ as } \varepsilon \rightarrow 0.$$

**Remark 4.** When all eigenvalues are real then one obtains the ratio of  $\lambda_1$  and  $\lambda_2$ , with  $|\lambda_2| \leq |\lambda_1|$ , from

$$\frac{\sigma_2}{\sigma_1^2} = \frac{\lambda_1\lambda_2 + \varepsilon(\dots)}{(\lambda_1 + \lambda_2 + \varepsilon(\dots))^2} = \frac{\lambda_2/\lambda_1}{(1 + \lambda_2/\lambda_1)^2} + \varepsilon(\dots)$$

and the arguments leading up to Lemma 4: With

$$\kappa_* := \inf_{x \in \widetilde{Y} \cap K} \left|\frac{\sigma_2(x, \widehat{\pi})}{\sigma_1(x, \widehat{\pi})^2}\right|, \quad \kappa^* := \sup_{x \in \widetilde{Y} \cap K} \left|\frac{\sigma_2(x, \widehat{\pi})}{\sigma_1(x, \widehat{\pi})^2}\right|, \quad (30)$$

the following hold for every  $\alpha > 0$ , with sufficiently small  $\varepsilon$ :

- On  $\widetilde{Y} \cap K$  one has

$$\left|\frac{\lambda_2}{\lambda_1}\right| \geq \frac{\kappa_*}{1 + \alpha}.$$

- If  $|\lambda_2/\lambda_1| \leq \delta$  for all  $x \in \widetilde{Y} \cap K$  then  $\kappa^* \leq \frac{\delta}{2\delta + 1}$ .

Large discrepancy between  $\lambda_1$  and  $\lambda_2$  (in addition to  $\mu^* \ll 1$ ) may indicate a scenario with three timescales (informally speaking): slow, fast and very fast. Cardin and Texeira [6] provided a rigorous extension of Fenichel theory for such settings, providing solid ground for their analysis. Note that large discrepancy between  $\varepsilon^*$  and  $\mu^*$  implies large discrepancy between  $\lambda_1$  and  $\lambda_2$ , in view of the definitions.

## 4 Michaelis–Menten reaction mechanism revisited

The reader may wonder why we include a rather long section on the most familiar reaction in biochemistry. The basic motivation is that some widely held beliefs on its QSS variants are problematic; see Eilertsen et al. [12]. Beyond this, the timescale ratio approach actually yields new results for the reversible MM system, as well as for MM with slow product formation.

## 4.1 The reversible network with low enzyme concentration

The reversible MM network with low enzyme concentration corresponds to the system

$$\begin{aligned}\dot{s} &= -k_1 e_0 s + (k_1 s + k_{-1})c \\ \dot{c} &= k_1 e_0 s - (k_1 s + k_{-1} + k_2)c + k_{-2}(e_0 - c)(s_0 - s - c)\end{aligned}\quad (31)$$

with standard initial conditions  $s(0) = s_0$ ,  $c(0) = 0$ . The earliest discussion of (31) dates back to Miller and Alberty [29], but the reversible network has garnered relatively little attention compared to the irreversible one.

The parameter space  $\Pi = \mathbb{R}_{\geq 0}^6$  has elements  $(e_0, s_0, k_1, k_{-1}, k_2, k_{-2})^{\text{tr}}$ , and we set  $x = (s, c)^{\text{tr}}$ . As is well known, setting  $e_0 = 0$  and all other parameters  $> 0$  defines a TFPV, with the critical manifold  $\tilde{Y}$  given by  $c = 0$ . For the reduced equation one finds

$$\dot{s} = -e_0 \cdot \frac{s(k_1 k_2 + k_{-1} k_{-2}) - k_{-1} k_{-2} s_0}{k_1 s + k_{-1} + k_2 + k_{-2}(s_0 - s)};$$

see e.g. Noethen and Walcher [32].

By the first blanket assumption in subsection 2.4 we restrict  $(s_0, k_1, k_{-1}, k_2, k_{-2})^{\text{tr}}$  to a compact subset of the open positive orthant.

With fixed  $e_0^* > 0$  (with dimension concentration) we let  $\rho = (e_0^*, 0, \dots, 0)^{\text{tr}}$ ; we will work with both  $e_0$  and  $\varepsilon e_0^*$ .

Rather than obtaining  $\varepsilon_*$  and  $\varepsilon^*$  directly from Lemma 4, we retrace their derivation and get error estimates in the process. The coefficients of the characteristic polynomial with  $x \in \tilde{Y}$  are

$$\begin{aligned}\sigma_1(x, \hat{\pi} + \varepsilon\rho) &= k_1 e_0 + k_1 s + k_{-1} + k_2 + k_{-2}(e_0 + s_0 - s); \\ \sigma_2(x, \hat{\pi} + \varepsilon\rho) &= e_0 (k_1 k_{-2}(e_0 + s_0) + k_1 k_2 + k_{-1} k_{-2}).\end{aligned}$$

The set  $K$  (compatible with the standard initial conditions), defined by  $0 \leq s \leq s_0$  and  $0 \leq c \leq e_0^*$ , is compact and positively invariant.

We only discuss the case  $k_1 \geq k_{-2}$ ; the other case amounts to reversing the roles of  $s$  and  $p$ . Note that  $\sigma_2$  is independent of  $s$ . The minimum of  $\sigma_1(x, \hat{\pi} + \varepsilon\rho)$  on  $\tilde{Y} \cap K$  equals

$$k_1 e_0 + k_{-1} + k_2 + k_{-2}(e_0 + s_0),$$

and the maximum is

$$k_1(e_0 + s_0) + k_{-1} + k_2 + k_{-2}e_0.$$

In particular the minimum of  $\sigma_1(x, \hat{\pi})$  on  $\tilde{Y} \cap K$  equals

$$k_{-1} + k_2 + k_{-2}s_0.$$

Moreover we have

$$\hat{\sigma}_2(x, \hat{\pi}, 0) = k_1 k_{-2} s_0 + k_1 k_2 + k_{-1} k_{-2},$$

a positive constant.

By Lemma 4 and its derivation we find

$$\frac{e_0 (k_1 k_{-2}(e_0 + s_0) + k_1 k_2 + k_{-1} k_{-2})}{(k_1(e_0 + s_0) + k_{-1} + k_2 + k_{-2}e_0)^2} \leq \frac{\sigma_2}{\sigma_1^2} \leq \frac{e_0 (k_1 k_{-2}(e_0 + s_0) + k_1 k_2 + k_{-1} k_{-2})}{(k_1 e_0 + k_{-1} + k_2 + k_{-2}(e_0 + s_0))^2},$$

valid for all  $\varepsilon > 0$ . Neglecting higher order terms in  $\varepsilon$  yields

$$\varepsilon_* = \frac{e_0 (k_1 k_{-2} s_0 + k_1 k_2 + k_{-1} k_{-2})}{(k_{-1} + k_2 + k_1 s_0)^2}; \quad \varepsilon^* = \frac{e_0 (k_1 k_{-2} s_0 + k_1 k_2 + k_{-1} k_{-2})}{(k_{-1} + k_2 + k_{-2} s_0)^2}.$$

Therefore it seems appropriate to define the distinguished local parameter for the reversible Michaelis–Menten system as

$$\varepsilon_{MMR} := \varepsilon^* = \frac{e_0 (k_1 k_{-2} s_0 + k_1 k_2 + k_{-1} k_{-2})}{(k_{-1} + k_2 + k_{-2} s_0)^2}. \quad (32)$$

It appears that this particular parameter has not been introduced so far, nor has any close relative. Indeed there seem to exist no parameters in the literature that were specifically derived for the reversible network. (In their discussion of the reversible system, Seshadri and Fritzsche [40] worked with the parameter  $\varepsilon_{RS}$  that Reich and Selkov had designed for the irreversible system; see (5).)

## 4.2 The irreversible network with low enzyme concentration

We specialize to the irreversible case, thus we have the differential equation (1) with  $e_0 = \varepsilon e_0^*$ . The QSS manifold of this system is defined by  $c = g(s) := e_0 s / (K_M + s)$ .

### 4.2.1 Distinguished small parameters

- The parameters from the reversible scenario simplify to

$$\varepsilon_* = \frac{e_0 k_1 k_2}{(k_1 s_0 + k_{-1} + k_2)^2}; \quad \varepsilon^* = \varepsilon_{MM} := \frac{e_0 k_1 k_2}{(k_{-1} + k_2)^2},$$

with

$$\min \sigma_1 = k_{-1} + k_2; \quad \hat{\sigma}_2 = k_1 k_2.$$

Note that the TFPV and nondegeneracy conditions, together with the compactness condition in parameter space, require that  $k_2$  is bounded below by some positive constant.

As in the previous subsection, one finds that  $\varepsilon_{MM}$  is a sharp upper estimate for the eigenvalue ratio. In fact

$$\frac{\sigma_2}{\sigma_1^2} \leq \frac{k_2 k_1 e_0}{(k_1 e_0 + k_{-1} + k_2)^2} \leq \varepsilon_{MM}$$

throughout.

Various small parameters have been proposed for the irreversible Michaelis–Menten system, as noted in the Introduction. Comparing these, we note

$$\varepsilon_{MM} = \frac{e_0 k_1}{k_{-1} + k_2} \cdot \frac{k_2}{k_{-1} + k_2} \leq \frac{e_0 k_1}{k_{-1} + k_2} = \varepsilon_{RS},$$

with the Reich–Selkov parameter. Whenever  $k_{-1}$  and  $k_2$  have the same order of magnitude (in any case  $k_2$  must be bounded away from 0 by nondegeneracy), the disparity between  $\varepsilon_{MM}$  and  $\varepsilon_{RS}$  may be seen as inessential.

The parameters  $\varepsilon_{MM}$  and  $\varepsilon_{RS}$  differ markedly from the most familiar small parameters, viz.  $\varepsilon_{BH}$  (see (4)) as used by Heineken et al. [23], and  $\varepsilon_{SSI}$  (see (6)) as introduced in Segel and Slemrod [39], which both involve the initial substrate concentration. As shown in [31], smallness of the Segel–Slemrod parameter is necessary and sufficient to ensure negligible loss of substrate in the initial phase. But as noted in Patsatzis and Goussis [34], and in Eilertsen et al. [12], large initial substrate concentration, while ensuring a fast approach to the QSS manifold, is not sufficient to guarantee a good QSS approximation over the whole course of the reaction. A general argument in favor of  $\varepsilon_*$  and  $\varepsilon_{MM}$  is that they directly measure the local ratio of timescales.

### 4.2.2 Further observations

- We briefly discuss what can be inferred from  $\varepsilon_{MM} = \frac{k_1 k_2 e_0}{(k_{-1} + k_2)^2} \rightarrow 0$  alone, with no further restriction on the limiting process. In the simplest imaginable scenario, letting a parameter tend to zero might automatically imply validity of some QSS approximation, but this is not the case here. The TFPV conditions on  $\sigma_1$  imply that  $k_{-1}$  is bounded above and we obtain three cases: In addition to the case  $e_0 \rightarrow 0$ , we have the case  $k_1 \rightarrow 0$ , yielding a singular perturbation reduction with the same critical manifold but a linear reduced equation. Furthermore we have the case  $k_2 \rightarrow 0$ , which leads to a singular perturbation scenario with a different critical manifold and different reduction; see the next

subsection. This observation supports a statement from the Introduction: A given small parameter by itself will in general not determine a unique singular perturbation scenario, and a transfer without reflection of the reduction procedure from one scenario to a different one may yield incorrect results. It is necessary to consider the complete setting, including TFPV, critical manifold and small parameter. Moreover, one needs to carefully stipulate how limits are taken. For instance, letting  $s_0 \rightarrow \infty$ , while ensuring  $\varepsilon_{SSL} \rightarrow 0$ , will fail to ensure convergence. Likewise, letting e.g.  $k_{-1} \rightarrow \infty$  in the Reich-Selkov parameter does not imply convergence.

- For the irreversible reaction with substrate inflow at rate  $k_0$ , one obtains the same expressions for  $\sigma_2/\sigma_1^2$  at the TFPV with  $k_0 = 0$  and  $e_0 = 0$  (all other parameters  $> 0$ ), the critical manifold being given by  $c = 0$ . Before obtaining  $\varepsilon_*$ ,  $\varepsilon^*$  one needs to choose appropriate initial conditions; we take  $s(0) = c(0) = 0$  here. Solutions are not necessarily confined to compact sets, so one may not be able to choose the set  $K$  from subsection 2.4 to be positively invariant. In the case  $s(0) = c(0) = 0$  the computation of the distinguished upper bound  $\varepsilon^*$  works as in the case with no influx; the supremum exists and is equal to  $\varepsilon_{MM}$ . However, one gets  $\varepsilon_* \rightarrow 0$  with increasing  $s$  when there exists no positive stationary point (all solutions are unbounded in positive time), hence the lower estimate provides no information. If there exists a finite positive stationary point  $\tilde{s}$  of the reduced equation then one obtains  $\varepsilon_* > 0$  by replacing  $s_0$  by  $\tilde{s}$  in the lower estimate in 4.2.1. In this case, a compact positively invariant set exists with  $s \leq \tilde{s}$ , as was shown in Eilertsen et al. [9].

### 4.3 The irreversible network with slow product formation

We turn to the scenario with slow product formation, the other reactions being fast. Here  $k_2 = 0$ , with all other parameters  $> 0$ , defines a TFPV with critical manifold  $\tilde{Y}$  given by  $c = \frac{k_1 e_0 s}{k_1 s + k_{-1}}$ . Although setting up  $k_2 = 0$  appears counterintuitive for an enzyme catalyzed reaction, there is a family of enzymes, known as pseudoenzymes, that have either zero catalytic activity ( $k_2 = 0$ ), or vestigial catalytic activity ( $k_2 \approx 0$ ) due to the lack of catalytic amino acids or motifs [16]. These enzymes exist in all the kingdoms of life and, are also named as “zombie” enzyme, dead enzyme, or prozymes. Pseudoenzymes play different functions in signalling network, such as serving as dynamic scaffolds, modulators of enzymes, or competitors in canonical signalling pathways [30].

#### 4.3.1 Distinguished small parameters

Intersecting  $\tilde{Y}$  with the positively invariant compact set  $K$  defined by  $0 \leq s \leq s_0$  and  $0 \leq c \leq e_0$ , amounts to restricting  $0 \leq s \leq s_0$ . The elements of the parameter space  $\Pi = \mathbb{R}_{\geq 0}^5$  have the form  $(e_0, s_0, k_1, k_{-1}, k_2)^{\text{tr}}$ , and a natural choice of ray direction is  $\rho = (0, 0, 0, 0, k_2^*)^{\text{tr}}$ , with  $k_2 = \varepsilon k_2^*$ .

The coefficients of the characteristic polynomial on  $\tilde{Y}$  are

$$\begin{aligned}\sigma_1 &= \frac{k_{-1} k_1 e_0}{k_1 s + k_{-1}} + k_1 s + k_{-1} + k_2, \\ \sigma_2 &= e_0 k_1 k_2 \cdot \frac{k_{-1}}{k_1 s + k_{-1}}.\end{aligned}$$

- We first evaluate the nondegeneracy conditions for the coefficients of the characteristic polynomial, from TFPV requirements and compactness. The minimum of  $\sigma_1(x, \hat{\pi})$  on  $\tilde{Y} \cap K$  is equal to  $k_{-1} + k_1 e_0$  when  $k_1 e_0 \leq k_{-1}$ , and equal to  $2\sqrt{k_{-1} k_1 e_0}$  otherwise. This minimum must be bounded below by some positive constant. Combining this observation with the boundedness of the maximum of  $\hat{\sigma}_2 = \frac{k_2^* k_{-1} k_1 e_0}{k_1 s + k_{-1}}$  on  $[0, s_0]$ , which is equal to  $k_2^* k_1 e_0$ , one sees that  $k_1 e_0$  and  $k_{-1}$  must be bounded above and below by positive constants.
- Turning to small parameters, in the asymptotic limit one obtains

$$\varepsilon^* = k_2 \sup \frac{av}{(a+v^2)^2} \text{ with } a = k_{-1} k_1 e_0, v = k_1 s + k_{-1},$$

where the supremum is taken over  $k_{-1} \leq v \leq k_{-1} + k_1 s_0$ . By elementary calculus one finds the global maximum of this function on the unbounded interval  $v \geq 0$ , thus for sufficiently large  $s_0$  we obtain the maximum at  $v = \sqrt{k_{-1} k_1 e_0 / 3}$ , and find the estimate

$$\varepsilon^* \leq \frac{3\sqrt{3}}{16} \frac{k_2}{\sqrt{k_{-1} \cdot k_1 e_0}} =: \frac{3\sqrt{3}}{8} \cdot \varepsilon_{PE}, \quad \text{with } \varepsilon_{PE} := \frac{2k_2}{\sqrt{k_{-1} \cdot k_1 e_0}}.$$

Note that  $\varepsilon_{PE}$  always yields an upper estimate for the eigenvalue ratio near the critical manifold. One can thus e.g. discard the factor  $1 + \alpha$  in Lemma 4.

- Depending on the given parameters, in some cases one may obtain sharper estimates for  $\varepsilon^*$  from the endpoints of the interval  $[0, s_0]$ . In any case, to determine  $\varepsilon_*$  one needs to consider the boundary points of this interval.
- The expression for  $\varepsilon_{PE}$  may look strange, but  $\sqrt{k_2/k_{-1}} \cdot \sqrt{k_2/(k_1 e_0)}$  is the geometric mean of two reaction rate ratios, thus admits a biochemical interpretation. There is little work in the literature on small parameters for the case of slow product formation: Heineken et al. [23] suggested  $k_2/(k_1 s_0)$ , while Patsatzis and Goussis introduced a parameter depending on  $s$  and  $c$  along a trajectory; taking the maximum over all  $s, c$  yields  $k_2/k_{-1}$ . The latter represents a commonly accepted “small parameter” for this scenario; see Keener and Sneyd [24], subsection 1.4.1. In the limiting case  $k_2 \rightarrow 0$  one also has  $\varepsilon_{MM} \rightarrow 0$ , but one should not conclude that the standard QSS approximation is valid here. (Recall that, in the low enzyme setting,  $k_2$  needs to be bounded away from zero by nondegeneracy.)

### 4.3.2 Approach to the slow manifold

For Michaelis–Menten with slow product formation, we specialize the arguments in the Appendix, 9.1.1 to determine  $\varepsilon_L$ , and show that  $\varepsilon_{PE}$  appears naturally in this estimate.<sup>9</sup> We use the results (and refer to the notation) of subsection 9.1.

First rewrite the system in Tikhonov standard form: Since  $\frac{d}{dt}(s + c) = -k_2 c$ ,  $s + c$  is a first integral of the fast system in the limit  $k_2 = 0$ , with  $x = s + c$ ,  $y = s$  (so  $c = x - y$ ,  $x \geq y \geq 0$ ), and  $k_2 = \varepsilon k_2^*$  one gets

$$\begin{aligned} \dot{x} &= -k_2(x - y) \\ \dot{y} &= -k_1 e_0 y + (k_1 y + k_{-1})(x - y) \\ &= -k_1(y - h_-(x)) \cdot (y - h_+(x)) \end{aligned} \tag{33}$$

with

$$h_{\pm}(x) := \frac{1}{2} (-(K_D + e_0 - x) \pm q(x)); \quad K_D := k_{-1}/k_1; \quad q(x) := \sqrt{(K_D + e_0 - x)^2 + 4K_D x}.$$

We focus on the particular initial conditions with zero complex, thus

$$x(0) = y(0) = s_0.$$

The QSS variety  $\tilde{Y}$  is defined by  $y = h_+(x)$ , and the reduced equation reads

$$\dot{x} = -\frac{k_2}{2} \left( (K_D + e_0 + x) - \sqrt{(K_D + e_0 - x)^2 + 4K_D x} \right). \tag{34}$$

We use the notation and apply the general procedure from the Appendix, subsection 9.1, with

$$A = -k_1(y - h_-(x)) = -k_1 q(x) \quad \text{on } \tilde{Y},$$

and  $g(x) = h_+(x)$ . We will use some properties of  $q$  in the following. First we have

$$q'(x) = \frac{K_D + x - e_0}{\sqrt{(K_D + e_0 - x)^2 + 4K_D x}},$$

---

<sup>9</sup>The scenario with low enzyme concentration is a more involved, and will be discussed in a separate paper.

hence  $|q'(x)| \leq 1$  for all  $x \geq 0$ . Moreover the sign of  $q'$  changes from  $-$  to  $+$  at  $x = e_0 - K_D$  when  $e_0 - K_D \geq 0$ , and is otherwise positive for all  $x \geq 0$ . Thus the minimum of  $q$  is attained at 0, with value  $K_D + e_0$ , when  $e_0 < K_D$ , and is attained at  $e_0 - K_D$ , with value  $2\sqrt{K_De_0}$ , when  $e_0 \geq K_D$ . By the arithmetic-geometric mean inequality we thus have

$$q(x) \geq 2\sqrt{K_De_0} \quad \text{for all } x \geq 0.$$

This shows

$$A \leq -2k_1\sqrt{K_De_0} = -2\sqrt{k_1e_0k_{-1}},$$

and we arrive at

$$\gamma = \sqrt{k_1e_0k_{-1}}.$$

According to subsection 9.1,  $\gamma^{-1}$  is an appropriate timescale for the approach to the slow manifold.

To determine  $\kappa$ , we have  $g(x) = h_+(x) = \frac{1}{2}(x - K_D - e_0 + q(x))$ , thus  $|g'(x)| \leq 1$ , and

$$|f_1(x, y)| = k_2(x - y) \leq k_2e_0, \quad \text{since } x - y = c \leq e_0,$$

hence we may set  $\kappa = k_2e_0$ .

Altogether, we obtain from the Lyapunov function the (dimensional) parameter

$$\varepsilon_L = \frac{2\kappa}{\gamma} = e_0 \cdot \varepsilon_{PE}. \quad (35)$$

To obtain a non-dimensional small parameter, normalization by  $e_0$  seems to be the natural choice here, which yields

$$\widehat{\varepsilon}_L = \varepsilon_{PE}. \quad (36)$$

In this particular setting the local timescale parameter completely characterizes the approach of the solution to the slow manifold.

### 4.3.3 Estimates for long times

We will not attempt to estimate a critical time for the onset of the slow dynamics, and without this we cannot determine approximation errors for solutions of the reduced equation (as outlined in 9.1.3); in this respect the discussion of the MM network with slow product formation remains incomplete. But the following observation provides a relevant condition for the long-term behavior. Since  $|y - g(x)| \rightarrow e_0 \cdot \varepsilon_{PE}$ , the solution will enter the domain with  $|y - g(x)| \leq 2e_0 \cdot \varepsilon_{PE}$  after some short transitory phase<sup>10</sup>. In this domain we obtain the reduced equation with error term:

$$\begin{aligned} \dot{x} &= -k_2(x - g(x)) + k_2(y - g(x)) \\ &\leq -\frac{k_2}{2} \left( (K_D + e_0 + x) - \sqrt{(K_D + e_0 - x)^2 + 4K_Dx} \right) + k_2 \cdot \frac{2k_2e_0}{\sqrt{k_1e_0 \cdot k_{-1}}} =: U(x). \end{aligned} \quad (37)$$

By a differential inequality argument, the solution of  $\dot{x} = U(x)$ , with positive initial value, is an upper bound for the first entry of the solution of (33), given appropriate initial values near the QSS variety. Moreover the solution of the reduced equation (34) with the same initial value remains positive. For  $t \rightarrow \infty$  the absolute value of the difference of these solutions converges to the stationary point of  $\dot{x} = U(x)$ , which therefore indicates the discrepancy. We determine the stationary point, neglecting terms of order  $> 1$  in  $k_2$ :

$$\begin{aligned} \left( (K_D + e_0 + x) - 4 \frac{k_2e_0}{\sqrt{k_1e_0 \cdot k_{-1}}} \right)^2 &= (K_D + e_0 - x)^2 + 4K_Dx \\ \Rightarrow e_0x &= \frac{2k_2e_0}{\sqrt{k_1e_0 \cdot k_{-1}}} \cdot (K_D + e_0 + x) + \dots \\ \Rightarrow \frac{x}{e_0} &= 2 \frac{k_2}{\sqrt{k_1e_0 \cdot k_{-1}}} \cdot \frac{k_1e_0 + k_{-1}}{k_1e_0} + \dots \end{aligned}$$

<sup>10</sup>The factor 2 could be replaced by any constant  $> 1$ .

Thus we obtain the parameter

$$\varepsilon_\infty = \frac{k_1 e_0 + k_{-1}}{k_1 e_0} \cdot \frac{2k_2}{\sqrt{k_1 e_0 \cdot k_{-1}}} = \frac{k_1 e_0 + k_{-1}}{k_1 e_0} \cdot \varepsilon_{PE}, \quad (38)$$

which provides an upper bound for the long-term discrepancy of the true solution and its approximation.

#### 4.4 A degenerate scenario

To illustrate the limitations of the approach via Proposition 2, consider the irreversible system with TFPV  $k_{-1} = k_2 = 0$ , the other parameters positive, and  $\rho = (0, 0, 0, k_{-1}^*, k_2^*)^{\text{tr}}$ . Here the critical variety is reducible, being the union of the lines  $Y_1, Y_2$  defined by  $e_0 - c = 0$  resp.  $s = 0$ , and the TFPV conditions fail at their intersection. We consider the case  $e_0 < s_0$ , and define  $\tilde{Y}_1$  by  $c = e_0, s > 0$ . The fast system admits the first integral  $s + c$ , so the initial value of the slow system on  $\tilde{Y}_1$  is close to  $(s_0 - e_0, e_0)^{\text{tr}}$ . Proceeding, one may choose

$$K = \{(s, c)^{\text{tr}}; s + c \leq s_0, s \geq \tilde{s}\}, \quad 0 < \tilde{s} < s_0 - e_0.$$

Then  $\tilde{Y}_1 \cap K$  is compact (but not positively invariant), and on this set one has

$$\sigma_1 = k_1 s, \quad \sigma_2 = 0, \quad \text{and} \quad \hat{\sigma}_2 = 0.$$

Here the nondegeneracy condition in (13) fails, and we obtain no timescale ratio by way of Lemma 4. A direct computation in a neighborhood of  $\tilde{Y}_1$  yields

$$\lambda_2/\lambda_1 = \varepsilon k_1 k_2^* (e_0 - c),$$

but this obscures the fact that both eigenvalues approach zero as  $s \rightarrow 0$ . Standard singular perturbation methods are not sufficient to analyze the dynamics of this system for small  $\varepsilon$ .

## 5 TFPV for higher dimensions

We keep the notation and conventions from subsections 2.1 and 2.4, but now we will focus on a TFPV  $\hat{\pi}$  for dimension  $s > 1$ . The goal of this technical section is to identify distinguished parameters and discuss their relation to timescales. There is a rather obvious direct extension of results from the  $s = 1$  case, but the timescale correspondence will be not as pronounced. Moreover, we will need to impose a stronger nondegeneracy condition. Abbreviate

$$\tilde{\sigma}_i(x, \varepsilon) := \sigma_i(x, \hat{\pi} + \varepsilon \rho), \quad 1 \leq i \leq n, \quad (39)$$

keeping in mind that  $\tilde{\sigma}_i(x, 0) > 0$  for all  $x \in \tilde{Y} \cap K$  and  $1 \leq i \leq n - s$ , due to  $\hat{\pi}$  being a TFPV. Additionally we set  $\tilde{\sigma}_0 := 1$ .

### 5.1 Distinguished small parameters

Some notions and results from Section 3 can easily be modified for the case  $s > 1$ . For suitable  $\varepsilon_{\max} > 0$  one has

$$\sigma_i(x, \hat{\pi} + \varepsilon \rho) > 0 \text{ for all } (x, \varepsilon) \in K^*, \quad 1 \leq i \leq n - s,$$

and due to  $\sigma_{n-s+1}(x, \hat{\pi}) = 0$  for  $x \in \tilde{Y} \cap K$  we have

$$\sigma_{n-s+1}(x, \hat{\pi} + \varepsilon \rho) = \varepsilon \hat{\sigma}_{n-s+1}(x, \hat{\pi}, \rho, \varepsilon)$$

with a polynomial  $\hat{\sigma}_{n-s+1}$ , for all  $(x, \varepsilon) \in K^*$ .

**Definition 3.** (i) Let

$$\begin{aligned} L(\hat{\pi}, \rho) &:= \inf_{x \in \tilde{Y} \cap K} \left| \frac{\hat{\sigma}_{n-s+1}(x, \hat{\pi}, \rho, 0)}{\sigma_1(x, \hat{\pi}) \cdot \sigma_{n-s}(x, \hat{\pi})} \right|, \\ U(\hat{\pi}, \rho) &:= \sup_{x \in \tilde{Y} \cap K} \left| \frac{\hat{\sigma}_{n-s+1}(x, \hat{\pi}, \rho, 0)}{\sigma_1(x, \hat{\pi}) \cdot \sigma_{n-s}(x, \hat{\pi})} \right|, \end{aligned} \quad (40)$$

(ii) We call

$$\varepsilon^*(\widehat{\pi}, \rho, \varepsilon) := \varepsilon U(\widehat{\pi}, \rho) \quad (41)$$

the *distinguished upper bound for the TFPV  $\widehat{\pi}$  for dimension  $s$ , with parameter direction  $\rho$* , of system (7). Moreover we call

$$\varepsilon_*(\widehat{\pi}, \rho, \varepsilon) := \varepsilon L(\widehat{\pi}, \rho) \quad (42)$$

the *distinguished lower bound for the TFPV  $\widehat{\pi}$  for dimension  $s$  with parameter direction  $\rho$* .

As in the case of reduction to dimension one, determining the distinguished parameters amounts to determining the extrema of a rational function on a compact set, or (when this is not possible, or not sensible) determining reasonably sharp estimates for these extrema. We note the following straightforward variant of Proposition 1.

**Proposition 5.** *Given  $\alpha > 0$ , for sufficiently small  $\varepsilon_{\max}$  the estimates*

$$\frac{\varepsilon}{(1+\alpha)} L(\widehat{\pi}, \rho) \leq \left| \frac{\sigma_{n-s+1}(x, \widehat{\pi} + \varepsilon\rho)}{\sigma_1(x, \widehat{\pi} + \varepsilon\rho) \cdot \sigma_{n-s}(x, \widehat{\pi} + \varepsilon\rho)} \right| \leq \varepsilon(1+\alpha) U(\widehat{\pi}, \rho) \quad (43)$$

hold on  $K^*$ .

## 5.2 The correspondence to timescales

Proofs of the following statements are given in the Appendix (Lemma 6 and Lemma 7).

- Let  $\widehat{\pi}$  be a TFPV for dimension  $s$ , with critical manifold  $\widetilde{Y}$ . Then for all  $x \in \widetilde{Y} \cap K$  one has

$$\widetilde{\sigma}_i(x, \varepsilon) = \varepsilon^{i-n+s} \widehat{\sigma}_i(x, \varepsilon) \text{ for all } x \in \widetilde{Y} \cap K, \quad n-s \leq i \leq n, \quad (44)$$

with polynomials  $\widehat{\sigma}_i$ .

- Assume that (44) is given, and furthermore assume the nondegeneracy condition:

$$\widehat{\sigma}_{n-s}(x, 0) \neq 0 \text{ and } \widehat{\sigma}_n(x, 0) \neq 0 \text{ on } \widetilde{Y} \cap K. \quad (45)$$

Then the zeros  $\lambda_i(x, \widehat{\pi} + \varepsilon\rho)$  of the characteristic polynomial can be labeled such that

$$\lambda_1(x, \widehat{\pi}) \neq 0, \dots, \lambda_{n-s}(x, \widehat{\pi}) \neq 0 \quad \text{on } \widetilde{Y} \cap K,$$

and

$$\lambda_i(x, \widehat{\pi} + \varepsilon\rho) = \varepsilon \widehat{\lambda}_i(x, \widehat{\pi}, \rho, \varepsilon), \quad n-s+1 \leq i \leq n$$

with continuous functions in  $\varepsilon$ .

Given the nondegeneracy assumptions, we turn to discussing the correspondence of  $\varepsilon_*$  and  $\varepsilon^*$  to timescales. By (11), and by the definition of  $\widetilde{\sigma}_i$  in (39), one has

$$\begin{aligned} -\widetilde{\sigma}_1 &= \lambda_1 + \dots + \lambda_{n-s} + \varepsilon(\dots); \\ (-1)^{n-s} \widetilde{\sigma}_{n-s} &= \sum \lambda_{j_1} \dots \lambda_{j_{n-s}} = \lambda_1 \dots \lambda_{n-s} + \varepsilon(\dots); \\ (-1)^{n-s+1} \widetilde{\sigma}_{n-s+1} &= \sum \lambda_{i_1} \dots \lambda_{i_{n-s+1}} \\ &= \lambda_1 \dots \lambda_{n-s} (\lambda_{n-s+1} + \dots + \lambda_n) + \varepsilon^2(\dots). \end{aligned}$$

This directly provides a result on separation of timescales.

**Proposition 6.** *Assume that the nondegeneracy condition (45) holds.*

(a) *The identity*

$$\frac{\widetilde{\sigma}_{n-s+1}}{\widetilde{\sigma}_1 \widetilde{\sigma}_{n-s}} = \frac{\lambda_{n-s+1} + \dots + \lambda_n}{\lambda_1 + \dots + \lambda_{n-s}} + \varepsilon^2(\dots) = \varepsilon \frac{\widehat{\lambda}_{n-s+1} + \dots + \widehat{\lambda}_n}{\lambda_1 + \dots + \lambda_{n-s}} + \varepsilon^2(\dots)$$

holds on  $K^*$ , with  $(\dots)$  representing a continuous function.

(b) Given  $\alpha > 0$ , and  $\varepsilon_{\max}$  sufficiently small, the estimates

$$\frac{1}{(1+\alpha)}\varepsilon_*(\widehat{\pi}, \rho, \varepsilon) \leq \left| \frac{\sum_{i \leq n-s} \lambda_i(x, \widehat{\pi} + \varepsilon\rho)}{\sum_{j > n-s} \lambda_j(x, \widehat{\pi} + \varepsilon\rho)} \right| \leq (1+\alpha)\varepsilon^*(\widehat{\pi}, \rho, \varepsilon) \quad (46)$$

hold for all  $(x, \varepsilon) \in K^*$ . In particular there exist constants  $C_1, C_2$  such that

$$C_1\varepsilon \leq \left| \frac{\sum_{i \leq n-s} \lambda_i(x, \widehat{\pi} + \varepsilon\rho)}{\sum_{j > n-s} \lambda_j(x, \widehat{\pi} + \varepsilon\rho)} \right| \leq C_2\varepsilon.$$

Thus, for higher dimensions of the critical manifold the coefficients of the characteristic polynomial still provide (albeit weaker) estimates for timescale ratios. Informally speaking,  $\tilde{\sigma}_{n-s+1}/(\tilde{\sigma}_1\tilde{\sigma}_{n-s})$  measures the ratio of the “fastest slow timescale” and the “fastest fast timescale”. Similar to the situation for  $s = 1$ , a more relevant ratio is the one of the “fastest slow timescale” and the “slowest fast timescale”; compare subsection 9.1 in the Appendix. We remark that for real or “essentially real”  $\lambda_1, \dots, \lambda_{n-s}$  one may obtain results similar to Proposition 3, but we will not pursue this further.

### 5.3 Further dimensionless parameters

Given the setting of (44) it is natural to ask about different types of dimensionless small parameters, in addition to the distinguished ones obtained from Proposition 5. We consider terms of the form

$$\frac{\tilde{\sigma}_{n-s+k}}{\tilde{\sigma}_{j_1} \cdots \tilde{\sigma}_{j_\ell} \cdot \tilde{\sigma}_{n-s+v_1} \cdots \tilde{\sigma}_{n-s+v_m}}$$

with  $k \geq 1$ ,  $\ell \geq 0$ ,  $m > 0$ , and the indices  $1 \leq j_1 \leq \dots \leq j_\ell$ ,  $1 \leq v_1 \leq \dots \leq v_m$  subject to the following conditions:

(1) “Dimensionless”: By Lemma 1 this means

$$j_1 + \dots + j_\ell + (n-s) + v_1 + \dots + (n-s) + v_m = (n-s) + k.$$

(2) “Order one in  $\varepsilon$ ”:

$$v_1 + \dots + v_m = k - 1.$$

**Proposition 7.** *The only classes of dimensionless small parameters that satisfy (1) and (2) are the following:*

(a)  $m = 1$  with  $\ell = 1$  and  $j_1 = 1$ ; with parameters

$$\frac{\tilde{\sigma}_{n-s+k}}{\tilde{\sigma}_1 \tilde{\sigma}_{n-s+k-1}}, \quad 2 \leq k \leq s. \quad (47)$$

(b)  $m = 2$ ,  $n \geq 4$ ,  $s = n - 1$  and  $\ell = 0$ ; with parameters

$$\frac{\tilde{\sigma}_{2+v_1+v_2}}{\tilde{\sigma}_{1+v_1} \tilde{\sigma}_{1+v_2}}, \quad 1 \leq v_1 \leq v_2, \quad v_1 + v_2 \leq n - 2. \quad (48)$$

*Proof.* Combining (1) and (2) one finds

$$j_1 + \dots + j_\ell + (m-1)(n-s) = 1,$$

thus necessarily  $m \leq 2$  due to  $s < n$ . In case  $m = 1$  one has  $\ell = 1$  and  $j_1 = 1$ ; in case  $m = 2$  one necessarily has  $s = n - 1$  and  $\ell = 0$ .  $\square$

To obtain explicit parameter bounds in the first case, use

$$\sigma_{n-s+j}(x, \widehat{\pi} + \varepsilon\rho) = \varepsilon^j \widehat{\sigma}_{n-s+j}(x, \widehat{\pi}, \rho, \varepsilon), \quad j \geq 1$$

to determine

$$\widetilde{L}_j(\widehat{\pi}, \rho) := \inf_{x \in \widetilde{Y} \cap K} \left| \frac{\widehat{\sigma}_{n-s+j}(x, \widehat{\pi}, \rho, 0)}{\widehat{\sigma}_{n-s+j-1}(x, \widehat{\pi}, \rho, 0) \sigma_1(x, \widehat{\pi})} \right|,$$

$$\widetilde{U}_j(\widehat{\pi}, \rho) := \sup_{x \in \widetilde{Y} \cap K} \left| \frac{\widehat{\sigma}_{n-s+j}(x, \widehat{\pi}, \rho, 0)}{\widehat{\sigma}_{n-s+j-1}(x, \widehat{\pi}, \rho, 0) \sigma_1(x, \widehat{\pi})} \right|,$$

and small parameters

$$\delta_{j*} := \varepsilon \cdot \widetilde{L}_j(\widehat{\pi}, \rho, 0), \quad \delta_j^* := \varepsilon \cdot \widetilde{U}_j(\widehat{\pi}, \rho, 0), \quad j \geq 2.$$

**Remark 5.** In the first case there is a notable correspondence to eigenvalues (thus to timescales). A variant of the argument in Proposition 6 shows that

$$\frac{\widetilde{\sigma}_{n-s+k}}{\widetilde{\sigma}_1 \widetilde{\sigma}_{n-s+k-1}} = \varepsilon \frac{\tau_k(\widehat{\lambda}_{n-s+1}, \dots, \widehat{\lambda}_n)}{(\lambda_1 + \dots + \lambda_{n-s}) \cdot \tau_{k-1}(\widehat{\lambda}_{n-s+1}, \dots, \widehat{\lambda}_n)} + \varepsilon^2(\dots),$$

where  $\tau_\ell$  denotes the  $\ell^{\text{th}}$  elementary symmetric polynomial in  $s$  variables.

## 5.4 Dimension three

We specialize the results to dimension three and  $s = 2$ , assuming nondegeneracy. By (44),  $\widetilde{\sigma}_2$  is of order  $\varepsilon$ , and  $\widetilde{\sigma}_3$  is of order  $\varepsilon^2$ .

- In view of Propositions 5 and 6 we consider

$$\frac{\widetilde{\sigma}_2}{\widetilde{\sigma}_1^2} = \varepsilon \frac{\widehat{\lambda}_2 + \widehat{\lambda}_3}{\lambda_1} + \varepsilon^2 \dots$$

Informally speaking, this expression governs the ratio of the fastest slow timescale to the fast timescale, which is the pertinent ratio according to the Appendix, subsection 9.1.2. We obtain

$$U = \sup_{x \in \widetilde{Y} \cap K} \left| \frac{\widehat{\sigma}_2(x, \widehat{\pi}, \rho, 0)}{\sigma_1(x, \widehat{\pi})^2} \right|, \quad \varepsilon^* = \varepsilon \cdot U$$

as well as

$$L = \inf_{x \in \widetilde{Y} \cap K} \left| \frac{\widehat{\sigma}_2(x, \widehat{\pi}, \rho, 0)}{\sigma_1(x, \widehat{\pi})^2} \right|, \quad \varepsilon_* = \varepsilon \cdot L.$$

- Similar to the observations in Remark 4, disparate slow eigenvalues may indicate a scenario with three timescales (informally speaking, fast, slow and very slow). To measure the disparity, we use Proposition 7 and consider

$$\frac{\widetilde{\sigma}_3}{\widetilde{\sigma}_1 \widetilde{\sigma}_2} = \varepsilon \frac{\lambda_1 \widehat{\lambda}_2 \widehat{\lambda}_3}{(\lambda_1 + \varepsilon \dots)(\lambda_1(\widehat{\lambda}_2 + \widehat{\lambda}_3) + \varepsilon \dots)} = \varepsilon \frac{\widehat{\lambda}_2 \widehat{\lambda}_3}{\lambda_1(\widehat{\lambda}_2 + \widehat{\lambda}_3)} + \varepsilon^2 \dots$$

Combining parameters shows

$$\frac{\widetilde{\sigma}_1 \widetilde{\sigma}_3}{\widetilde{\sigma}_2^2} = \frac{\widehat{\lambda}_2 \widehat{\lambda}_3}{(\widehat{\lambda}_2 + \widehat{\lambda}_3)^2} + \varepsilon \dots = \frac{\widehat{\lambda}_3 / \widehat{\lambda}_2}{(1 + \widehat{\lambda}_3 / \widehat{\lambda}_2)^2} + \varepsilon \dots$$

Thus the constants

$$\kappa^* := \sup_{x \in \widetilde{Y} \cap K} \frac{\sigma_1(x, \widehat{\pi}) \widehat{\sigma}_3(x, \widehat{\pi}, \rho, 0)}{\widehat{\sigma}_2(x, \widehat{\pi}, \rho, 0)^2} \quad \text{and} \quad \kappa_* := \inf_{x \in \widetilde{Y} \cap K} \frac{\sigma_1(x, \widehat{\pi}) \widehat{\sigma}_3(x, \widehat{\pi}, \rho, 0)}{\widehat{\sigma}_2(x, \widehat{\pi}, \rho, 0)^2}$$

measure the disparity of  $\widehat{\lambda}_2$  and  $\widehat{\lambda}_3$ . In particular, given that  $|\lambda_3| \leq |\lambda_2|$  one has

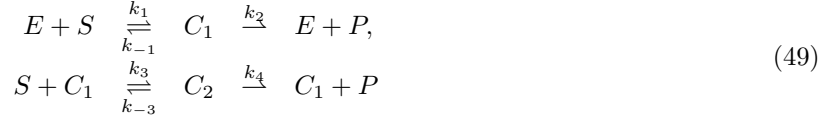
$$\left| \frac{\lambda_3}{\lambda_2} \right| \geq \kappa_* \quad \text{throughout } \widetilde{Y} \cap K.$$

## 6 Case studies: Reduction from dimension three to one

In this section we discuss two biochemically relevant modifications of the Michaelis–Menten reaction mechanism and a non-Michaelis–Menten reaction mechanism, with low enzyme concentration, and their familiar (quasi-steady state) reductions to dimension one. This seems to be the first instance that small parameters in the spirit of Segel and Slemrod – although consistently based on linear timescales – are derived for these reaction networks in a systematic manner. (In the application-oriented literature the perturbation parameter of choice mostly seems to be  $\varepsilon_{BH} = e_0/s_0$ , on loan from the Michaelis–Menten system.) We will directly consider the asymptotic small parameters  $\varepsilon^*$ ,  $\varepsilon_*$ ,  $\mu^*$  by application of the results in Section 3, and obtain rather satisfactory estimates for these. Considering the steps outlined in the Introduction, we thus complete a substantial part of step 1. Proceeding beyond this, along the lines of the Appendix, subsection 9.1, would involve considerable and lengthy work for each system, so we will not go further. However, to test and illustrate the efficacy of the parameters, we include extensive numerical simulations. We also include examples that demonstrate the limitations of the local timescale approach, and in particular show that the nondegeneracy conditions imposed on the “non-small” parameters are necessary.

### 6.1 Cooperativity

The (irreversible) cooperative reaction mechanism



is a non-Michaelis–Menten reaction mechanism of enzyme action, and is modelled by the mass action equations

$$\begin{aligned} \dot{s} &= -k_1(e_0 - c_1 - c_2)s + k_{-1}c_1 - k_3sc_1 + k_{-3}c_2, \\ \dot{c}_1 &= k_1(e_0 - c_1 - c_2)s - (k_{-1} + k_2)c_1 - k_3sc_1 + (k_4 + k_{-3})c_2, \\ \dot{c}_2 &= k_3sc_1 - (k_4 + k_{-3})c_2, \end{aligned} \quad (50)$$

via stoichiometric conservation laws. Typical initial conditions are  $s(0) = s_0$ ,  $e(0) = e_0$ , and  $c_1(0) = c_2(0) = p(0) = 0$ . The conservation laws yield the compact positively invariant set

$$K := \{(s, c_1, c_2) \in \mathbb{R}_{\geq 0}^3 : 0 \leq s \leq s_0, 0 \leq c_1 + c_2 \leq e_0^*\}, \quad (51)$$

with some reference value  $e_0^* > 0$ . The parameter space  $\Pi = \mathbb{R}_{\geq 0}^8$  has elements  $(e_0, s_0, k_1, k_{-1}, k_2, k_3, k_{-3}, k_4)^{\text{tr}}$ , and setting  $e_0 = 0$  defines a TFPV,

$$\hat{\pi} := (0, s_0, k_1, k_{-1}, k_2, k_3, k_{-3}, k_4)^{\text{tr}}$$

for dimension one, subject to certain nondegeneracy conditions on the  $k_i$ . The associated critical manifold is

$$\tilde{Y} := \{(s, c_1, c_2) \in \mathbb{R}_{\geq 0}^3 : c_1 = c_2 = 0\}. \quad (52)$$

We now set  $\rho = (e_0^*, 0, \dots, 0)^{\text{tr}}$ , and consider the perturbed system with parameter  $\pi = \hat{\pi} + \varepsilon\rho$ . The singular perturbation reduction (according to formula (9) in subsection 2.1) was carried out in Noethen and Walcher [31], Section 4 and Goeke and Walcher [19], Examples 8.2 and 8.7. This reduction agrees with the well known classical quasi-steady state reduction for complexes (see Keener and Sneyd [24], subsection 1.4.4). We have

$$\dot{s} = -\frac{k_1 e_0 s (k_3 k_4 s + k_2 (k_{-3} + k_4))}{(k_1 s + k_{-1} + k_2)(k_{-3} + k_4) + k_1 k_3 s^2}, \quad s(0) = s_0. \quad (53)$$

The quasi-steady state variety (see Keener and Sneyd [24]) is given parametrically by

$$\begin{pmatrix} c_1 \\ c_2 \end{pmatrix} = \frac{k_1 e_0 s}{(k_{-1} + k_2)(k_{-3} + k_4) + k_1(k_{-3} + k_4)s + k_1 k_3 s^2} \cdot \begin{pmatrix} k_{-3} + k_4 \\ k_3 s \end{pmatrix}, \quad 0 \leq s \leq s_0,$$

and agrees with the first order approximation of the slow manifold. Fenichel theory guarantees that (53) holds for sufficiently small  $e_0 = \varepsilon e_0^*$ , up to errors of order  $\varepsilon^2$ . The initial value for the reduced equation is generally chosen as  $s_0$ , and we adopt this choice here (refraining from a closer analysis of the approximation error).

### 6.1.1 Asymptotic small parameters

According to the first blanket assumption in subsection 2.4 we will assume that  $(s_0, k_1, k_{-1}, k_2, k_3, k_{-3}, k_4)^{\text{tr}}$  is contained in a compact subset of  $\mathbb{R}_{\geq 0}^7$ ; in particular  $s_0$  and all the  $k_i$  are bounded above by some positive constants. We now further specify this compact parameter set. On  $\tilde{Y} \cap K$ , with  $\pi = \hat{\pi}$  we have

$$\begin{aligned}\sigma_1 &= (k_1 + k_3)s + k_{-1} + k_2 + k_{-3} + k_4; \\ \sigma_2 &= k_1 k_3 s^2 + k_1(k_{-3} + k_4)s + (k_{-1} + k_2)(k_{-3} + k_4); \\ \hat{\sigma}_3 &= k_1 e_0^* \cdot (k_3 k_4 s + k_2(k_{-3} + k_4)).\end{aligned}$$

Due to the TFPV requirement,  $\sigma_1$  and  $\sigma_2$  must be bounded below on  $K \cap \tilde{Y}$  by positive constants,

$$\begin{aligned}k_{-1} + k_2 + k_{-3} + k_4 &= \min \sigma_1 > 0, \\ (k_{-1} + k_2)(k_{-3} + k_4) &= \min \sigma_2 > 0,\end{aligned}$$

and from this one sees that the TFPV conditions hold if and only if both  $k_{-1} + k_2$  and  $k_{-3} + k_4$  are bounded below by positive constants. Nontriviality of the reduced equation (53) also imposes conditions on  $k_1, k_2, k_3, k_4$ . Moreover, for instance, in the limit  $k_3 \rightarrow 0$ , with  $k_4$  bounded below by a positive constant, the reduced equation is nontrivial but approaches the Michaelis–Menten equation. We will take a closer look at this situation below.

Generally, the TFPV and nondegeneracy conditions will certainly hold whenever  $(s_0, k_1, k_{-1}, k_2, k_3, k_{-3}, k_4)^{\text{tr}}$  is contained in a compact subset of the open positive orthant.

Our aim is now to determine a suitable dimensionless parameter that corresponds to the legitimacy of (53). The typical requirement in the literature, that  $e_0/s_0 \ll 1$ , yields a sufficient asymptotic condition for bounded  $s_0$ , since singular perturbation theory guarantees convergence as  $e_0 \rightarrow 0$ , but no quantitative information can be inferred. In contrast, we use the results of Section 3 to provide a correspondence to linear timescales.

- The explicit calculation of  $\varepsilon^*$  according to Proposition 2, i.e. determining the maximum of

$$s \mapsto r(s) := \frac{\hat{\sigma}_3}{\sigma_1 \sigma_2}, \quad 0 \leq s \leq s_0 \quad (55)$$

involves the computation of the roots of the numerator of the derivative, thus of a parameter dependent cubic polynomial  $q$  in  $s$ . The signs of all the coefficients<sup>11</sup> are negative, except possibly the constant coefficient. By the Descartes rule of signs, the polynomial  $q$  has at most one positive zero. If there exists no positive zero, then  $r$  is strictly decreasing for  $0 \leq s < \infty$  and attains its maximum at  $s = 0$ ,<sup>12</sup> and in any case one has

$$\varepsilon^* \geq r(0) = \varepsilon_{MM} \cdot \frac{k_{-1} + k_2}{k_{-1} + k_2 + k_{-3} + k_4}.$$

If a positive zero  $s^*$  exists<sup>13</sup> then the maximum of  $r$  will be attained there. An exact calculation via Cardano does not provide any palatable information, but an upper bound for  $\varepsilon^*$  is obtained rather easily from the monotonicity of the  $\sigma_j$ :

$$\begin{aligned}\varepsilon^* &\leq \varepsilon \frac{\sup_{\tilde{Y} \cap K} \hat{\sigma}_3}{\inf_{\tilde{Y} \cap K} \sigma_1 \inf_{\tilde{Y} \cap K} \sigma_2} \\ &= \frac{k_1 e_0}{k_{-1} + k_2} \cdot \left( \frac{k_3 k_4 s_0 + k_2(k_{-3} + k_4)}{(k_{-1} + k_2 + k_{-3} + k_4)(k_{-3} + k_4)} \right) \\ &= \varepsilon_{MM} \cdot \left( \frac{k_3 k_4 s_0 (k_{-1} + k_2)}{k_2 (k_{-1} + k_2 + k_{-3} + k_4)(k_{-3} + k_4)} + \frac{k_{-1} + k_2}{k_{-1} + k_2 + k_{-3} + k_4} \right) =: \varepsilon_C.\end{aligned} \quad (56)$$

Comparing this to the lower estimate  $r(0)$ , one finds that the upper estimate by  $\varepsilon_C$  is acceptable as long as  $s_0$  is not too large, but weakens with increasing  $s_0$ . As noted in Section 3 above,  $\varepsilon^*$  (and by extension  $\varepsilon_C$ ) provides an estimate for the ratio of slowest to fastest timescale. Thus smallness of  $\varepsilon^*$  is a necessary condition, but it may not be sufficient when the fast timescales are far apart.

<sup>11</sup>It is unproblematic to determine these explicitly, but the expressions are unwieldy.

<sup>12</sup>Straightforward computation yields a condition on  $k_3$  that ensures the maximum of  $r$  being attained at  $s = 0$ .

<sup>13</sup>This case does occur.

- We therefore consider an estimate for the ratio of the slow timescale to the slower of the fast ones via  $\mu^*$ . It is straightforward to verify that  $\sigma_1^2 - 4\sigma_2 \geq 0$ , thus all eigenvalues are real, and Proposition 4(b) is applicable. The explicit calculation of  $\mu^*$  again involves a cubic polynomial in  $s$ , for  $0 \leq s \leq s_0$ . In this case the Descartes sign rule allows for two or no positive zeros, and there exist at most two local maxima for  $0 \leq s < \infty$ . One of these is located at  $s = 0$ , yielding in any case the lower estimate

$$\mu^* \geq \varepsilon_{MM} \cdot \frac{k_{-1} + k_2 + k_{-3} + k_4}{k_{-3} + k_4}, \quad (57)$$

but an explicit computation of the maximum provides little information. Instead, we again resort to an upper bound:

$$\begin{aligned} \mu^* &\leq \varepsilon \frac{\sup_{\tilde{Y} \cap K} \hat{\sigma}_3 \sup_{\tilde{Y} \cap K} \sigma_1}{\inf_{\tilde{Y} \cap K} \sigma_2^2} \\ &= \varepsilon_{MM} \cdot \left( \frac{k_3 k_4 s_0 + k_2(k_{-3} + k_4)}{k_2(k_{-3} + k_4)} \cdot \frac{(k_1 + k_3)s_0 + k_{-1} + k_2 + k_{-3} + k_4}{k_{-3} + k_4} \right) =: \mu_C. \end{aligned} \quad (58)$$

Comparison with (57) shows that the estimate by  $\mu_C$  is satisfactory as long as  $s_0$  is not too large, but it will become rather weak with increasing  $s_0$ .

All estimates involve the distinguished Michaelis–Menten parameter  $\varepsilon_{MM}$ , multiplied by some positive factor. For both estimates in (57), (58) this factor is  $> 1$ .

### 6.1.2 Numerical simulations

While we have obtained asymptotic timescale estimates for given reaction parameters, these estimates are unsatisfactory for large substrate concentrations. Moreover, by its nature our approach alone does not provide an upper estimate for the distance of the solution to the slow manifold. So, to obtain an a priori gauge of the efficacy of (53), it is natural to resort to numerical simulations. These simulations serve two purposes. On the positive side, they illustrate that the small parameters  $\varepsilon^*$  and  $\mu^*$  are good indicators for viability of the QSS reduction, in a wide parameter range. On the negative side, numerical examples highlight parameter combinations where consideration of  $\varepsilon^*$  and  $\mu^*$  is misleading. Such cases can be traced back to problems with the blanket assumptions from subsection 2.4, or with assumptions implicit in the proofs of Propositions 2 and 3.

We will consider some specific examples, and instead of relying on  $\varepsilon_C$  and  $\mu_C$  we will compute both  $\varepsilon^*$  and  $\mu^*$  numerically in the simulations that follow. (This is still far less computationally involved than working with eigenvalues of linearizations on  $\tilde{Y} \cap K$ .)

In the figures illustrating all the simulations, to show the behavior of trajectories over the interval  $0 \leq t < \infty$ , time is mapped to

$$\tau = t/T, \quad \tau \in [0, 1],$$

where the numerical solution has been computed on the interval  $[0, T]$ , and  $T$  is chosen large enough to ensure the numerical simulations capture the long-time dynamics of the reaction. We start with some examples that document the efficacy of the parameters in “normal” parameter domains.

1. In a first numerical study, we compare the numerical solution to the mass action equations (50) with the numerical solution to (53) in the scenario when all parameters except  $e_0$  are of the same order of magnitude. In the simulations, all parameter values except  $e_0$  are set equal to 1, and  $e_0$  is varied from  $10^0$ – $10^{-3}$ . The simulation results are reported in FIGURE 1, which reinforces the assertion that  $\varepsilon^* \ll 1$  and  $\mu^* \ll 1$  support the validity of (53); moreover one sees that smallness of  $\mu^*$  is the more relevant condition.
2. In a second numerical study, we examine a case with varied parameter values, but all (except  $e_0$ ) within the same order of magnitude. The results are reported in FIGURE 2, and once again support the claim that the accuracy of (53) improves as  $\varepsilon^* \rightarrow 0$  and  $\mu^* \rightarrow 0$ , with higher relevance for  $\mu^*$ .

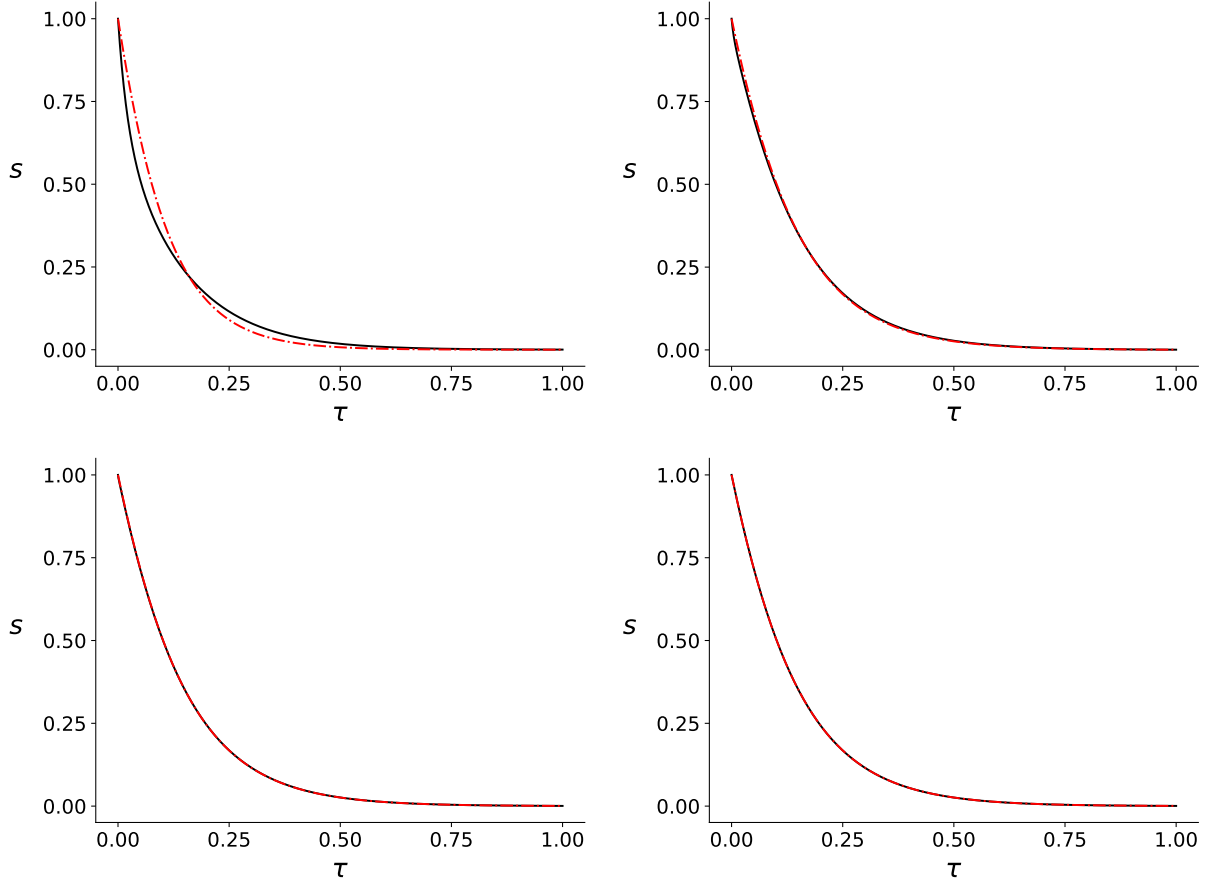


Figure 1: **Cooperativity: Numerical simulations indicate that the accuracy of (53) improves along the parameter ray direction as both  $\varepsilon^* \rightarrow 0$  and  $\mu^* \rightarrow 0$ .** In both panels, the parameters (in arbitrary units) are:  $s_0 = 1.0, k_1 = 1.0, k_2 = 1.0, k_{-1} = 1.0, k_3 = 1.0, k_{-3} = 1.0$  and  $k_4 = 1.0$ . Time has been mapped to the  $\tau$  scale:  $\tau = t/T, \tau \in [0, 1]$ . The solid black curve is the numerical solution to the mass action system (50); the broken red curve is the numerical solution to (53). TOP LEFT PANEL: Simulation performed with  $e_0 = 1.0$ . The numerically-computed dimensionless parameters are:  $\varepsilon^* = 1.25 \times 10^{-1}, \mu^* = 5 \times 10^{-1}$ , and there is visible error. TOP RIGHT PANEL: Simulation performed with  $e_0 = 10^{-1}$ . The numerically-computed dimensionless parameters are:  $\varepsilon^* = 1.25 \times 10^{-2}, \mu^* = 5 \times 10^{-2}$ . There is visible error, but the approximation (53) appears to improve. BOTTOM LEFT PANEL: Simulation performed with  $e_0 = 10^{-2}$ . The numerically-computed dimensionless parameters are:  $\varepsilon^* = 1.25 \times 10^{-3}, \mu^* = 5 \times 10^{-3}$ . The QSS reduction (53) is virtually indistinguishable from (50). BOTTOM RIGHT PANEL: Simulation performed with  $e_0 = 10^{-3}$ . The numerically-computed dimensionless parameters are:  $\varepsilon^* = 1.25 \times 10^{-4}, \mu^* = 5 \times 10^{-4}$ . The QSS reduction (53) is again virtually indistinguishable from (50).

3. As a third numerical example, we consider a combination of parameter values that are somewhat disparate in terms of the magnitudes. Nevertheless, we once again confirm that that the accuracy of (53) improves as  $\varepsilon^* \rightarrow 0$  and  $\mu^* \rightarrow 0$ , again with higher relevance for  $\mu^*$ ; see FIGURE 3. This simulation also debunks the commonly accepted notion that  $e_0/s_0 \ll 1$  is sufficient for the accuracy of (53).

Throughout these simulations we observe that the magnitude of  $\mu^*$  is more relevant for the quality of the QSS approximation than the magnitude of  $\varepsilon^*$ . This is in accordance with the results of subsection 3.2.

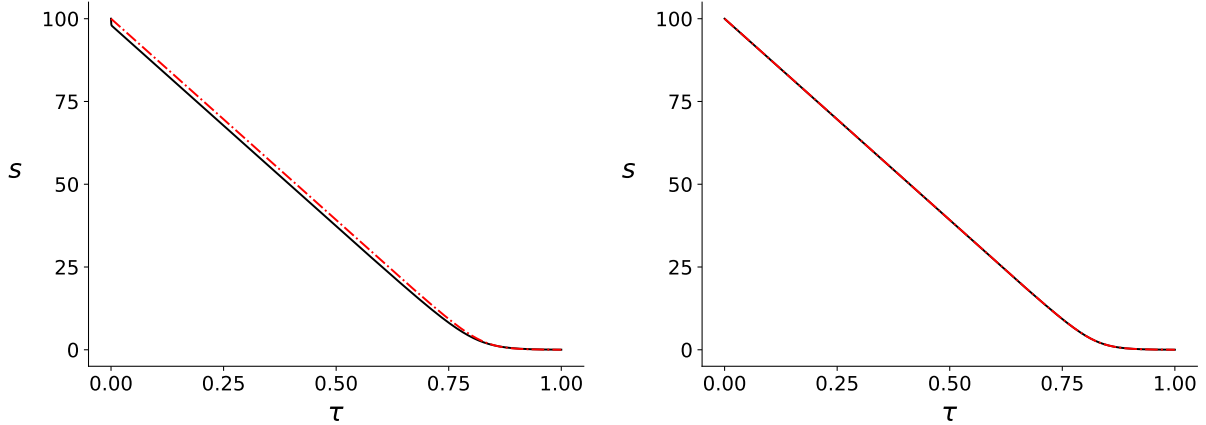


Figure 2: **Cooperativity: Numerically-computed  $\mu^*$  and  $\varepsilon^*$  give an a priori indication of the accuracy of (53).** In both panels, the parameters (in arbitrary units) are:  $s_0 = 10^2$ ,  $k_1 = 20$ ,  $k_2 = 50$ ,  $k_{-1} = 50$ ,  $k_3 = 10$ ,  $k_{-3} = 20$  and  $k_4 = 40$ . The solid black curve is the numerical solution to the mass action system (50); the broken red curve is the numerical solution to (53). Time has been mapped to the  $\tau$  scale:  $\tau = t/T$ ,  $\tau \in [0, 1]$ . LEFT PANEL:  $e_0 = 1.0$  and  $\varepsilon^* = 6.25 \times 10^{-2}$  but  $\mu^*$  is roughly  $2.67 \times 10^{-1}$  and the QSS approximation (53) is inaccurate. RIGHT PANEL:  $e_0 = 10^{-2}$ ,  $\varepsilon^*$  is numerically estimated to be  $6.25 \times 10^{-4}$  and  $\mu^*$  is numerically-estimated to be roughly  $2.67 \times 10^{-3}$ . In this simulation the validity of (53) clearly improves along the parameter ray  $\rho = (e_0^*, 0, \dots, 0)^{\text{tr}}$  as  $\mu^* \rightarrow 0$ . Thus,  $e_0$  must be small enough so that  $0 < \mu^* \ll 1$  (recall that  $\mu^* \ll 1$  implies  $\varepsilon^* \ll 1$ ). We see that  $\varepsilon^* \ll 1$  provides a too optimistic prediction, and that  $\mu^* \ll 1$  is a better indicator for the accuracy of the reduction (50).

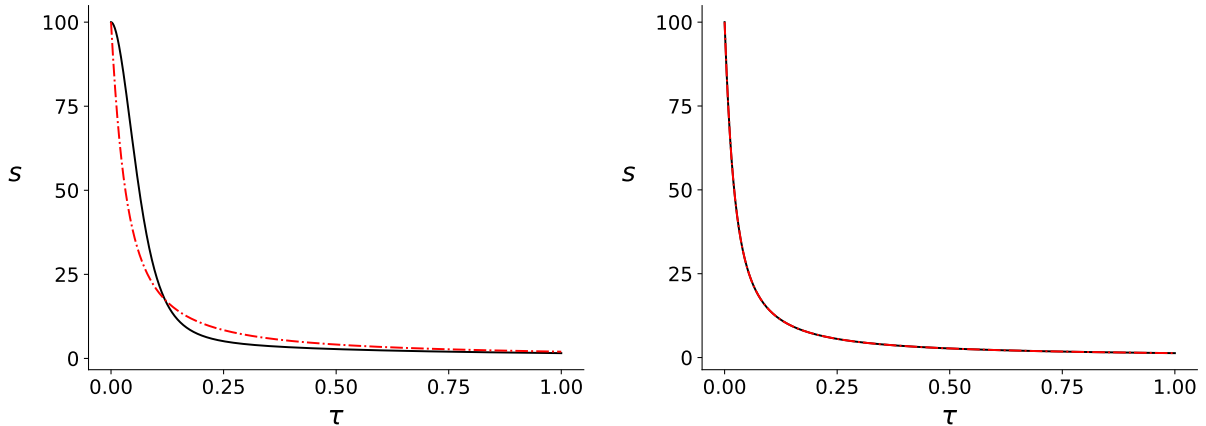


Figure 3: **Cooperativity: Numerically-computed  $\mu^*$  and  $\varepsilon^*$  give an a priori indication of the long-time accuracy of (53).** In both panels, the parameters (in arbitrary units) are:  $s_0 = 100$ ,  $k_1 = 1.0$ ,  $k_2 = k_{-1} = 10^2$ ,  $k_3 = 2 \times 10^3$ ,  $k_{-3} = k_4 = 10^5$ . The solid black curve is the numerical solution to the mass action system (50); the broken red curve is the numerical solution to (53). Time has been mapped to the  $\tau$  scale:  $\tau = t/T$ ,  $\tau \in [0, 1]$ . LEFT PANEL:  $e_0 = 1.0$  and  $\varepsilon^* \approx 6.5 \cdot 10^{-4}$  but  $\mu^*$  is roughly 1.0. RIGHT PANEL:  $e_0 = 10^{-3}$ ,  $\varepsilon^* \approx 6.5 \times 10^{-7}$  and  $\mu^* \approx 10^{-3}$ ; the reduction (53) is an excellent approximation to (50). Note that although  $e_0/s_0 \ll 1$  the reduction (53) is inaccurate: The failure in the left panel is immediate (and severe), despite the fact that  $e_0/s_0 = 10^{-2}$ .

### 6.1.3 Exceptional cases: Near-degeneracy and near-invariance

Here we briefly discuss two special scenarios with  $\mu^* \gg 1$ , but precede this by a word of caution: Obviously, whenever  $\mu^* > 1$  then the implicit assumptions in the proofs of Propositions 3 and 4 are violated for the given values of  $e_0$ , and the propositions are not applicable in this range. (To enable applicability,  $\varepsilon_{\max}$  would have to be adjusted to a smaller value.) However, the consideration of such extreme cases provides insight into the significance of various parameters.

The first case involves a near-degeneracy scenario: The critical variety contains a degenerate point and  $1 \ll \mu^*$ , while at first sight the QSS reduction (53) *appears* to be highly accurate. In the second case a two-dimensional nearly-invariant subspace emerges within phase space.

1. Consider the parameter point

$$\pi^\ddagger = (s_0, 0, k_1, 0, 0, k_3, k_{-3}, k_4)^{\text{tr}},$$

thus in addition to  $e_0 = 0$  one has  $k_{-1} = k_2 = 0$  (which is problematic in view of nondegeneracy conditions). The associated critical variety,  $Y$ , consists of two intersecting lines of equilibria (and is therefore not a manifold)<sup>14</sup>:

$$Y := \{(s, c_1, c_2) \in \mathbb{R}_{\geq 0}^3 : c_1 = c_2 = 0\} \cup \{(s, c_1, c_2) \in \mathbb{R}_{\geq 0}^3 : s = c_2 = 0\}.$$

The perturbation form of the mass action equations with  $e_0 = \varepsilon e_0^*$ ,  $k_2 = \varepsilon k_2^*$  and  $k_{-1} = \varepsilon k_{-1}^*$  is

$$\begin{pmatrix} \dot{s} \\ \dot{c}_1 \\ \dot{c}_2 \end{pmatrix} = \begin{pmatrix} (k_1 - k_3) & k_1 s + k_{-3} \\ -(k_1 + k_3) & -k_1 s + k_4 + k_{-3} \\ k_3 & -(k_{-3} + k_4) \end{pmatrix} \begin{pmatrix} s c_1 \\ c_2 \end{pmatrix} + \varepsilon \begin{pmatrix} k_1 e_0^* s + k_{-1}^* c_1 \\ k_1 e_0^* s - (k_{-1}^* + k_2^*) c_1 \\ 0 \end{pmatrix}. \quad (59)$$

In this case the rank of the Jacobian is not constant:

$$\begin{aligned} \text{rank } D_1 h(s, c_1, c_2, \pi^\ddagger) &= 1, \quad \text{if } (s_1, c_1, c_2) = (0, 0, 0); \\ \text{rank } D_1 h(s, c_1, c_2, \pi^\ddagger) &= 2, \quad \text{otherwise.} \end{aligned}$$

While the rank condition from subsection 2.1 fails<sup>15</sup> on  $Y$ , it is straightforward to verify that the compact submanifolds defined by

$$\begin{aligned} \tilde{Y}_1 &:= \{(s, c_1, c_2) \in K : c_1 = c_2 = 0 \text{ and } s \geq \theta_1\}, \quad 0 < \theta_1 < s_0, \\ \tilde{Y}_2 &:= \{(s, c_1, c_2) \in K : s = c_2 = 0 \text{ and } c_1 \geq \theta_2\}, \quad 0 < \theta_2 < e_0^*, \end{aligned}$$

are normally hyperbolic and attracting. Thus, for  $\pi$  sufficiently close to  $\pi^\ddagger$ , and for  $s_0 > 0$ , trajectories will rapidly approach the attracting branch  $\tilde{Y}_1$ . Projection of the perturbation onto the tangent space of  $\tilde{Y}_1$ , according to (9), yields

$$\begin{pmatrix} \dot{s} \\ \dot{c}_1 \\ \dot{c}_2 \end{pmatrix} = \varepsilon \begin{pmatrix} 1 & \frac{k_1(k_3 s + k_4 + k_{-3}) - k_3 k_4}{k_1(k_3 s + k_4 + k_{-3})} & \frac{(2k_3 s + k_4 + 2k_{-3})k_1 - k_3 k_4}{k_1(k_3 s + k_4 + k_{-3})} \\ 0 & 0 & 0 \\ 0 & 0 & 0 \end{pmatrix} \begin{pmatrix} -k_1 e_0^* s \\ k_1 e_0^* s \\ 0 \end{pmatrix}$$

and the corresponding reduction on  $\tilde{Y}_1$  is:

$$\dot{s} = -\frac{e_0 k_4 k_3 s}{k_{-3} + k_4 + k_3 s}. \quad (62)$$

Remarkably, one can recover (62) by setting  $k_{-1} = k_2 = 0$  in (53). Thus, equation (62) can be viewed as a special case of (53) in the limit of small  $k_2$  and  $k_{-1}$ . Moreover, numerical simulations seem to indicate that the reduction (53) is valid over the full time course, even when  $\mu^*$  is quite large; see FIG

<sup>14</sup>Recall a similar scenario for Michaelis–Menten in subsection 4.4.

<sup>15</sup>A dynamic transcritical bifurcation occurs at the point where the rank of  $D_1 h(x, \pi^\ddagger)$  is 1. See Krupa and Szmolyan [26] for a general discussion of such scenarios.

4, left panel. But this is illusory: Both (53) and (62) fail to approximate the depletion of  $s$  near the origin, as the right panel shows. Thus, near-degeneracy scenarios can generate conditions in which (53) may appear to yield an excellent approximation. But recall that small  $\varepsilon^*$  combined with large  $\mu^*$  indicates that two eigenvalues are small, and this necessarily prohibits the reduction from being valid over the complete time course.

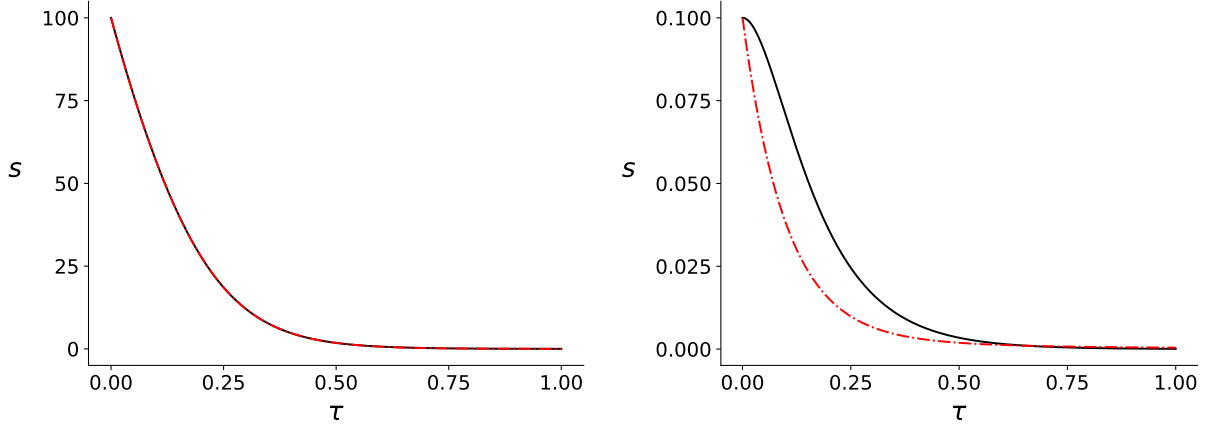


Figure 4: **Cooperativity: Numerically-computed  $\mu^*$  and  $\varepsilon^*$  give an a priori indication of the long-time accuracy of (53).** In both panels, the parameters (in arbitrary units) are:  $e_0 = 10^{-5}$ ,  $k_1 = 1.0$ ,  $k_2 = k_{-1} = 10^{-3}$ ,  $k_3 = 10^4$ ,  $k_{-3} = 10^2$  and  $k_4 = 10^6$ . The solid black curve is the numerical solution to the mass action system (50); the broken red curve is the numerical solution to (53). Time has been mapped to the  $\tau$  scale:  $\tau = t/T$ ,  $\tau \in [0, 1]$ . LEFT PANEL:  $s_0 = 100$  and  $\varepsilon^* \approx 10^{-8}$  but numerically-computed  $\mu^*$  is roughly  $10^1$ . Nevertheless, the QSS reduction (53) appears to be very good. However, the reduction fails near the origin, which is not captured in the LEFT PANEL due to limited resolution. RIGHT PANEL:  $s_0 = 10^{-1}$ , and the reduction (53) clearly fails to approximate the timecourse of  $s$ . This example illustrates that  $\mu^* \ll 1$  is necessary for the long-time validity of (53).

There are other degenerate scenarios for this reaction (for instance,  $k_{-3} = k_4 = 0$  or  $k_{-3} = k_4 = k_2 = k_{-1} = 0$  with all other parameters bounded below by a positive constant). We will not further investigate these.

2. In the final numerical example of this case study, we exhibit a scenario for which (53) provides a valid approximation even though  $1 \ll \mu^*$ . This can happen, for instance, in the limit of small  $e_0$  and small  $k_3$ : For  $k_3 = 0$  the two-dimensional subspace  $V := \{(s, c_1, c_2) \in \mathbb{R}^3 : c_2 = 0\}$  is invariant. One approach to such a scenario is to consider a singular perturbation reduction with both  $e_0 = \varepsilon e_0^*$ ,  $k_3 = \varepsilon k_3^*$  of order  $\varepsilon$ . The perturbation form of the mass action system is

$$\begin{pmatrix} \dot{s} \\ \dot{c}_1 \\ \dot{c}_2 \end{pmatrix} = \begin{pmatrix} k_1 s + k_{-1} & k_1 s + k_{-3} \\ -k_1 s - (k_{-1} + k_2) & k_1 s + (k_{-3} + k_4) \\ 0 & -(k_{-3} + k_4) \end{pmatrix} \begin{pmatrix} c_1 \\ c_2 \end{pmatrix} + \varepsilon \begin{pmatrix} -k_1 e_0^* s - k_3^* c_1 s \\ k_1 e_0^* s - k_3^* c_1 s \\ k_3^* c_1 s \end{pmatrix}, \quad (63)$$

with the critical manifold given by  $c_1 = c_2 = 0$ . Projection onto the critical manifold according to (9) yields

$$\begin{pmatrix} \dot{s} \\ \dot{c}_1 \\ \dot{c}_2 \end{pmatrix} = \varepsilon \begin{pmatrix} 1 & \frac{k_1 s + k_{-1}}{k_1 s + k_{-1} + k_2} & \frac{k_1 s(k_2 + k_4) + k_4 k_{-1} - k_2 k_{-3}}{(k_1 s + k_{-1} + k_2)(k_{-3} + k_4)} \\ 0 & 0 & 0 \\ 0 & 0 & 0 \end{pmatrix} \begin{pmatrix} -k_1 e_0^* s \\ k_1 e_0^* s \\ 0 \end{pmatrix},$$

and thus the QSS reduction

$$\dot{s} = -\frac{k_1 k_2 e_0 s}{k_1 s + k_{-1} + k_2},$$

which corresponds to the sQSSA of the Michaelis–Menten system.

One may regard this also from a different perspective: For fixed  $k_3$  one obtains the reduction (53); then letting  $k_3 \rightarrow 0$  yields the Michaelis–Menten equation. Notably, the lower estimate (57) for  $\mu^*$  is independent of  $k_3$ , and thus large  $\mu^*$  will remain large as  $k_3 \rightarrow 0$ . On the other hand, the upper estimate for  $\varepsilon^*$  decreases as  $k_3 \rightarrow 0$ . We recover the Michaelis–Menten rate law because a slight perturbation to  $k_3 = 0$  results in  $V$  being *nearly* invariant (see e.g. Goeke et al. [22] for the notion). Biochemically, near invariance of  $V$  is equivalent to gradually “turning off” the cooperative mechanism, since the secondary complex  $C_2$  is being produced at a very small rate. Mathematically, the near invariance of  $V$  implies for the given initial values, thus  $c_2(0) = 0$ , that the relevant dynamics are essentially two-dimensional even prior to reduction, and further reduction to a one-dimensional manifold depends only on a single eigenvalue ratio. In the simulation example, the fast eigenvalue with smaller absolute value – which generally is responsible for the slow-fast separation – has negligible influence, since the dynamics evolves on an invariant manifold very near  $c_2 = 0$ . Consequently  $\varepsilon^*$  (or indeed  $\varepsilon_{MM}$ ) is the relevant quantity rather than  $\mu^*$ ; see FIGURE 5.

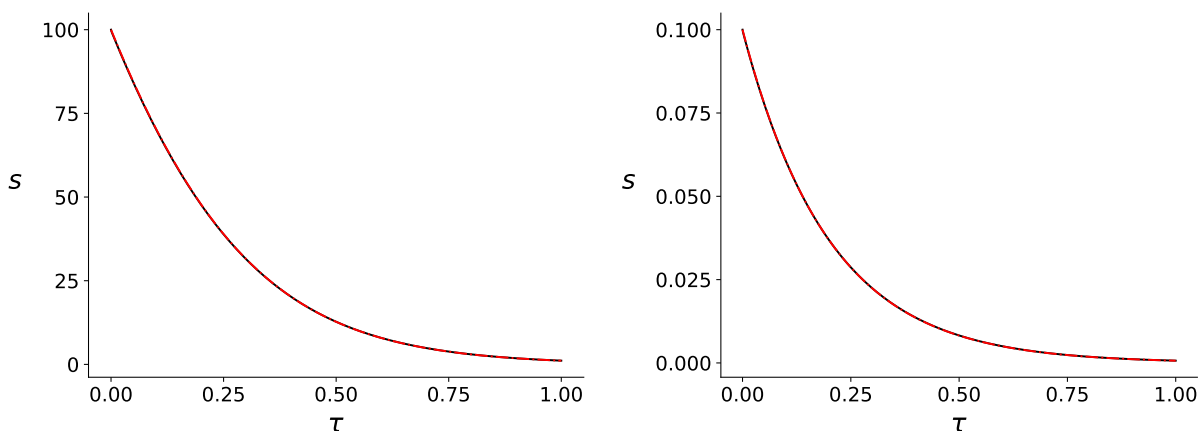
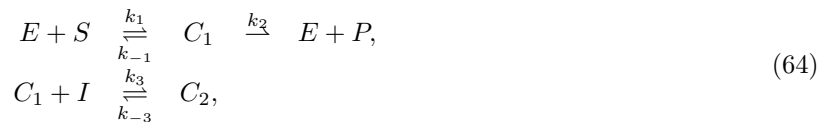


Figure 5: **Cooperative system with nearly invariant subspace: When the three-dimensional dynamics is nearly two-dimensional,  $\varepsilon^*$  provides a good a priori measure for the accuracy of (53).** In both panels the solid black curve is the numerical solution to the mass action equations (50); the broken red curve is the numerical solution to the QSS reduction (53). Time has been mapped to the  $\tau$  scale:  $\tau = t/T$ ,  $\tau \in [0, 1]$ , and the parameters (in arbitrary units) are:  $e_0 = 1.0$ ,  $k_1 = 1.0$ ,  $k_2 = k_{-1} = 10^2$ ,  $k_3 = 10^{-5}$ ,  $k_{-3} = 10^{-1}$  and  $k_4 = 10^{-1}$ . LEFT PANEL:  $s_0 = 100$  and  $\varepsilon^* \approx 2.5 \times 10^{-3}$  but the numerically-computed  $\mu^*$  is roughly 2.5. Nevertheless, the QSS reduction (53) is very accurate. By near-invariance of  $V$ , (53) effectively reduces to the Michaelis–Menten equation, and the pertinent dynamics unfold in the two-dimensional subspace  $V$ . RIGHT PANEL:  $s_0 = 10^{-1}$ , and we have confirmation that the long-time accuracy of the reduction (53) holds, even though  $\mu^* \approx 2.5$  remains of order unity.

## 6.2 Uncompetitive Inhibition

The irreversible Michaelis–Menten reaction mechanism in the presence of an uncompetitive inhibitor



is modelled deterministically by the system

$$\begin{aligned}
 \dot{s} &= -k_1(e_0 - c_1 - c_2)s + k_{-1}c_1, \\
 \dot{c}_1 &= k_1(e_0 - c_1 - c_2)s - (k_{-1} + k_2)c_1 - k_3(i_0 - c_2)c_1 + k_{-3}c_2, \\
 \dot{c}_2 &= k_3(i_0 - c_2)c_1 - k_{-3}c_2,
 \end{aligned} \tag{65}$$

via stoichiometric conservation laws. The standard initial conditions are  $(s, c_1, c_2)(0) = (s_0, 0, 0)$ . We fix a reference value  $e_0^*$  and obtain from the conservation laws the compact positively invariant set

$$K := \{(s, c_1, c_2) \in \mathbb{R}_{\geq 0}^3 : 0 \leq s \leq s_0, \quad c_1 + c_2 \leq e_0^*, \quad c_2 \leq \min\{e_0^*, i_0\}\}.$$

The parameter space  $\Pi = \mathbb{R}_{\geq 0}^8$  has elements  $\pi = (e_0, s_0, k_1, k_{-1}, k_2, k_3, k_{-3}, i_0)^{\text{tr}}$ . Given suitable nondegeneracy conditions on the parameters (to be specified below), setting  $e_0 = 0$  defines a TFPV for dimension one:

$$\hat{\pi} := (0, s_0, k_1, k_{-1}, k_2, k_3, k_{-3}, i_0)^{\text{tr}},$$

with associated critical manifold

$$\tilde{Y} := \{(s, c_1, c_2) \in \mathbb{R}_{\geq 0}^3 : c_1 = c_2 = 0\}.$$

We set  $\rho = (e_0^*, 0, \dots, 0)^{\text{tr}}$  and consider the ray  $\varepsilon \mapsto \hat{\pi} + \varepsilon\rho$  in parameter space. Then the perturbed system has the form

$$\begin{pmatrix} \dot{s} \\ \dot{c}_1 \\ \dot{c}_2 \end{pmatrix} = \begin{pmatrix} k_1 s + k_{-1} & k_1 s \\ -k_1 s - (k_{-1} + k_2) - k_3(i_0 - c_2) & -k_1 s + k_{-3} \\ k_3(i_0 - c_2) & -k_{-3} \end{pmatrix} \begin{pmatrix} c_1 \\ c_2 \end{pmatrix} + \varepsilon \begin{pmatrix} -k_1 e_0^* s \\ k_1 e_0^* s \\ 0 \end{pmatrix}. \quad (66)$$

According to (9), the singular perturbation reduction of (66) is given by

$$\begin{pmatrix} \dot{s} \\ \dot{c}_1 \\ \dot{c}_2 \end{pmatrix} = \varepsilon \begin{pmatrix} 1 & \frac{(k_1 s + k_{-1})k_{-3} + i_0 k_1 k_3 s}{(k_1 s + k_2 + k_{-1})k_{-3} + i_0 k_1 k_3 s} & \frac{(k_1 s + k_{-1})k_{-3} + (i_0 k_3 + k_2)k_1 s}{(k_1 s + k_2 + k_{-1})k_{-3} + i_0 k_1 k_3 s} \\ 0 & 0 & 0 \\ 0 & 0 & 0 \end{pmatrix} \begin{pmatrix} -k_1 e_0^* s \\ k_1 e_0^* s \\ 0 \end{pmatrix}, \quad (67)$$

thus  $\dot{c}_1 = \dot{c}_2 = 0$  and

$$\dot{s} = -\frac{k_1 e_0 k_2 k_{-3} s}{(k_1 s + k_2 + k_{-1})k_{-3} + i_0 k_1 k_3 s}, \quad s(0) = s_0, \quad (68)$$

in the limiting case of small  $e_0 = \varepsilon e_0^*$ , up to errors of order  $\varepsilon^2$ .

(The reduced equation (68) is different from the classical QSS reduction, which is obtained by substituting exact equations for the  $c_1$ - and  $c_2$ -nullclines into (65). But, in accordance with Goeke et al. [22], Proposition 5, the difference between the classical reduction and (68) will be of order  $\varepsilon^2$ . Typically, in numerical simulations there will only be noticeable differences between the classical reduction and the Fenichel reduction at very large substrate concentrations.)

### 6.2.1 Asymptotic small parameters

On  $\tilde{Y} \cap K$  we have at  $\pi = \hat{\pi}$ :

$$\begin{aligned} \sigma_1 &= k_1 s + k_{-1} + k_2 + k_3 i_0 + k_{-3}, \\ \sigma_2 &= k_1 s (k_3 i_0 + k_{-3}) + (k_{-1} + k_2) k_{-3}, \\ \hat{\sigma}_3 &= k_2 k_1 e_0^* k_{-3}. \end{aligned}$$

As always, we assume that all the parameters are contained in a suitable compact subset of parameter space, in particular they are bounded above by positive constants. The TFPV property requires, in addition, that  $\sigma_1$  and  $\sigma_2$  are bounded below on  $K \cap \tilde{Y}$  by positive constants, thus

$$\begin{aligned} k_3 i_0 + k_{-3} + k_{-1} + k_2 &= \min \sigma_1 > 0, \\ (k_{-1} + k_2) k_{-3} &= \min \sigma_2 > 0, \end{aligned}$$

and therefore the TFPV conditions hold if and only if both  $k_{-1} + k_2$  and  $k_{-3}$  are bounded below by positive constants. Moreover the reduction (68) should be significantly different from a trivial equation, hence one also requires  $k_2$  to be bounded below by some positive constant. No lower bound for  $k_3 i_0$  is imposed by the TFPV conditions, but note that (68) approaches the Michaelis–Menten equation as  $i_0 \rightarrow 0$  or  $k_3 \rightarrow 0$ . We will discuss this scenario below.

As before, we will obtain usable estimates for the timescale ratio from Propositions 2, 3 and 4. For uncompetitive inhibition the maxima can be determined explicitly.

- The distinguished small parameter  $\varepsilon^*$ , with  $\sigma_1, \sigma_2$  and  $\widehat{\sigma}_3$  evaluated at  $\pi = \widehat{\pi}$ , may be determined from

$$\begin{aligned}
\varepsilon^* &= \varepsilon \max_{0 \leq s \leq s_0} \frac{\widehat{\sigma}_3(s, \widehat{\pi}, \rho, 0)}{\sigma_1(s, \widehat{\pi})\sigma_2(s, \widehat{\pi})} \\
&= \varepsilon \frac{\widehat{\sigma}_3(0, \widehat{\pi}, \rho, 0)}{\sigma_1(0, \widehat{\pi})\sigma_2(0, \widehat{\pi})} \\
&= \frac{k_2 k_1 e_0}{(k_{-1} + k_2)^2} \cdot \frac{k_{-1} + k_2}{k_3 i_0 + k_{-3} + k_{-1} + k_2} \\
&= \varepsilon_{MM} \cdot \frac{k_{-1} + k_2}{k_3 i_0 + k_{-3} + k_{-1} + k_2} =: \varepsilon_U,
\end{aligned} \tag{69}$$

with the distinguished parameter  $\varepsilon_{MM}$  from the Michaelis–Menten system. (To see why the first equality sign in (69) holds, determine the derivative and verify that it is negative for  $s \geq 0$ .)

- It is straightforward to verify that all eigenvalues are real, since  $\sigma_1^2 - 4\sigma_2 \geq 0$ . Thus from  $\sigma_1, \sigma_2$  and  $\widehat{\sigma}_3$  evaluated at  $\widehat{\pi}$ , the parameter  $\mu^*$  is obtained from

$$\begin{aligned}
\mu^* &= \varepsilon \max_{0 \leq s \leq s_0} \frac{\widehat{\sigma}_3(s, \widehat{\pi}, \rho, 0)\sigma_1(s, \widehat{\pi})}{\sigma_2(s, \widehat{\pi})^2} \\
&= \frac{k_2 k_1 e_0}{(k_{-1} + k_2)^2} \cdot \left( \frac{k_3 i_0 + k_2 + k_{-1} + k_{-3}}{k_{-3}} \right) \\
&= \varepsilon_{MM} \cdot \left( \frac{k_3 i_0 + k_2 + k_{-1} + k_{-3}}{k_{-3}} \right) =: \mu_U.
\end{aligned} \tag{70}$$

(The first equality holds because the derivative of  $s \mapsto \frac{\widehat{\sigma}_3(s, \widehat{\pi}, \rho, 0)\sigma_1(s, \widehat{\pi})}{\sigma_2(s, \widehat{\pi})^2}$  is negative for all  $s \geq 0$ .)

### 6.2.2 Numerical simulations

We turn to numerical simulations, with the same dual motivation as in subsection 6.1. Parallel to our analysis of (56) and (58), we discuss the reliability of the qualifiers  $\varepsilon_U \ll 1$  and  $\mu_U \ll 1$  in gauging the validity of (68).

1. We begin with the special case  $\pi = (e_0, 1, 1, 1, 1, 1, 1)$ , representing a scenario where all parameters except  $e_0$  are of the same order 1, and vary  $e_0$  from 1 to  $10^{-3}$ . The results are reported in FIGURE 6, and collectively support the statement that (68) holds when  $\mu_U$  is sufficiently less than 1. With all “non-small” parameters having the same order, one also sees that sufficiently small  $\varepsilon_U$  suffices.
2. Parallel to our analysis of the cooperative reaction, we next consider parameters with widely disparate magnitude. In this simulation the accuracy of (68) improves only as  $\mu_U \rightarrow 0$ , and this illustrates the relevance of  $\mu_U$  as the dimensionless parameter that indicates the accuracy of (68); see FIGURE 7.

### 6.2.3 Near-invariance

As in the case of the cooperative reaction, near-invariance scenarios also exist for uncompetitive inhibition: Setting  $e_0 = i_0 = 0$  (also) yields a TFPV for dimension one, viz.

$$\widehat{\pi} := (0, s_0, k_1, k_{-1}, k_2, k_3, k_{-3}, 0)^{\text{tr}},$$

with the same associated critical manifold  $\widetilde{Y}$ , defined by  $c_1 = c_2 = 0$ . We fix a further reference value  $i_0^*$  and consider the ray direction  $\rho^\dagger = (e_0^*, 0, \dots, 0, i_0^*)^{\text{tr}}$ . Then the perturbed system with  $\pi = \widehat{\pi} + \varepsilon \rho^\dagger$  has the form

$$\begin{pmatrix} \dot{s} \\ \dot{c}_1 \\ \dot{c}_2 \end{pmatrix} = \begin{pmatrix} k_1 s + k_{-1} & k_1 s \\ -k_1 s - (k_{-1} + k_2) + k_3 c_2 & -k_1 s + k_{-3} \\ -k_3 c_2 & k_{-3} \end{pmatrix} \begin{pmatrix} c_1 \\ c_2 \end{pmatrix} + \varepsilon \begin{pmatrix} -k_1 e_0^* s \\ k_1 e_0^* s - k_3 i_0^* c_1 \\ k_3 i_0^* c_1 \end{pmatrix} \tag{71}$$

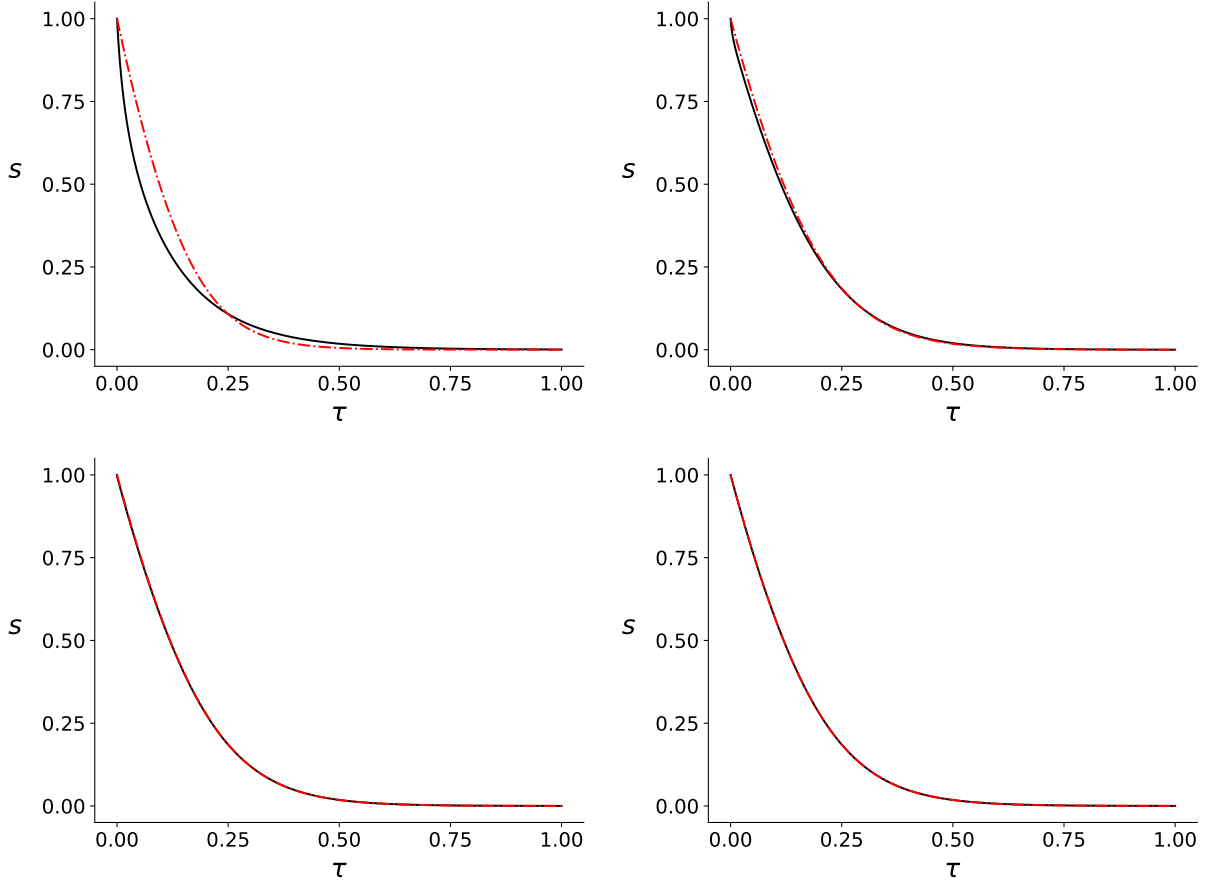


Figure 6: **Uncompetitive inhibition: Numerical simulations indicate that the accuracy of (68) improves as both  $\varepsilon_U \rightarrow 0$  and  $\mu_U \rightarrow 0$  along the parameter ray direction.** In both panels, the parameters (in arbitrary units) are:  $s_0 = 1.0$ ,  $k_1 = 1.0$ ,  $k_2 = 1.0$ ,  $k_{-1} = 1.0$ ,  $k_3 = 1.0$ ,  $k_{-3} = 1.0$  and  $i_0 = 1.0$ . The solid black curve is the numerical solution for  $s$  to the mass action system (65); the broken red curve is the numerical solution to (68). Time has been mapped to the  $\tau$  scale:  $\tau = t/T$ ,  $\tau \in [0, 1]$ . TOP LEFT PANEL: Simulation performed with  $e_0 = 1.0$ . There is visible error with  $\varepsilon_U = 1.25 \times 10^{-1}$  and  $\mu_U = 1.0$ . TOP RIGHT PANEL: Simulation performed with  $e_0 = 10^{-1}$ . Although there is visible error with  $\mu_U = 10^{-1}$  and  $\varepsilon_U = 1.25 \times 10^{-2}$ , the approximation (68) does appear to be improving along the parameter ray direction. BOTTOM LEFT PANEL: Simulation performed with  $e_0 = 10^{-2}$  and thus  $\mu_U = 10^{-2}$  and  $\varepsilon_U = 1.25 \times 10^{-3}$ . The QSS reduction (68) is nearly indistinguishable from (65). BOTTOM RIGHT PANEL: Simulation performed with  $e_0 = 10^{-3}$  with  $\mu_U = 10^{-3}$  and  $\varepsilon_U = 1.25 \times 10^{-4}$ . The QSS reduction (68) is again practically indistinguishable from (65). Note that  $\mu_U \ll 1$  is still a better indicator of accuracy than  $\varepsilon_U \ll 1$ .

Applying the reduction according to (9) yields

$$\begin{pmatrix} \dot{s} \\ \dot{c}_1 \\ \dot{c}_2 \end{pmatrix} = \varepsilon \begin{pmatrix} 1 & \frac{k_1 s + k_{-1}}{k_1 s + k_{-1} + k_2} & \frac{(k_1 s + k_{-1})k_{-3} + k_1 k_2 s}{k_{-3}(k_1 s + k_{-1} + k_2)} \\ 0 & 0 & 0 \\ 0 & 0 & 0 \end{pmatrix} \begin{pmatrix} -k_1 e_0^* s \\ k_1 e_0^* s \\ 0 \end{pmatrix}$$

and thus, with  $\dot{c}_1 = \dot{c}_2 = 0$ ,

$$\dot{s} = -\frac{k_1 e_0 k_2 s}{k_1 s + k_2 + k_{-1}}, \quad s(0) = s_0, \quad (72)$$

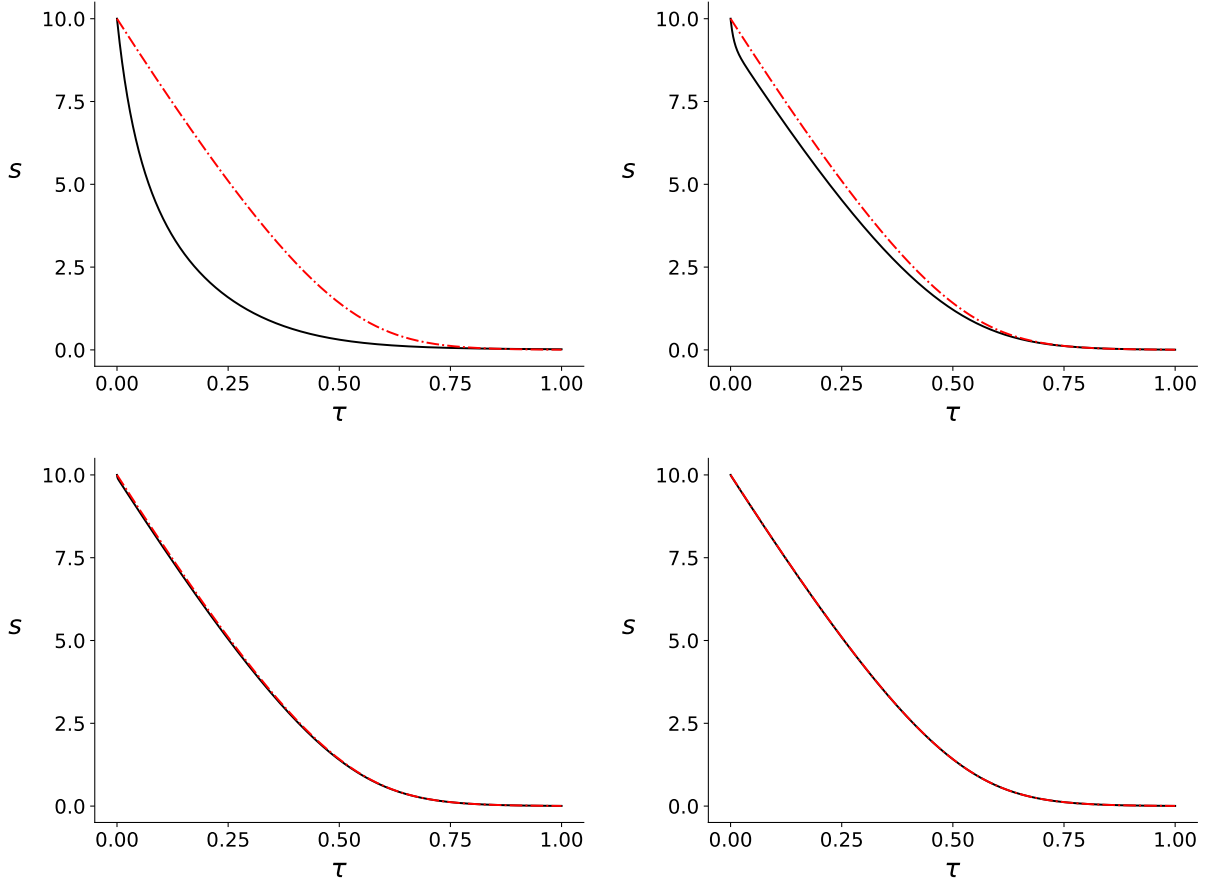


Figure 7: **Uncompetitive inhibition: The accuracy of (68) is reflected in the magnitude of the dimensionless parameter  $\mu_U$ .** The solid black curve is the numerical solution for  $s$  to (65); the broken red curve is the numerical solution to (68). Time has been mapped to the  $\tau$  scale:  $\tau = t/T$ ,  $\tau \in [0, 1]$ . The parameters (in arbitrary units) are:  $s_0 = 10^1$ ,  $k_{-3} = 10^{-1}$ ,  $k_3 = 10^1$ ,  $i_0 = 10^1$ ,  $k_1 = 1.0$ ,  $k_2 = k_{-1} = 10^3$ . TOP LEFT PANEL:  $e_0 = 1.0$  and  $\varepsilon_U \approx 2.38 \times 10^{-4}$ ,  $\mu_U \approx 5.25$ . TOP RIGHT PANEL:  $e_0 = 10^{-1}$  and  $\varepsilon_U \approx 2.38 \times 10^{-5}$ ,  $\mu_U \approx 5.25 \times 10^{-1}$ . BOTTOM LEFT PANEL:  $e_0 = 10^{-2}$  and  $\varepsilon_U \approx 2.38 \times 10^{-6}$ ,  $\mu_U \approx 5.25 \times 10^{-2}$ . BOTTOM RIGHT PANEL:  $e_0 = 10^{-3}$  and  $\varepsilon_U = 2.38 \times 10^{-7}$ ,  $\mu_U \approx 5.25 \times 10^{-3}$ . Note that the solutions to (65) and (68) are virtually indistinguishable in the last panel.

which is valid asymptotically as  $\varepsilon \rightarrow 0$ . Here one recovers the familiar Michaelis–Menten equation in the limit when the concentrations of both enzyme and inhibitor approach zero of order  $\varepsilon$ . (The same reduction is obtained for  $k_3 = \varepsilon k_3^*$  and  $e_0 = \varepsilon e_0^*$ .)

From a different perspective, when the term  $k_3 i_0$  vanishes, the subspace  $W := \{(s, c_1, c_2) \in \mathbb{R}^3 : c_2 = 0\}$  is invariant, and a slight perturbation (not necessarily of order  $\varepsilon$ ) results in the near-invariance of  $W$ . Considering the expressions (69) and (70) for  $\varepsilon^*$  and  $\mu^*$ , respectively, one sees that  $k_3 i_0 \rightarrow 0$  has no strong effect on these parameters, and that  $\varepsilon_{MM}$  is a good upper estimate for  $\varepsilon_U$ . One may rewrite (68) as

$$\dot{s} = -\frac{k_1 e_0 k_2 s}{k_1 s (1 + k_3 i_0 / k_{-3}) + k_{-1} + k_2}, \quad (73)$$

thus when  $k_3 i_0 / k_{-3} \ll 1$ , then the standard Michaelis–Menten reduction is approximately valid. In this case, the dynamics are effectively two-dimensional. Hence (for the given initial values) the magnitude of  $\mu_U$  is irrelevant, and (68) will hold even if  $1 < k_1 e_0 / k_{-3}$  and  $1 < \mu_U$ <sup>16</sup> since  $\varepsilon_{MM} \ll 1$  automatically ensures

<sup>16</sup>The implicit assumptions in the proof of Proposition 3 are then not satisfied.

the validity of (68) when  $W$  is nearly invariant; see FIGURE 8.

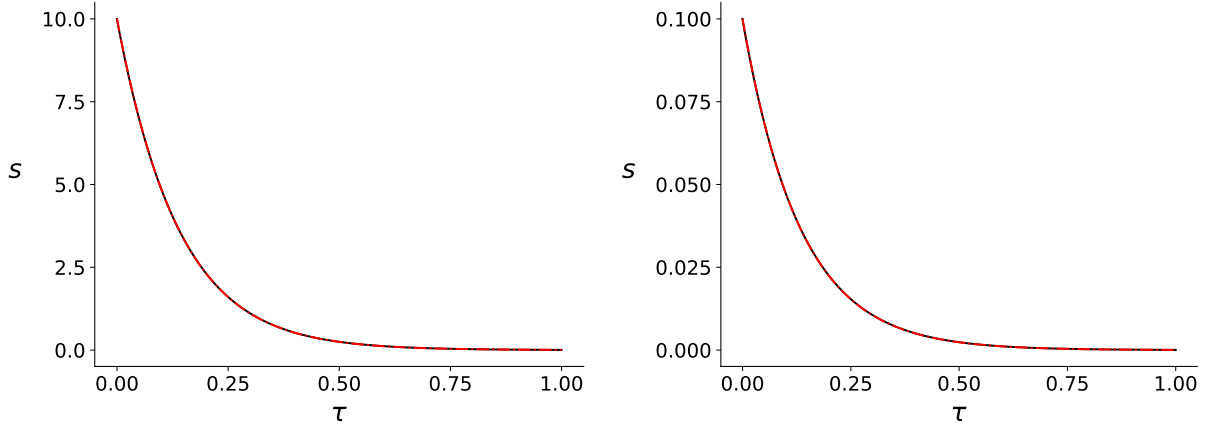
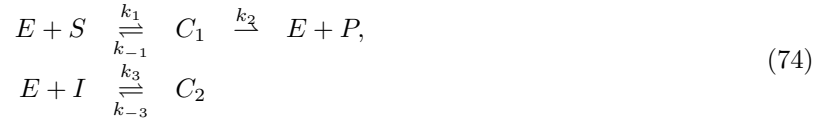


Figure 8: **Uncompetitive inhibition: Near-invariance may lead to scenarios in which the reduction (68) is accurate even when  $1 < \mu_U$ .** The solid black curve is the numerical solution to (65); the broken red curve is the numerical solution to (68). Time has been mapped to the  $\tau$  scale:  $\tau = t/T$ ,  $\tau \in [0, 1]$ . The parameters (in arbitrary units) are:  $k_1 = 1.0$ ,  $e_0 = 1.0$ ,  $k_{-3} = 10^{-1}$ ,  $k_3 = 10^{-2}$ ,  $i_0 = 10^{-3}$ ,  $k_2 = k_{-1} = 10^2$  with  $\varepsilon_U \approx 2.5 \times 10^{-3}$  and  $\mu_U \approx 5.0$ . LEFT PANEL:  $s_0 = 10.0$ . RIGHT PANEL: The long-time validity is verified with  $s_0 = 10^{-1}$ . Note that  $k_1 e_0 / k_{-3}$  is large, thus  $\mu_U$  is of order one. However, since  $k_3 i_0 / k_{-3} = 10^{-2}$  and  $c_1(0) = c_2(0) = 0$ , the dynamics prior to reduction are essentially two-dimensional. Consequently, (68) holds since  $\varepsilon_{MM} \ll 1$ .

### 6.3 Competitive Inhibition

The irreversible competitive inhibition mechanism



corresponds (with mass action kinetics and stoichiometric conservation laws) to the ODE system

$$\begin{aligned} \dot{s} &= -k_1(e_0 - c_1 - c_2)s && + k_{-1}c_1, \\ \dot{c}_1 &= k_1(e_0 - c_1 - c_2)s && - (k_{-1} + k_2)c_1, \\ \dot{c}_2 &= k_3(e_0 - c_1 - c_2)(i_0 - c_2) && - k_{-3}c_2. \end{aligned} \quad (75)$$

The usual initial conditions are  $s(0) = s_0$ ,  $e(0) = e_0$ ,  $i(0) = i_0$  and  $c_1(0) = c_2(0) = p(0) = 0$ . We fix a reference value  $e_0^*$ , then from the conservation laws we obtain the compact positively invariant set

$$K := \{(s, c_1, c_2) \in \mathbb{R}_{\geq 0}^3 : 0 \leq s \leq s_0, \quad 0 \leq c_1 \leq e_0^*, \quad 0 \leq c_2 \leq \min\{e_0^*, i_0\}\}.$$

The parameter space  $\Pi = \mathbb{R}_{\geq 0}^8$  has elements

$$(e_0, s_0, i_0, k_1, k_{-1}, k_2, k_3, k_{-3})^{\text{tr}},$$

and it is known that  $e_0 = 0$ , with all other parameters positive, defines a TFPV,

$$\hat{\pi} := (0, s_0, i_0, k_1, k_{-1}, k_2, k_3, k_{-3})^{\text{tr}} \quad (76)$$

with corresponding critical manifold

$$\tilde{Y} := \{(s, c_1, c_2) \in \mathbb{R}_{\geq 0}^3 : c_1 = c_2 = 0\}.$$

(See below for nondegeneracy conditions on the remaining parameters.) We choose the parameter ray direction  $\rho = (e_0^*, 0, \dots, 0)^{\text{tr}}$ , with  $e_0 = \varepsilon e_0^*$ . The singular perturbation reduction (see Goeke and Walcher [20], subsection 3.2) yields the equation

$$\dot{s} = -\frac{k_1 k_{-3} k_2 e_0 s}{(k_1 s + k_{-1} + k_2) k_{-3} + k_3 i_0 (k_{-1} + k_2)}. \quad (77)$$

(The reduction (77) again differs from the classical QSS reduction (see e.g. Keener and Sneyd [24], subsection 1.4.3); however, (77) and the classical reduction agree up to a term of order  $\varepsilon^2$  and are therefore asymptotically equivalent.)

### 6.3.1 Asymptotic small parameters

The coefficients of the characteristic polynomial on the critical manifold are

$$\begin{aligned} \sigma_1 &= k_1 s + k_{-1} + k_2 + k_3 i_0 + k_{-3}; \\ \sigma_2 &= k_{-3} k_1 s + (k_3 i_0 + k_{-3})(k_{-1} + k_2); \\ \hat{\sigma}_3 &= k_2 k_1 e_0^* \cdot (k_3 i_0 + k_{-3}). \end{aligned}$$

We generally assume that all parameters are contained in a compact subset of the positive orthant, hence are bounded above by certain positive constants. Moreover  $\sigma_1(\hat{\pi}, s)$  and  $\sigma_2(\hat{\pi}, s)$  satisfy the TFPV property

$$\begin{aligned} k_3 i_0 + k_{-3} + k_{-1} + k_2 &= \min \sigma_1 > 0, \\ (k_{-1} + k_2)(k_3 i_0 + k_{-3}) &= \min \sigma_2 > 0 \end{aligned}$$

if and only if  $k_{-1} + k_2$  and  $k_3 i_0 + k_{-3}$  are bounded below by certain positive constants. More restrictively, we will assume that  $i_0$  is bounded below by some positive constant. Finally  $k_2$  and  $k_{-3}$  should be bounded below by positive constants, lest the reduced equation (77) is too close to trivial.

- With  $\sigma_1, \sigma_2$  and  $\hat{\sigma}_3$  evaluated at  $\hat{\pi}$ , we obtain the distinguished small parameter:

$$\begin{aligned} \varepsilon^* &= \varepsilon \sup_{\hat{Y} \cap K} \frac{\hat{\sigma}_3(s, \hat{\pi}, \rho, 0)}{\sigma_1(s, \hat{\pi}) \sigma_2(s, \hat{\pi})} \\ &= \frac{k_2 k_1 e_0}{(k_{-1} + k_2)^2} \cdot \frac{k_{-1} + k_2}{k_{-1} + k_2 + k_3 i_0 + k_{-3}} \\ &= \varepsilon_{MM} \cdot \frac{k_{-1} + k_2}{k_{-1} + k_2 + k_3 i_0 + k_{-3}} := \varepsilon_I \end{aligned} \quad (78)$$

To verify the equalities, note that  $\hat{\sigma}_3$  is constant while  $\sigma_1, \sigma_2$  are increasing with  $s$ .

- It is straightforward to check that  $\sigma_1^2 - 4\sigma_2 \geq 0$ , thus all eigenvalues are real and Proposition 3 is applicable. Determining the parameter  $\mu^*$  requires a distinction of cases: The derivative of  $s \mapsto q(s) := \frac{\hat{\sigma}_3(s, \hat{\pi}, \rho, 0) \sigma_1(s, \hat{\pi})}{\sigma_2(s, \hat{\pi})^2}$  is a rational function in  $s$  with numerator of degree one. Both coefficients are negative if and only if

$$2k_{-3}(k_3 i_0 + k_{-3}) + k_{-3}(k_{-1} + k_2) \geq (k_{-1} + k_2) i_0 k_3, \quad (79)$$

otherwise they have opposite signs. Note that (79) is satisfied whenever  $\frac{k_3 i_0}{k_{-3}} \leq 1$ ; this inequality admits a direct interpretation in terms of the reaction network. On the one hand, it places a lower bound on the allowable size of  $k_{-3}$ . On the other hand it holds whenever the inhibitor concentration is not too high, thus it is controllable by experimental design.

- When (79) holds then  $s \mapsto q(s)$  is strictly decreasing for  $s \geq 0$ , and

$$\mu^* = \mu_I^{(1)} := \varepsilon \frac{\hat{\sigma}_3(0, \hat{\pi}, \rho, 0) \sigma_1(0, \hat{\pi})}{\sigma_2(0, \hat{\pi})^2} = \varepsilon_{MM} \cdot \frac{k_{-1} + k_2 + k_3 i_0 + k_{-3}}{k_3 i_0 + k_{-3}}. \quad (80)$$

- Whenever (79) does not hold then a straightforward calculation shows that the maximum of  $s \mapsto q(s)$  for  $0 \leq s < \infty$  is given by

$$\begin{aligned}\mu^* = \mu_I^{(2)} &= \frac{k_2 k_1 e_0 \cdot (k_3 i_0 + k_{-3})}{4k_{-3} \cdot \left( k_3 i_0 (k_{-1} + k_2) - k_{-3} (k_3 i_0 + k_{-3}) \right)} \\ &= \varepsilon_{MM} \cdot \frac{(k_{-1} + k_2)^2 \cdot (k_3 i_0 + k_{-3})}{4k_{-3} \cdot \left( k_3 i_0 (k_{-1} + k_2) - k_{-3} (k_3 i_0 + k_{-3}) \right)}.\end{aligned}\tag{81}$$

This expression is somewhat unwieldy. But  $\mu_I^{(2)}$  admits an obvious lower bound, obtained by discarding the negative term in the denominator:

$$\mu_I^{(2)} \geq \frac{1}{4} \cdot \frac{k_1 k_2 e_0}{k_{-3} (k_{-1} + k_2)} \cdot \left( 1 + \frac{k_{-3}}{k_3 i_0} \right).$$

Moreover, the negation of (79) provides an estimate for the denominator which yields an upper bound:

$$\mu_I^{(2)} \leq \frac{1}{4} \cdot \frac{k_2 k_1 e_0 (k_3 i_0 + k_{-3})}{k_{-3}^2 (k_3 i_0 + k_{-3} + k_{-1} + k_2)}.$$

The lower bound shows that it is necessary to require  $k_1 e_0 \ll \min\{k_{-3}, k_3 i_0\}$  whenever  $k_{-1}$  and  $k_2$  are of the same order.

- Finally, whenever  $s_0$  is not too large one may also consider the estimate

$$\begin{aligned}\mu^* &\leq \varepsilon \frac{\widehat{\sigma}_3(s_0, \widehat{\pi}, \rho, 0) \sigma_1(s_0, \widehat{\pi})}{\sigma_2(0, \widehat{\pi})^2} \\ &= \frac{k_2 k_1 e_0}{(k_{-1} + k_2)^2} \cdot \frac{k_1 s_0 + k_{-1} + k_2 + k_3 i_0 + k_{-3}}{k_3 i_0 + k_{-3}} \\ &= \varepsilon_{MM} \cdot \frac{k_1 s_0 + k_{-1} + k_2 + k_3 i_0 + k_{-3}}{k_3 i_0 + k_{-3}} =: \widetilde{\mu}_I,\end{aligned}\tag{82}$$

which is a direct consequence of monotonicity properties of the  $\sigma_j$ . This inequality is exact whenever (79) does not hold and  $s_0$  is smaller than the argument of  $\max q$ .

### 6.3.2 Numerical simulations

Generally, by Fenichel theory the accuracy of the reduction (77) improves along the parameter ray as  $\varepsilon_I \rightarrow 0$  and  $\mu_I^{(i)} \rightarrow 0$ , for  $i = 1, 2$ , respectively. Continuing the procedure employed in the previous case studies, we illustrate the efficacy of the qualifiers  $\varepsilon_I \ll 1, \mu_I^{(i)} \ll 1$  (with appropriate index  $i$ ) with several numerical simulations.

1. For our first example, we once again consider the case in which all parameters except  $e_0$  are equal, which is a representative of parameters of the same magnitude. Numerical simulations confirm that the accuracy of (77) improves as  $\varepsilon_I \rightarrow 0$  and  $\mu_I^{(1)} \rightarrow 0$ ; see FIGURE 9.
2. In our second example we demonstrate the effectiveness of  $\varepsilon_I$  and  $\mu_I^{(i)}$  with parameters that have disparate magnitudes. We observe that  $\mu_I^{(1)}$  is the definitive indicator of the accuracy of (77) when (79) holds, while  $\mu_I^{(2)}$  is the indicator of the accuracy of (77) whenever (79) fails, reflecting the fact that one eigenvalue must have much smaller absolute value than the other two; see FIGURES 10 and 11.

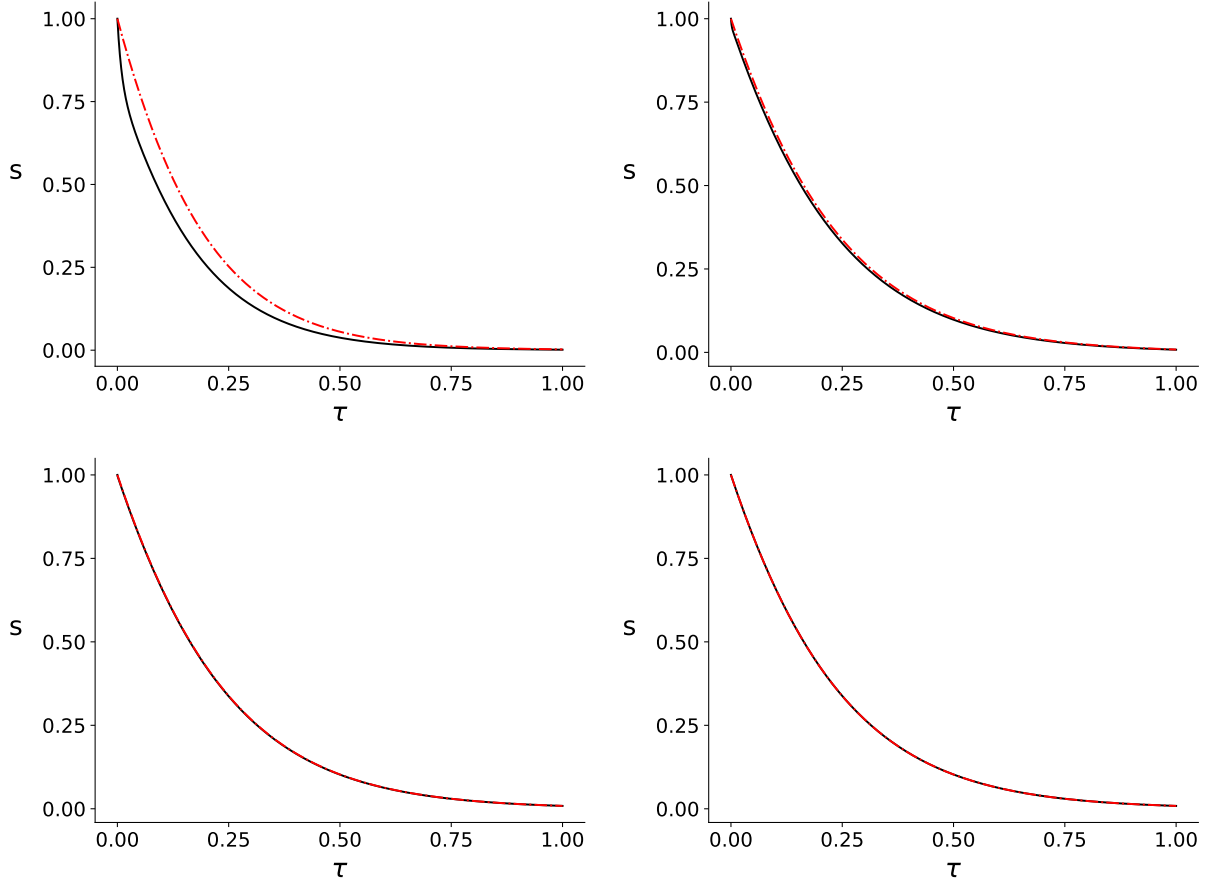


Figure 9: **Competitive inhibition: With parameters of unit magnitude, and (79) valid, numerical simulations indicate that the accuracy of (77) improves along the parameter ray as both  $\varepsilon_I \rightarrow 0$  and  $\mu_I^{(1)} \rightarrow 0$ .** In all panels, the parameters (in arbitrary units) are:  $s_0 = 1.0$ ,  $k_1 = 1.0$ ,  $k_2 = 1.0$ ,  $k_{-1} = 1.0$ ,  $k_3 = 1.0$ ,  $k_{-3} = 1.0$  and  $i_0 = 1.0$ . The solid black curve is the numerical solution to the mass action system (75); the broken red curve is the numerical solution to (77). Time has been mapped to the  $\tau$  scale:  $\tau = t/T$ ,  $\tau \in [0, 1]$  TOP LEFT PANEL:  $e_0 = 1.0$  with  $\varepsilon_I = 1.25 \times 10^{-1}$  and  $\mu_I^{(1)} = 5 \times 10^{-1}$ . TOP RIGHT PANEL:  $e_0 = 10^{-1}$  with  $\varepsilon_I = 1.25 \times 10^{-2}$  and  $\mu_I^{(1)} = 5 \times 10^{-2}$ . BOTTOM LEFT PANEL:  $e_0 = 10^{-2}$  with  $\varepsilon_I = 1.25 \times 10^{-3}$  and  $\mu_I^{(1)} = 5 \times 10^{-3}$ . The reduction (77) is nearly indistinguishable from (75). BOTTOM RIGHT PANEL:  $e_0 = 10^{-4}$  with  $\varepsilon_I = 1.25 \times 10^{-4}$  and  $\mu_I^{(1)} = 5 \times 10^{-4}$ . The QSS reduction (77) is again practically indistinguishable from (75).

### 6.3.3 Near-invariance

As in the previous subsections we now discuss special instances of near-invariance. The inhibitory mechanism can be turned off by requiring  $k_3 i_0 = 0$ , which implies that, for sufficiently small  $k_3$  or  $i_0$ , the subspace  $U := \{(s, c_1, c_2) \in \mathbb{R}^3 : c_2 = 0\}$  will be nearly invariant. One perspective is to define the parameter ray by  $k_3 = \varepsilon k_3^*$  and  $e_0 = \varepsilon e_0^*$ . Then the perturbation form of the mass action equations is

$$\begin{pmatrix} \dot{s} \\ \dot{c}_1 \\ \dot{c}_2 \end{pmatrix} = \begin{pmatrix} k_1 s + k_{-1} & k_1 s \\ -k_1 s - (k_{-1} + k_2) & -k_1 s \\ 0 & -k_{-3} \end{pmatrix} \begin{pmatrix} c_1 \\ c_2 \end{pmatrix} + \varepsilon \begin{pmatrix} -k_1 e_0^* s \\ k_1 e_0^* s \\ -k_3^* (c_1 + c_2)(i_0 - c_2) \end{pmatrix} + \mathcal{O}(\varepsilon^2).$$

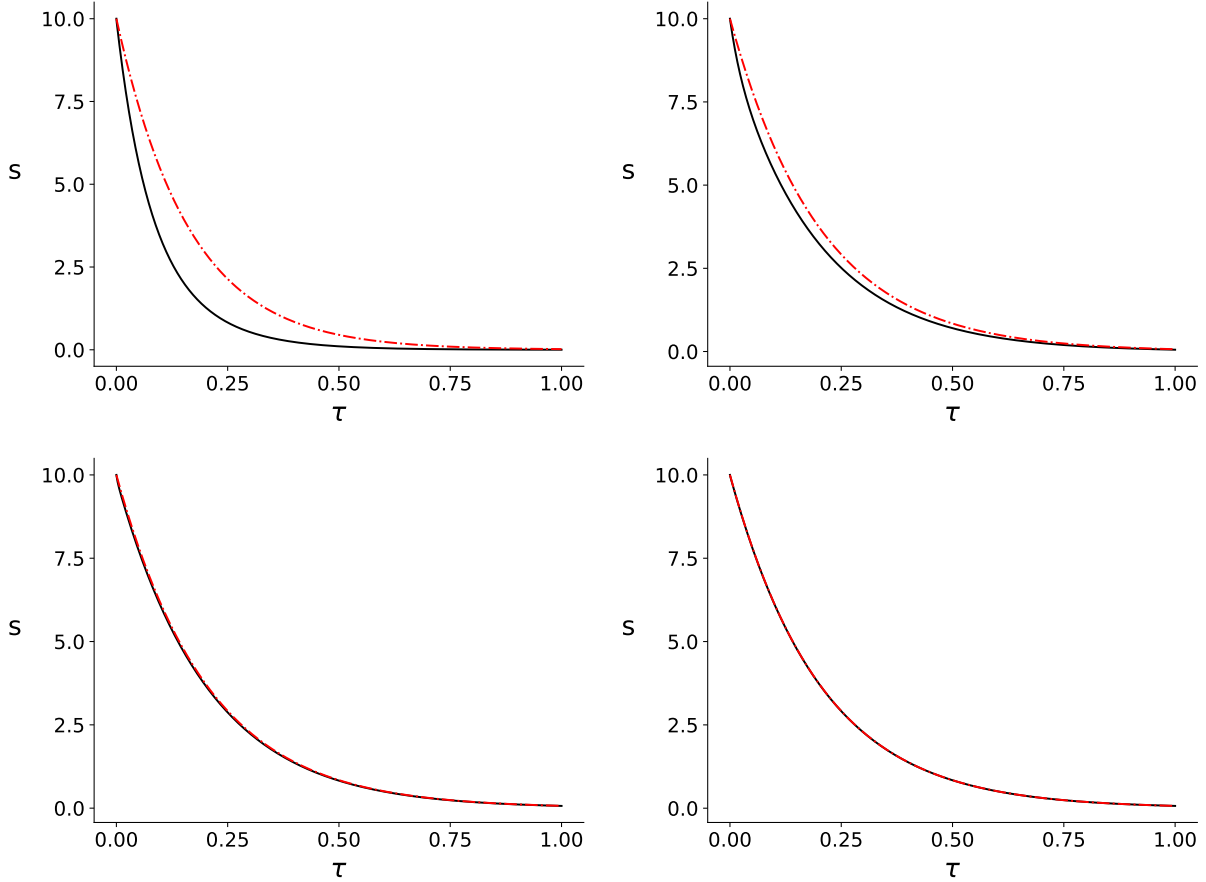


Figure 10: **Competitive inhibition: When parameter values are disparate in magnitude, numerical simulations indicate that the accuracy of (77) improves along the parameter ray as  $\mu_I^{(1)} \rightarrow 0$  when (79) holds.** In all panels, the parameters (in arbitrary units) are:  $s_0 = 10.0$ ,  $k_1 = 1.0$ ,  $k_2 = k_{-1} = 10^2$ ,  $k_3 = k_{-3} = 10^{-1}$  and  $i_0 = 1.0$ . The solid black curve is the numerical solution for  $s$  to the mass action system (75); the broken red curve is the numerical solution to (77). Time has been mapped to the  $\tau$  scale:  $\tau = t/T$ ,  $\tau \in [0, 1]$ . TOP LEFT PANEL:  $e_0 = 1.0$ ,  $\varepsilon_I \approx 2.5 \times 10^{-3}$ , and  $\mu_I^{(1)} \approx 2.5$ . TOP RIGHT PANEL:  $e_0 = 10^{-1}$ ,  $\varepsilon_I \approx 2.5 \times 10^{-4}$ , and  $\mu_I^{(1)} \approx 2.5 \times 10^{-1}$ . BOTTOM LEFT PANEL:  $e_0 = 10^{-2}$ ,  $\varepsilon_I \approx 2.5 \times 10^{-5}$ , and  $\mu_I^{(1)} \approx 2.5 \times 10^{-2}$ . BOTTOM RIGHT PANEL:  $e_0 = 10^{-3}$ ,  $\varepsilon_I \approx 2.5 \times 10^{-6}$ ,  $\mu_I^{(1)} \approx 2.5 \times 10^{-3}$  and the QSS reduction (77) is nearly indistinguishable from (75). Collectively, these simulations indicate that  $\mu_I^{(1)} \ll 1$  is the qualifier that ensures the validity of (77) when (79) holds.

The QSS reduction is obtained by projecting the leading order perturbation onto the critical manifold, thus

$$\begin{pmatrix} \dot{s} \\ \dot{c}_1 \\ \dot{c}_2 \end{pmatrix} = \varepsilon \begin{pmatrix} 1 & \frac{k_1 s + k_{-1}}{k_1 s + k_{-1} + k_2} & \frac{k_1 k_2 s}{(k_1 s + k_{-1} + k_2) k_{-3}} \\ 0 & 0 & 0 \\ 0 & 0 & 0 \end{pmatrix} \begin{pmatrix} -k_1 e_0^* s \\ k_1 e_0^* s \\ 0 \end{pmatrix},$$

from which we recover

$$\dot{s} = -\frac{k_1 k_2 e_0 s}{k_1 s + k_{-1} + k_2},$$

i.e., the sQSSA of the MM reaction mechanism. This is not surprising: With initial conditions  $s(0) = s_0$ ,  $c_1(0) = c_2(0) = 0$ , the dynamics are approximately two-dimensional. From a different perspective (taking

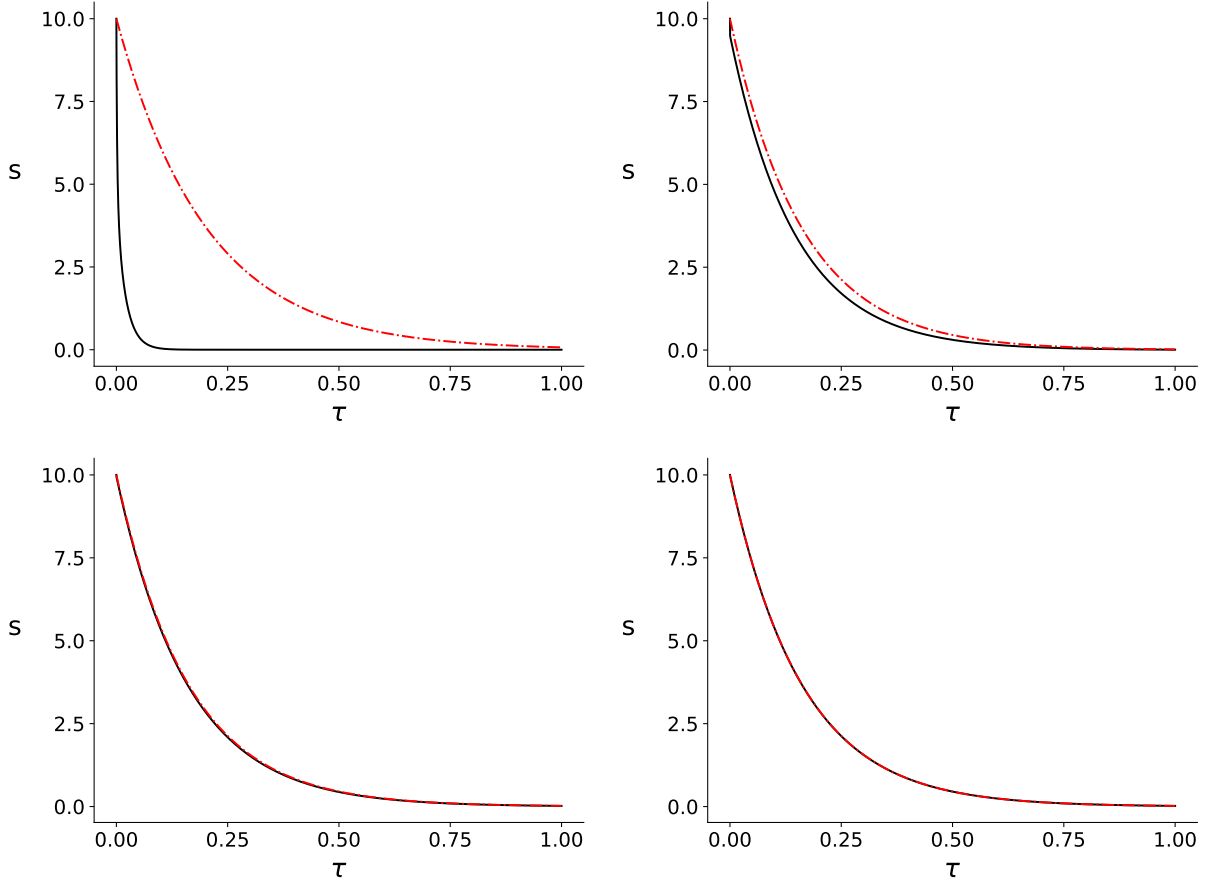


Figure 11: **Competitive inhibition: When parameter values are disparate in magnitude, numerical simulations indicate that the accuracy of (77) improves along the search direction as  $\mu_I^{(2)} \rightarrow 0$  when (79) fails.** In all panels, the parameters (in arbitrary units) are:  $s_0 = 10.0$ ,  $k_1 = 1.0$ ,  $k_2 = k_{-1} = 10^2$ ,  $k_{-3} = 10^{-2}$  and  $k_3 = i_0 = 1.0$ . The solid black curve is the numerical solution for  $s$  to the mass action system (75); the broken red curve is the numerical solution to (77). Time has been mapped to the  $\tau$  scale:  $\tau = t/T$ ,  $\tau \in [0, 1]$ . TOP LEFT PANEL:  $e_0 = 1.0$ ,  $\varepsilon_I \approx 2.5 \times 10^{-3}$ , and  $\mu_I^{(2)} \approx 12.6$ . TOP RIGHT PANEL:  $e_0 = 10^{-1}$ ,  $\varepsilon_I \approx 2.5 \times 10^{-4}$ , and  $\mu_I^{(2)} \approx 12.6 \times 10^{-1}$ . BOTTOM LEFT PANEL:  $e_0 = 10^{-2}$ ,  $\varepsilon_I \approx 2.5 \times 10^{-5}$ , and  $\mu_I^{(2)} \approx 12.6 \times 10^{-2}$ . BOTTOM RIGHT PANEL:  $e_0 = 10^{-3}$ ,  $\varepsilon_I \approx 2.5 \times 10^{-6}$ , and  $\mu_I^{(2)} \approx 12.6 \times 10^{-3}$ . Observe the QSS reduction (77) is nearly indistinguishable from (75), which indicates that  $\mu_I^{(2)} \ll 1$  is the qualifier that ensures the validity of (77) when (79) fails.

independent limits), we can write (77) as

$$\dot{s} = - \frac{k_1 k_2 e_0 s}{k_1 s + (k_{-1} + k_2) \left( 1 + \frac{k_3 i_0}{k_{-3}} \right)},$$

from which it is clear by inspection that the sQSSA is recoverable from (77) whenever  $k_3 i_0 / k_{-3} \ll 1$ . Consequently, whenever  $k_3 i_0 / k_{-3} \ll 1$  we need only consider the magnitude of  $\varepsilon_I$  to ascertain the accuracy of (77); see FIGURE 12.

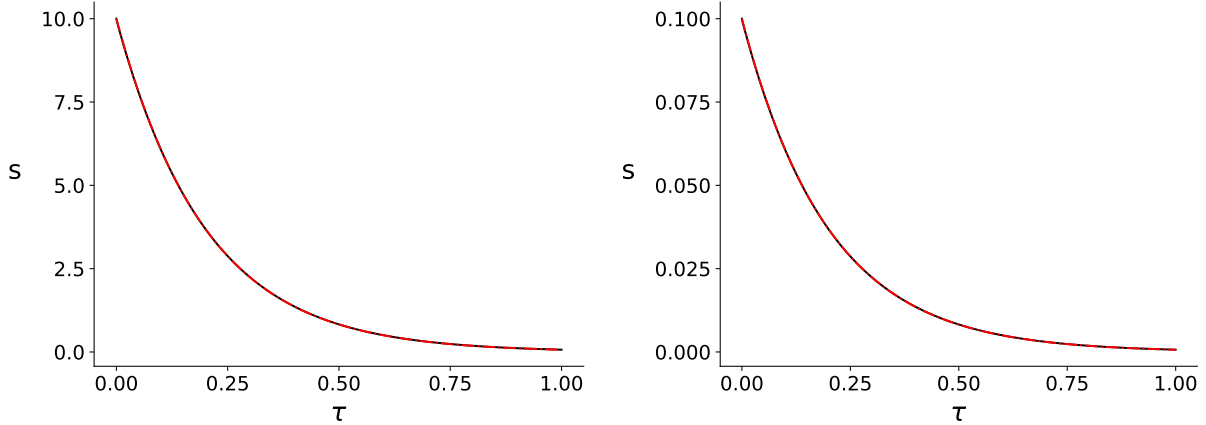


Figure 12: **Competitive inhibition: If  $k_3 i_0 / k_{-3} \ll 1$ , the subspace  $U$  is nearly invariant, and (77) will be accurate provided  $\varepsilon_{RS} \ll 1$ .** In both panels, the parameters (in arbitrary units) are:  $e_0 = 10.0$ ,  $k_1 = 1.0$ ,  $k_2 = k_{-1} = 10^3$ ,  $k_3 = 10^{-7}$ ,  $k_{-3} = 10^{-1}$  and  $i_0 = 10^0$ . It is straightforward to verify that (79) is satisfied, and that  $\varepsilon_{MM} = 2.5 \times 10^{-3}$ , and  $\mu_I^{(1)} \approx 50$ . The solid black curve is the numerical solution for  $s$  to the mass action system (75); the broken red curve is the numerical solution to (77). Time has been mapped to the  $\tau$  scale:  $\tau = t/T$ ,  $\tau \in [0, 1]$ . LEFT PANEL:  $s_0 = 10.0$  and the reduction (77) is very accurate. RIGHT PANEL: Here  $s_0 = 10^{-1}$  and the reduction (77) is still accurate; this confirms the long-time validity of (77) is regulated by the magnitude of  $\varepsilon_{MM}$  whenever  $k_3 i_0 / k_{-3} \ll 1$ .

## 7 Case Studies: Reduction from dimension three to two

In this section we further discuss the uncompetitive and competitive inhibition networks, but now we consider exemplary cases of reduction to dimension two. These scenarios are of less practical relevance than those in the previous section, but we present them for illustrative purposes. We will provide less detailed discussions, and will be content to show the feasibility of the method. The results from Section 5, in particular Proposition 5 and subsection 5.4, will be employed. The determination of distinguished parameters now amounts to finding (or estimating) the maximum and minimum of rational functions in two variables on some compact set.

### 7.1 Uncompetitive inhibition

For the uncompetitive inhibition network (64), (65), one sees that  $k_1 = k_{-3} = 0$ , with all other parameters contained in some compact subset of the open positive orthant, defines a TFPV  $\hat{\pi}$ , with a two-dimensional critical manifold  $\tilde{Y}$  given by  $c_1 = 0$ . The TFPV conditions mean that both elementary reactions responsible for the formation of  $C_1$  are slow.

We consider system (65) with initial values  $s(0) = s_0$ ,  $c_1(0) = c_2(0) = 0$  on the compact positively invariant set

$$K := \{(s, c_1, c_2) \in \mathbb{R}_{\geq 0}^3 : 0 \leq s \leq s_0, \quad c_1 + c_2 \leq e_0, \quad c_2 \leq \min\{e_0, i_0\}\},$$

and take the ray direction

$$\rho = (0, 0, k_1^*, 0, 0, 0, k_{-3}^*)^{\text{tr}}$$

in parameter space, with  $k_i = \varepsilon k_i^*$ ,  $k_i^* > 0$ , for  $i \in \{1, -3\}$ . Straightforward computations yield the reduced system

$$\begin{pmatrix} \dot{s} \\ \dot{c}_2 \end{pmatrix} = \frac{1}{k_{-1} + k_2 + k_3(i_0 - c_2)} \begin{pmatrix} -k_1(e_0 - c_2)(k_2 + k_3(i_0 - c_2))s + k_{-3}k_{-1}c_2 \\ k_1k_3(e_0 - c_2)(i_0 - c_2)s - k_{-3}(k_{-1} + k_2)c_2 \end{pmatrix}, \quad (83)$$

with initial conditions  $s(0) = s_0$ ,  $c_2(0) = 0$ . A straightforward phase plane analysis of system (83) (respectively, of the orbitally equivalent system with the common denominator discarded) shows that every solution in the positive quadrant converges to the stationary point 0.

### 7.1.1 Asymptotic small parameters

We now determine dimensionless parameters that gauge the accuracy of (83). For the sake of brevity, we will restrict attention to the case  $e_0 > i_0$ . The coefficients of the characteristic polynomial on  $\tilde{Y}$  are given by

$$\begin{aligned}\tilde{\sigma}_1 &= k_{-1} + k_2 + k_3(i_0 - c_2) + \varepsilon(\dots) \\ \tilde{\sigma}_2 &= k_1(k_3(i_0 - c_2)(e_0 - c_2 + s) + k_2(e_0 - c_2)) + k_{-3}(k_{-1} + k_2) + \varepsilon^2(\dots) \\ \tilde{\sigma}_3 &= k_1 k_{-3} k_2 (e_0 - c_2).\end{aligned}$$

Thus

$$\begin{aligned}\sigma_1 &= k_{-1} + k_2 + k_3(i_0 - c_2) \\ \hat{\sigma}_2 &= k_1^*(k_3(i_0 - c_2)(e_0 - c_2 + s) + k_2(e_0 - c_2)) + k_{-3}^*(k_{-1} + k_2) \\ \hat{\sigma}_3 &= k_1^* k_{-3}^* k_2 (e_0 - c_2),\end{aligned}$$

and the first nondegeneracy condition from Lemma 7 is satisfied since  $e_0 > i_0$ .

According to Propositions 5 and 6 and their proofs, for timescale comparisons we consider the rational function

$$q(s, c_2) = \frac{\hat{\sigma}_2(s, c_2, \hat{\pi}, \rho, 0)}{\sigma_1(s, c_2, \hat{\pi})^2}, \quad 0 \leq s \leq s_0, \quad 0 \leq c_2 \leq i_0.$$

Since  $\hat{\sigma}_2$  decreases with  $c_2$  and increases with  $s$ , while  $\sigma_1$  decreases with  $c_2$ , we obtain an upper estimate from

$$\varepsilon^* \leq \varepsilon \frac{\max \hat{\sigma}_2}{(\min \sigma_1)^2} = \frac{k_1(k_3 i_0 (e_0 + s_0) + k_2 e_0) + k_{-3}(k_{-1} + k_2)}{(k_{-1} + k_2)^2} =: \delta^*.$$

Moreover from  $\varepsilon^* \geq q(s_0, 0)$  we find that

$$\frac{k_1(k_3 i_0 (e_0 + s_0) + k_2 e_0) + k_{-3}(k_{-1} + k_2)}{(k_{-1} + k_2 + k_3 i_0)^2} \leq \varepsilon^*.$$

Likewise, we obtain lower timescale estimates from

$$\varepsilon_* \geq \varepsilon \frac{\min \hat{\sigma}_2}{(\max \sigma_1)^2} = \frac{k_1 k_2 (e_0 - i_0) + k_{-3}(k_{-1} + k_2)}{(k_{-1} + k_2 + k_3 i_0)^2} =: \delta_*.$$

Thus, for  $i_0$  not too large, the estimates by  $\delta^*$  and  $\delta_*$  are quite acceptable.

To estimate the disparity of the slow eigenvalues, according to subsection 5.4 we consider

$$\kappa^* = \max \frac{\sigma_1 \hat{\sigma}_3}{\hat{\sigma}_2^2} \leq \frac{(k_{-1} + k_2 + k_3 i_0) k_1^* k_{-3}^* k_2 e_0}{(k_1^* k_2 e_0 + k_{-3}^* (k_{-1} + k_2))^2} =: \nu^*$$

as well as

$$\kappa_* = \min \frac{\sigma_1 \hat{\sigma}_3}{\hat{\sigma}_2^2} \geq \frac{(k_{-1} + k_2) k_1^* k_{-3}^* k_2 (e_0 - i_0)}{(k_1^* (k_3 i_0 (e_0 + s_0) + k_2 e_0) + k_{-3}^* (k_{-1} + k_2))^2} =: \nu_*.$$

Whenever  $i_0$  is not too large, these two parameters are close, and so are the slow eigenvalues.

### 7.1.2 Numerical Simulations

We include some numerical simulations to gauge the efficacy of the parameter  $\delta^*$ . From Fenichel theory it is known that the accuracy of the reduction (83) improves along the perturbation direction as  $\varepsilon \rightarrow 0$ .

1. Following the outline established in Section 6, we first consider a case when all parameters are of unit order. Numerical simulations confirm that the accuracy of (83) improves as  $\delta^* \rightarrow 0$  along the parameter ray direction; see FIGURE 13. We include the values of  $\delta_*$  to indicate the variation of timescale ratios.
2. In a second set of simulations, we consider the case of parameter values that are disparate in magnitude. Numerical simulations confirm once again that the accuracy of (83) improves along the parameter ray direction as  $\delta^* \rightarrow 0$ ; see FIGURE 14.

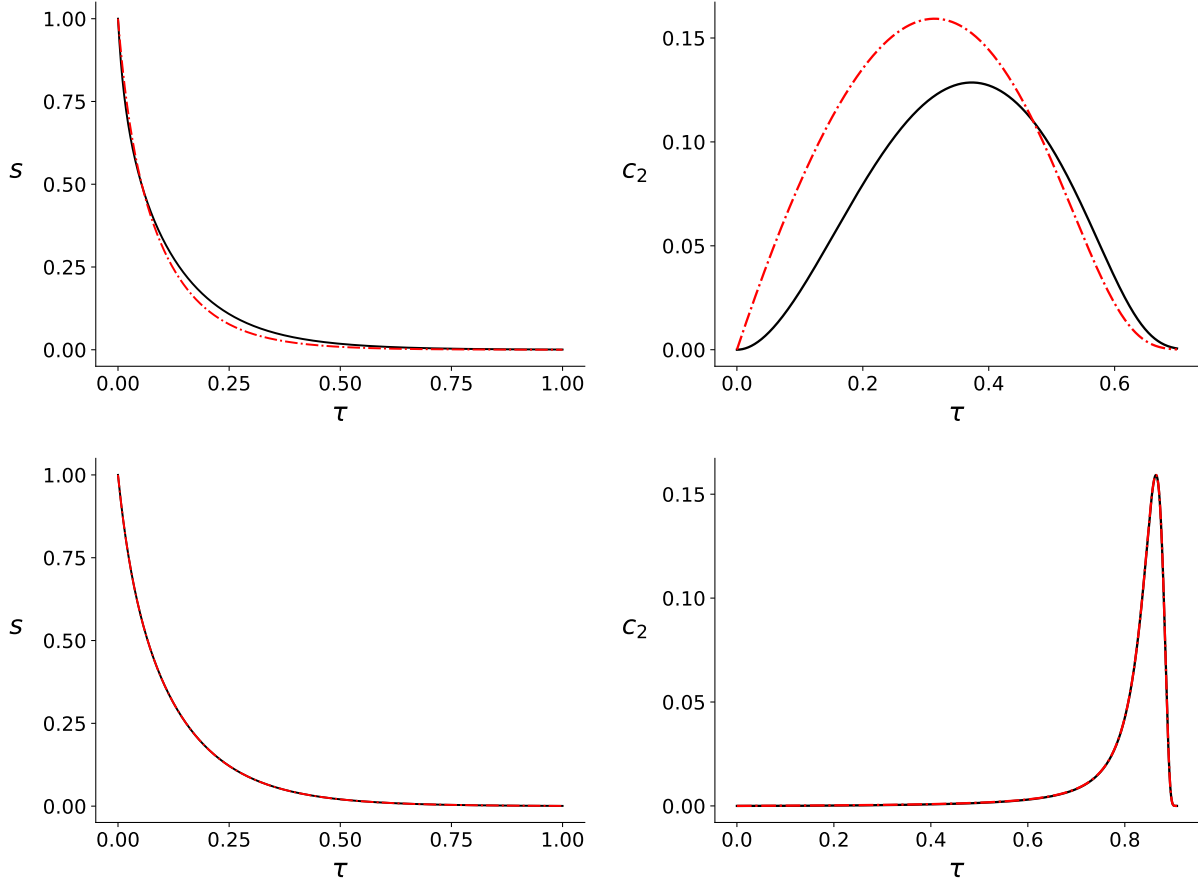


Figure 13: **Uncompetitive inhibition, reduction to dimension two.** In all panels, the parameters (in arbitrary units) are:  $e_0 = 2.0$ ,  $s_0 = 1.0$ ,  $k_2 = k_{-1} = 1.0$ ,  $k_3 = 1.0$ , and  $i_0 = 1.0$ . The solid black curve is the numerical solution to the mass action system (65); the dashed/dotted red curve is the numerical solution to (83). Time has been mapped to the  $\tau$  scale:  $\tau = t/T$ ,  $\tau \in [0, 1]$ . TOP PANELS:  $k_1 = k_{-3} = 10^{-1}$  with  $\delta^* = 1.75 \times 10^{-1}$  and  $\delta_* = 3.33 \times 10^{-2}$ . BOTTOM PANELS:  $k_1 = k_{-3} = 10^{-3}$  with  $\delta^* = 1.75 \times 10^{-3}$  and  $\delta_* = 3.33 \times 10^{-4}$ . As expected, the accuracy of (83) improves as the perturbation decreases along the parameter ray.

## 7.2 Competitive inhibition

For the competitive inhibition network (74), (75), we consider the case that formation of complex  $C_1$ , and both formation and degradation of complex  $C_2$ , are slow: Setting  $k_1 = k_3 = k_{-3} = 0$ , with all the other parameters contained in a compact subset of the positive orthant, defines a TFPV  $\hat{\pi}$  for dimension  $s = 2$ , the critical manifold  $\tilde{Y}$  being given by  $c_1 = 0$ ; see Kruff and Walcher [25]. We consider the system on the compact positively invariant set  $K$  defined by

$$K := \{(s, c_1, c_2) \in \mathbb{R}_{\geq 0}^3 : 0 \leq s \leq s_0, 0 \leq c_1 \leq e_0, 0 \leq c_2 \leq \min\{e_0, i_0\}\},$$

choosing the ray direction

$$\rho = (0, 0, k_1^*, 0, 0, k_3^*, k_{-3}^*)^{\text{tr}}$$

in parameter space, and  $k_i = \varepsilon k_i^*$  with  $k_i^* > 0$  for  $i \in \{1, 3, -3\}$ . Standard computations yield the reduced system

$$\begin{aligned} \dot{s} &= -\frac{k_1 k_2}{k_{-1} + k_2} (e_0 - c_2) s \\ \dot{c}_2 &= k_3 (e_0 - c_2) (i_0 - c_2) - k_{-3} c_2 \end{aligned} \quad (84)$$

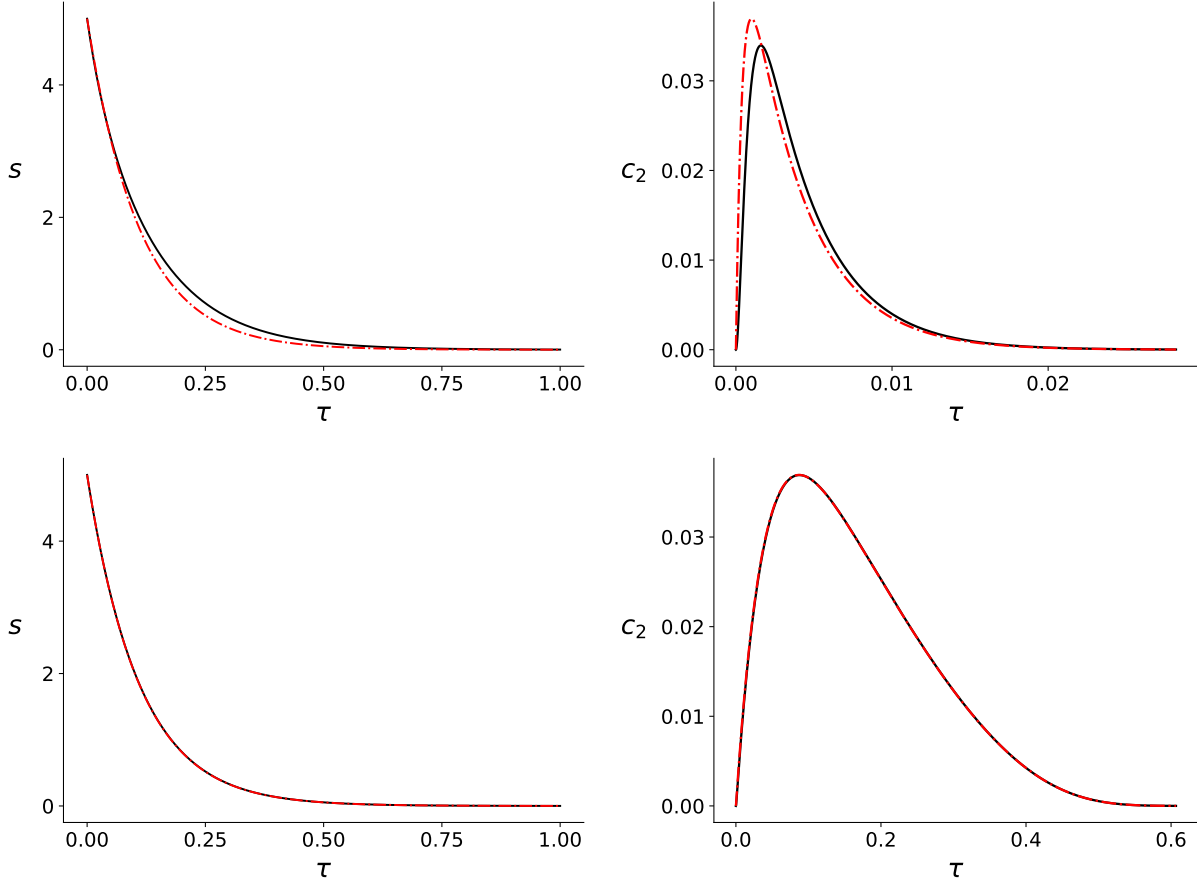


Figure 14: **Uncompetitive inhibition, reduction to dimension two; disparate parameter values.** In all panels, the parameters (in arbitrary units) are:  $e_0 = 10.0$ ,  $s_0 = 5.0$ ,  $k_2 = 10^3$ ,  $k_{-1} = 10^2$ ,  $k_3 = 10.0$ , and  $i_0 = 1.0$ . The solid black curve is the numerical solution to the mass action system (65); the broken red curve is the numerical solution to (83). Time has been mapped to the  $\tau$  scale:  $\tau = t/T$ ,  $\tau \in [0, 1]$ . TOP PANELS:  $k_1 = k_{-3} = 10^2$  with  $\delta^* \approx 9.3 \times 10^{-1}$  and  $\delta_* \approx 8.2 \times 10^{-1}$ . BOTTOM PANELS:  $k_1 = k_{-3} = 1.0$  with  $\delta^* \approx 9.3 \times 10^{-3}$  and  $\delta_* \approx 8.3 \times 10^{-3}$ . Again, it is clear that the accuracy of (83) improves as the perturbation decreases along the parameter ray. Notably, the approximation in the second case is very good although  $k_1 = k_{-3} = 1$ . (As always, the expression “ $\ll 1$ ” should not be taken too literally.) As for measuring the discrepancy of the “slow” eigenvalues, one finds  $\kappa_* \geq \nu_* \approx 7.8 \cdot 10^{-2}$  and  $\kappa^* \leq \nu^* \approx 9.0 \cdot 10^{-2}$ . This indicates a ratio of about  $10^{-1}$ .

with initial conditions  $s(0) = s_0$ ,  $c_2(0) = 0$ . The qualitative behavior of this system is easily determined: All solutions in the positive quadrant converge to a stationary point  $(0, c_2^*)$ , with  $0 < c_2^* < \min\{e_0, i_0\}$ <sup>17</sup>.

### 7.2.1 Asymptotic small parameters

For the sake of brevity we will consider only the case  $e_0 > i_0$ . The coefficients of the characteristic polynomial on  $\tilde{Y}$  are

$$\begin{aligned} \tilde{\sigma}_1 &= k_{-1} + k_2 + \varepsilon(\dots) \\ \tilde{\sigma}_2 &= k_1 k_2 (e_0 - c_2) + k_3 (e_0 + i_0 - 2c_2)(k_{-1} + k_2) + k_{-3}(k_{-1} + k_2) + \varepsilon^2(\dots) \\ \tilde{\sigma}_3 &= k_1 k_3 \cdot (k_2 e_0 (e_0 + i_0 - 2c_2) + k_2 c_2 (2c_2 - e_0 - i_0)) + k_1 k_{-3} \cdot k_2 (e_0 - c_2), \end{aligned}$$

<sup>17</sup>Incidentally, it is possible to compute the solutions to (84) via quadratures: The second equation is separable, and upon substitution the first equation is non-autonomous linear.

and we obtain

$$\begin{aligned}\sigma_1 &= k_{-1} + k_2 \\ \widehat{\sigma}_2 &= k_1^* k_2 (e_0 - c_2) + k_3^* (e_0 + i_0 - 2c_2)(k_{-1} + k_2) + k_{-3}^* (k_{-1} + k_2) \\ \widehat{\sigma}_3 &= k_1^* k_2 (e_0 - c_2) (k_3^* (e_0 + i_0 - 2c_2) + k_{-3}^*).\end{aligned}$$

The nondegeneracy conditions are satisfied (also at  $c_2 = i_0$ ), due to  $e_0 > i_0$ . As for timescales, we need to analyze the rational function

$$q(s, c_2) = \frac{\widehat{\sigma}_2(s, c_2, \widehat{\pi}, \rho, 0)}{\sigma_1(s, c_2, \widehat{\pi})^2}, \quad 0 \leq s \leq s_0, \quad 0 \leq c_1 \leq e_0, \quad 0 \leq c_2 \leq i_0.$$

Since  $\sigma_1$  is constant and  $\widehat{\sigma}_2$  is decreasing with  $c_2$ , attaining its maximum at  $c_2 = 0$ , and its minimum at  $c_2 = i_0$ , we find the distinguished parameters

$$\varepsilon^* = \frac{k_1 k_2 e_0 + (k_3(e_0 + i_0) + k_{-3})(k_{-1} + k_2)}{(k_{-1} + k_2)^2}$$

and

$$\varepsilon_* = \frac{k_1 k_2 (e_0 - i_0) + (k_3(e_0 - i_0) + k_{-3})(k_{-1} + k_2)}{(k_{-1} + k_2)^2}.$$

Furthermore, according to subsection 5.4 we consider

$$\kappa^* = \max \frac{\sigma_1 \widehat{\sigma}_3}{\widehat{\sigma}_2^2} \leq \frac{k_1^* k_2 e_0 (k_3^* (e_0 + i_0) + k_{-3}^*) (k_{-1} + k_2)}{(k_1^* k_2 (e_0 - i_0) + (k_3^* (e_0 - i_0) + k_{-3}^*) (k_{-1} + k_2))^2} =: \nu^* \quad (85)$$

and

$$\kappa_* = \min \frac{\sigma_1 \widehat{\sigma}_3}{\widehat{\sigma}_2^2} \geq \frac{k_1^* k_2 (e_0 - i_0) (k_3^* (e_0 - i_0) + k_{-3}^*) (k_{-1} + k_2)}{(k_1^* k_2 e_0 + (k_3^* (e_0 + i_0) + k_{-3}^*) (k_{-1} + k_2))^2} =: \nu_* \quad (86)$$

to measure the disparity between the eigenvalues  $\lambda_2$  and  $\lambda_3$ .

### 7.2.2 Numerical simulations

We present numerical examples to gauge the accuracy of the reduction (84) with decreasing  $\varepsilon^*$ .

1. For our first example, we consider the case with  $\pi := \varepsilon(k_1^*, 1.0, 1.0, 1.0, 1.0, k_3^*, k_{-3}^*, 1.0)^{\text{tr}}$ ; see FIGURE 15. We include the values of  $\varepsilon^*$ ,  $\varepsilon_*$  to indicate the variation of timescale ratios.
2. For our second example we again consider a case when parameters are of differing magnitudes. Again, numerical simulations confirm that the QSS reduction (84) improves as  $\varepsilon^* \rightarrow 0$  along the parameter ray; see FIGURE 16.

### 7.2.3 The case of very small $k_1$ : Three timescales

Finally, we discuss a scenario mentioned in subsection 5.4. From equations (86), (85) below one sees that both  $\kappa^*$  and  $\kappa_*$  approach zero as  $k_1^* \rightarrow 0$ ; this may indicate three timescales. Moreover from equation (75) one sees that the plane defined by  $c_1 = 0$  is invariant when  $k_1 = 0$ , thus nearly invariant when  $k_1$  is small. A coordinate-independent approach to a three-timescale scenario was presented in Kruff and Walcher [25], based on work of Cardin and Teixeira [6]: Introduce two small parameters  $\varepsilon_1, \varepsilon_2$  and

$$k_3 = \varepsilon_1 k_3^\dagger, \quad k_{-3} = \varepsilon_1 k_{-3}^\dagger, \quad k_1 = \varepsilon_1 \varepsilon_2 k_1^\dagger,$$

and rewrite system (75) with three timescales. As detailed in [25] the system admits a sequence of two reductions, with nested invariant manifolds:

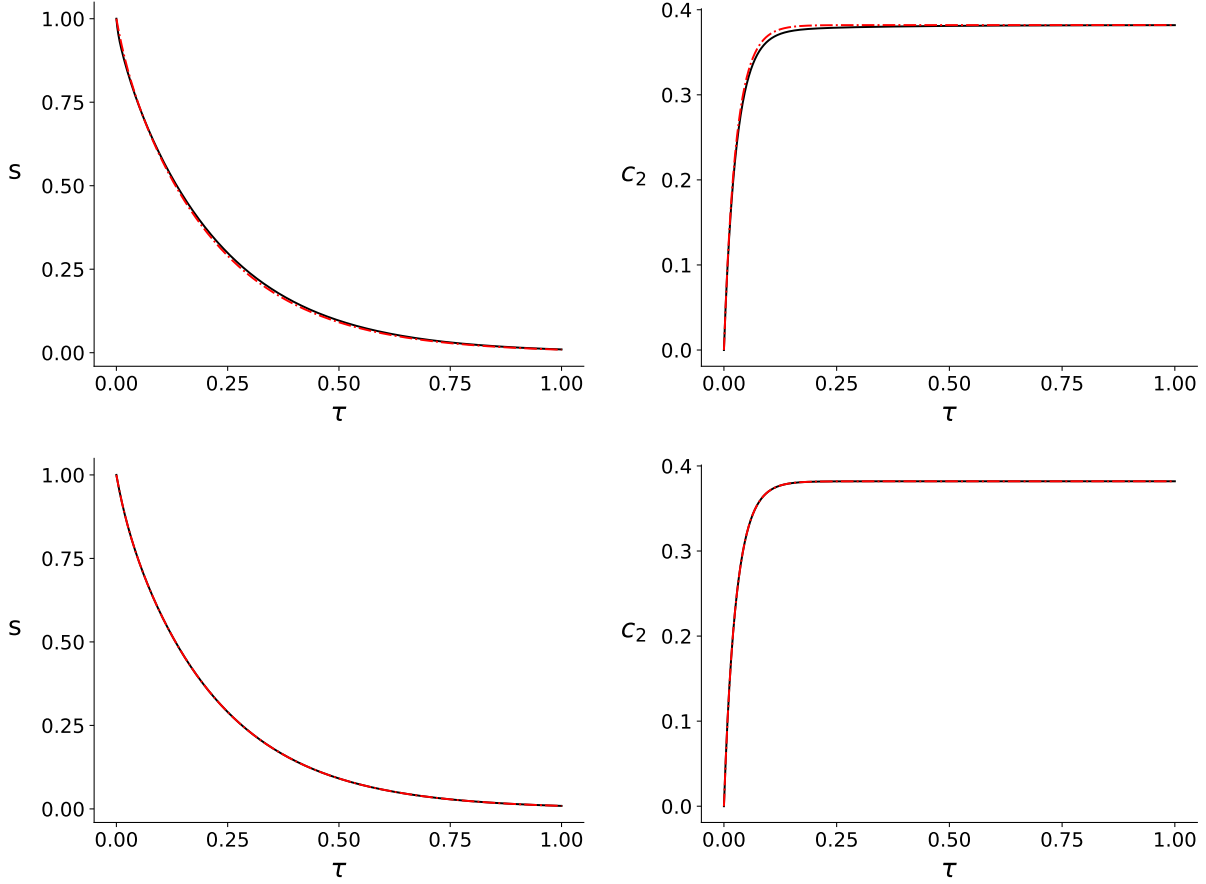


Figure 15: **Competitive inhibition, reduction to dimension two. The accuracy of (84) improves along the parameter ray.** In all panels, the parameters (in arbitrary units) are:  $e_0 = 1.0$ ,  $s_0 = 1.0$ ,  $k_2 = 1.0$ ,  $k_{-1} = 1.0$ , and  $i_0 = 1.0$ . The solid black curve is the numerical solution to the mass action system (75); the broken red curve is the numerical solution to (84). Time has been mapped to the  $\tau$  scale:  $\tau = t/T$ ,  $\tau \in [0, 1]$ . TOP PANELS: Simulation performed with  $k_1 = k_{-3} = k_3 = 10^{-1}$  and  $\varepsilon^* = 1.75 \times 10^{-1}$ ,  $\varepsilon_* = 5.0 \times 10^{-2}$ . BOTTOM PANELS: Simulation performed with  $k_1 = k_{-3} = k_3 = 10^{-3}$  and  $\varepsilon^* = 1.75 \times 10^{-3}$ ,  $\varepsilon_* = 5.0 \times 10^{-4}$ . The singular perturbation reduction (84) is practically indistinguishable from (75).

- A reduction to slow dynamics on a two-dimensional invariant manifold close to  $c_1 = 0$ , with reduced system

$$\begin{pmatrix} \frac{ds}{d\tau_1} \\ \frac{dc_2}{d\tau_1} \end{pmatrix} = \begin{pmatrix} 0 \\ k_3^\dagger(e_0 - c_2)(i_0 - c_2) - k_{-3}^\dagger c_2 \end{pmatrix} \quad (87)$$

with  $\tau_1 = \varepsilon_1 t$ .

- A subsequent reduction to “very slow” dynamics on a one-dimensional invariant manifold close to  $c_1 = 0$ ,  $c_2 = \tilde{c}_2$ , with

$$\tilde{c}_2 = \frac{k_3(e_0 + i_0) + k_{-3} - \sqrt{(k_3(e_0 + i_0) + k_{-3})^2 - 4e_0 i_0 k_3^2}}{2k_3}.$$

The fully reduced one-dimensional equation is then

$$\frac{ds}{d\tau_2} = -\frac{k_2 \cdot k_1^\dagger (e_0 - \tilde{c}_2)}{k_{-2} + k_{-1}} s$$

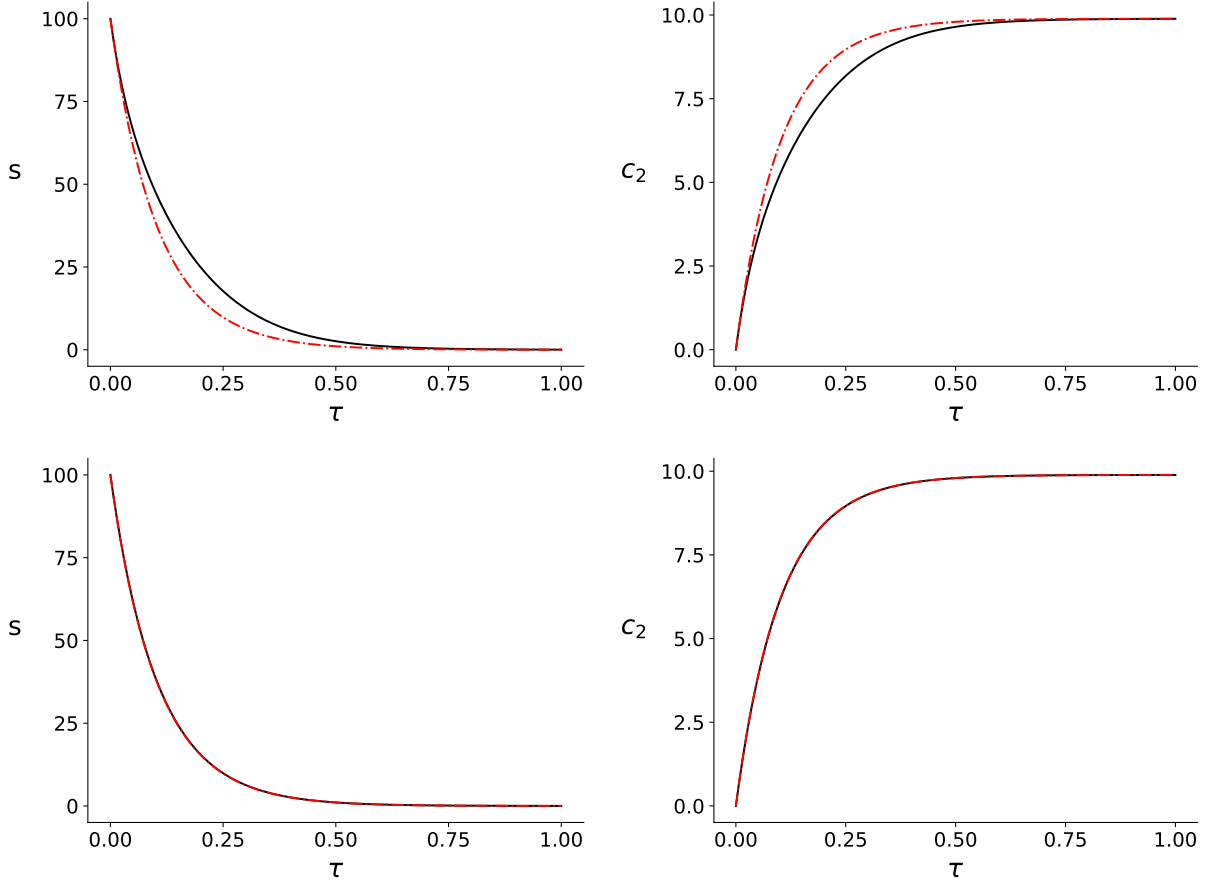


Figure 16: **Competitive inhibition, reduction to dimension two, disparate parameters.** In all panels, the “non-small” parameters (in arbitrary units) are:  $e_0 = 10^2$ ,  $s_0 = 10^2$ ,  $k_2 = 10^2$ ,  $k_{-1} = 1.0$ , and  $i_0 = 10.0$ . The solid black curve is the numerical solution to the mass action system (75); the broken red curve is the numerical solution to (84). Time has been mapped to the  $\tau$  scale:  $\tau = t/T$ ,  $\tau \in [0, 1]$ . TOP PANELS: Simulation performed with  $k_1 = k_{-3} = k_3 = 1.0$  and  $\varepsilon^* \approx 2.08$ ,  $\varepsilon_* \approx 1.78$ . This scenario is outside the range of applicability for Proposition 6. BOTTOM PANELS: Simulation performed with  $k_1 = k_{-3} = k_3 = 10^{-2}$  and  $\varepsilon^* \approx 2.08 \times 10^{-2}$ ,  $\varepsilon_* \approx 1.78 \times 10^{-2}$ . The singular perturbation reduction (84) here is very close to (75).

with  $\tau_2 = \varepsilon_1 \varepsilon_2 t$ ,

or, restated in fast time,

$$\dot{s} = -\frac{k_2 \cdot k_1 (e_0 - \tilde{c}_2)}{k_{-2} + k_{-1}} s. \quad (88)$$

FIGURE 17 illustrates the “slow - very slow” dynamics for a numerical example.

## 8 Discussion

We finish by briefly reviewing the results in this paper.

1. We introduced a general consistent method to obtain perturbation parameters, based on local linear timescales. (By its nature, the approach is focused on and limited to the local behavior.) We start from a singular perturbation scenario with a well-defined critical manifold; this is crucial for the appropriateness of linearizability. Thus we completed an essential part of step 1 (as stated in the Introduction) toward a quantitative analysis of the reduction.

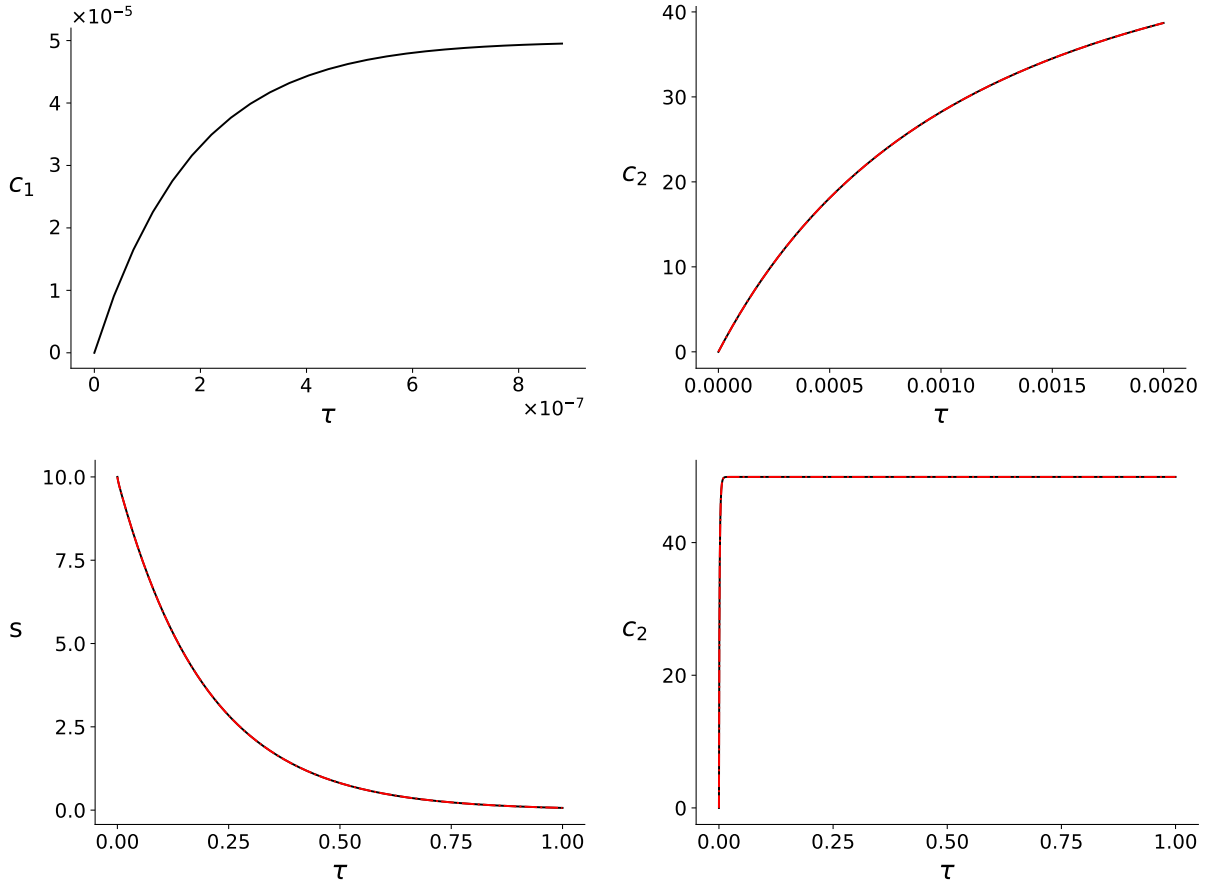


Figure 17: **Competitive inhibition with a three timescale scenario.** In both panels, the parameters (in arbitrary units) are:  $s_0 = 10.0$ ,  $e_0 = 10^2$ ,  $k_1 = 1 \times 10^{-4}$ ,  $k_2 = 2 \times 10^3$ ,  $k_{-1} = 1.0$ ,  $k_3 = 10^{-1}$ ,  $k_{-3} = 10^{-3}$  and  $i_0 = 50.0$ . The solid black curve is the numerical solution to the mass action system (75); the dashed/dotted red curves are the numerical solutions to (87) and (88). Time has been mapped to the  $\tau$  scale:  $\tau = t/T$ . For the chosen parameter values,  $\varepsilon^* \approx 7.5 \times 10^{-3}$  and  $\varepsilon_* \approx 2.5 \times 10^{-3}$ . Moreover, the two slow eigenvalues are disparate since  $\nu^* \approx 6 \times 10^{-3}$ , this is consistent with a three timescale scenario. TOP LEFT PANEL: The initial accumulation of  $c_1$  occurs on the fast timescale; the concentrations of  $c_2$  and  $s$  are approximately constant on the fast timescale. TOP RIGHT PANEL: The reduction (87) is accurate on the slow timescale as  $c_2$  approaches its threshold value,  $\tilde{c}_2$ . BOTTOM LEFT PANEL: The reduction (88) is accurate on the the very slow timescale,  $\tau_2$ , on which the depletion of  $s$  is significant. BOTTOM RIGHT PANEL: On the very slow timescale,  $c_2$  is effectively constant:  $c_2 \approx \tilde{c}_2$ .

2. Using classical results from algebra to approximate eigenvalue ratios in the asymptotic limit, we obtained parameters that are computable, palatable, and admit a biochemical interpretation.
3. We first applied our methods to the Michaelis–Menten reaction mechanism system. As it turns out, even for such a familiar network our approach provides new and elucidating perturbation parameters. Moreover, we included a partial discussion of step 3 for the irreversible system with small product formation rate.
4. For two relevant extensions of the Michaelis–Menten reaction mechanism – uncompetitive inhibition, competitive inhibition – and a non-Michaelis–Menten reaction mechanism – a cooperative system with two complexes, we derived perturbation parameters in the spirit of Segel and Slemrod [39], but without resorting to nonlinear timescales. This stands in contrast to the practice of using  $\varepsilon_{BH}$  or  $\varepsilon_{SSI}$ , or ad-hoc modifications of these. We augmented these results by an extensive discussion of numerical examples

to illustrate the efficacy of these parameters, but also to highlight the importance of the compactness requirements we impose throughout. We also discussed one case that leads to a system with three timescales.

5. Finally, we discussed exemplary cases of reduction from dimension three to dimension two for both inhibition scenarios, to verify the feasibility of our approach. Numerical simulations illustrate the quality and accuracy of the approximations.

The remaining items (step 2 and step 3) as stated in the Introduction need to be handled on a case-by-case basis. We will provide a complete analysis of the irreversible Michaelis–Menten reaction mechanism with low enzyme in forthcoming work.

## 9 Appendix

In this section we collect some technical matters and proofs, as well as recalling some known results for which a concise presentation seems appropriate and useful.

### 9.1 Lyapunov function arguments

Lyapunov functions can be used to estimate the approach to the slow manifold in a singularly perturbed system, as was mentioned in the Introduction. This estimate gives rise to a small parameter  $\varepsilon_L$  which controls the distance of the solution to the slow manifold. We give an account of the relevant facts here.

We first state an auxiliary result that goes back to Lyapunov.

**Lemma 5.** *Let  $Q$  be a real  $n \times n$ -matrix, with eigenvalues  $\mu_1, \dots, \mu_n$ , and let  $\delta > 0$ . Then there exists a scalar product  $\langle \cdot, \cdot \rangle$  on  $\mathbb{R}^n$  such that for all  $x$  one has*

$$\left( \min_{1 \leq i \leq n} \operatorname{Re} \mu_i - \delta \right) \langle x, x \rangle \leq \langle x, Qx \rangle \leq \left( \max_{1 \leq i \leq n} \operatorname{Re} \mu_i + \delta \right) \langle x, x \rangle,$$

and

$$\left( \min_{1 \leq i \leq n} |\mu_i|^2 - \delta \right) \langle x, x \rangle \leq \langle Qx, Qx \rangle \leq \left( \max_{1 \leq i \leq n} |\mu_i|^2 + \delta \right) \langle x, x \rangle.$$

This can be proven as in Walter [45], Chapter VII, §30 (see also Arnold [2], Ch. 22): For matrices that are diagonalizable over  $\mathbb{C}$  build a real basis from real and imaginary parts of a complex eigenbasis; for the non-diagonalizable case, by suitable choice of basis elements the nilpotent part can be chosen to have norm  $< \delta$ .

#### 9.1.1 Estimates

This presentation follows Berglund and Gentz [3], subsection 2.1 ff.; but (for the purpose of illustration) we are satisfied with a local version. Consider a smooth system

$$\begin{aligned} \dot{x} &= \varepsilon \tilde{f}_1(x, y, \varepsilon) \\ \dot{y} &= f_2(x, y, \varepsilon) \end{aligned}, \quad \text{briefly } \begin{pmatrix} \dot{x} \\ \dot{y} \end{pmatrix} = F \left( \begin{pmatrix} x \\ y \end{pmatrix} \right) \tag{89}$$

with  $\begin{pmatrix} x \\ y \end{pmatrix}$  in some open subset of  $\mathbb{R}^n$ ,  $x \in \mathbb{R}^m$ , and a nonnegative parameter  $\varepsilon$ . Moreover let  $\begin{pmatrix} x_0 \\ y_0 \end{pmatrix}$  be such that  $f_2(x_0, y_0, 0) = 0$ , and  $M$  a suitable compact neighborhood of this point. (More conditions on  $M$  will be implicitly imposed below, by further assumptions.)

- Assume furthermore that

$$f_2(x, y, \varepsilon) = 0 \iff y = g(x, \varepsilon)$$

for  $\begin{pmatrix} x \\ y \end{pmatrix} \in M$  and  $\varepsilon \leq \varepsilon_{\max}$ , with some positive  $\varepsilon_{\max}$  and a smooth function  $g$ . The zero set  $Y_\varepsilon$  of  $f_2(\cdot, \cdot, \varepsilon)$  in  $M$  will be called the slow manifold, or QSS manifold,<sup>18</sup> for  $\varepsilon$ . By Hadamard's lemma, after possibly shrinking  $M$  there exists a smooth matrix valued function  $A$  such that

$$f_2(x, y, \varepsilon) = A(x, y, \varepsilon) \cdot (y - g(x, \varepsilon)).$$

Thus we may rewrite system (89) as

$$\begin{aligned} \dot{x} &= \varepsilon \tilde{f}_1(x, y, \varepsilon) \\ \dot{y} &= A(x, y, \varepsilon) \cdot (y - g(x, \varepsilon)). \end{aligned} \quad (90)$$

With

$$D_y f_2(x, y, \varepsilon) = A(x, y, \varepsilon) + (D_y A(x, y, \varepsilon)) (y - g(x, \varepsilon)),$$

one finds in particular

$$D_y f_2(x, y, \varepsilon) = A(x, y, \varepsilon) \text{ on } Y_\varepsilon.$$

- Now assume that all eigenvalues of  $A(x_0, y_0, 0)$  have negative real parts. By continuity and suitable choice of  $M$  and  $\varepsilon_{\max}$ , all eigenvalues of  $A(x, y, \varepsilon)$  have negative real part for  $\begin{pmatrix} x \\ y \end{pmatrix} \in M$  and  $0 \leq \varepsilon \leq \varepsilon_{\max}$ . Due to Lemma 5 there exists a scalar product  $\langle \cdot, \cdot \rangle$  on  $\mathbb{R}^{n-m}$  and some  $\gamma > 0$  such that

$$\langle z, A(x_0, y_0, 0)z \rangle \leq -2\gamma \langle z, z \rangle, \quad \text{all } z \in \mathbb{R}^{n-m}.$$

(Recall the correspondence between  $2\gamma$  and eigenvalues.) Thus we may assume that

$$\langle z, A(x, y, \varepsilon)z \rangle \leq -\gamma \langle z, z \rangle, \quad \text{all } z \in \mathbb{R}^{n-m}, \quad (91)$$

on  $M$ , with  $0 \leq \varepsilon \leq \varepsilon_{\max}$ . Denote by  $\|\cdot\|$  the norm associated with this scalar product.

The following line of arguments is a slight variant of classical reasoning (which uses Gronwall's lemma; see e.g. Evans [15], Appendix B for the latter). For solutions of (89) we find

$$\begin{aligned} \frac{d}{dt} \langle y - g(x, \varepsilon), y - g(x, \varepsilon) \rangle &= 2 \langle y - g(x, \varepsilon), \dot{y} - D_x g(x, \varepsilon) f_1(x, y, \varepsilon) \rangle \\ &= 2 \langle y - g(x, \varepsilon), A(x, y, \varepsilon) (y - g(x, \varepsilon)) \rangle \\ &\quad - 2 \langle y - g(x, \varepsilon), D_x g(x, \varepsilon) f_1(x, y, \varepsilon) \rangle. \end{aligned}$$

The first term on the right hand side can be estimated by  $-\gamma \cdot \langle y - g(x, \varepsilon), y - g(x, \varepsilon) \rangle$ . As for the second term, by Cauchy-Schwarz one has

$$\begin{aligned} 2 |\langle y - g(x, \varepsilon), D_x g(x, \varepsilon) f_1(x, y, \varepsilon) \rangle| &\leq 2 \|y - g(x, \varepsilon)\|_2 \cdot \|D_x g(x, \varepsilon) f_1(x, y, \varepsilon)\|_2 \\ &\leq 2 \|y - g(x, \varepsilon)\|_2 \cdot (\|D_x g(x, \varepsilon)\| \cdot \|f_1(x, y, \varepsilon)\|) \end{aligned}$$

with suitable norms in the second and third factor.

Now there exists a positive constant  $\kappa = \varepsilon \tilde{\kappa}$  such that

$$\|D_x g(x, \varepsilon)\| \cdot \|f_1(x, y, \varepsilon)\| \leq \kappa.$$

So, for  $V := \|y - g(x, \varepsilon)\|_2^2$  one obtains the differential inequality

$$\frac{dV}{dt} \leq -2\gamma V + 2\kappa \sqrt{V}.$$

Comparison with the solution of the corresponding Bernoulli equation yields

$$V \leq V(0) \exp(-\gamma t) + \left(\frac{\kappa}{\gamma}\right)^2 \cdot (1 - \exp(-\gamma t)), \quad (92)$$

<sup>18</sup>This is an order  $\varepsilon$  approximation of the slow manifold in a singular perturbation setting.

thus  $\|y - g(x, \varepsilon)\| = \sqrt{V(t)}$  can be estimated e.g. by  $\sqrt{2}\frac{\kappa}{\gamma}$  as  $t \rightarrow \infty$ .<sup>19</sup> Therefore, after a transient phase the proximity of the solution to the slow manifold is controlled by

$$\varepsilon_L := \sqrt{2}\frac{\kappa}{\gamma} = \sqrt{2}\varepsilon\frac{\tilde{\kappa}}{\gamma}. \quad (93)$$

More precisely, once  $V(0)\exp(-\gamma t) \leq \left(\frac{\kappa}{\gamma}\right)^2$ , the stated estimate holds. The inequality is satisfied whenever

$$t \geq \frac{1}{\gamma} \log\left(\frac{\gamma^2 V(0)}{\kappa^2}\right) \sim \log\frac{1}{\varepsilon_L},$$

and this indicates that the time span for the approach to the QSS manifold is of order  $|\log \varepsilon_L|$  in the fast timescale, and of order  $\varepsilon_L |\log \varepsilon_L|$  in the slow timescale  $\varepsilon_L t$ . (A more detailed analysis will provide a lower estimate by a variant of (91), and confirm that the asymptotic estimate cannot be improved.) In particular time spans of order 1 will not suffice for the transient.

In reaction network settings,  $\varepsilon_L$  is a dimensional parameter (with dimension concentration); a suitable normalization needs to be chosen.

### 9.1.2 A correspondence to eigenvalues

We sketch the relation of the small parameter  $\varepsilon_L$  to eigenvalues of the Jacobian. For the sake of simplicity, we only consider the linearization here, disregarding higher order terms. Given the system

$$\begin{aligned} \dot{x} &= -\varepsilon\tilde{U}x + \varepsilon\tilde{V}y \\ \dot{y} &= Wx - Zy = -Z(y - Z^{-1}W)x \end{aligned}, \text{ briefly } \begin{pmatrix} \dot{x} \\ \dot{y} \end{pmatrix} = F(x, y, \varepsilon),$$

and keeping the notation from above, we have  $A = -Z$ ,  $g(x) = Z^{-1}Wx$ ,  $D_x g = Z^{-1}W$ . The slow manifold  $Y_\varepsilon$  is given by  $Wx - Zy = 0$ , up to higher order terms. Moreover

$$\tilde{f}_1 = -\tilde{U}x + \tilde{V}y = \left(-\tilde{U} + \tilde{V}Z^{-1}W\right)x \quad \text{on } Y_\varepsilon.$$

Now consider the eigenvalues of the matrix  $DF = \begin{pmatrix} -\varepsilon\tilde{U} & \varepsilon\tilde{V} \\ W & -Z \end{pmatrix}$ ; see also Lemma 7. Thus let  $\alpha_0 + \varepsilon\alpha_1 + \dots$

be an eigenvalue with eigenvector  $\begin{pmatrix} x_0 + \varepsilon x_1 + \dots \\ y_0 + \varepsilon y_1 + \dots \end{pmatrix}$ ;  $\begin{pmatrix} x_0 \\ y_0 \end{pmatrix} \neq 0$ . For  $\alpha_0 \neq 0$ , comparing lowest order terms in the eigenvalue condition yields

$$x_0 = 0 \text{ and } Wx_0 - Zy_0 = \alpha_0 y_0,$$

thus  $-\alpha_0$  is an eigenvalue of  $Z$ . By Lemma 5, we see that  $2\gamma$  can be chosen near the nonzero eigenvalue of  $DF(x, y, 0)$  with smallest absolute real part.

For  $\alpha_0 = 0$ , thus the eigenvalue has order  $\varepsilon$ , comparing lowest orders in the eigenvalue condition yields

$$-\tilde{U}x_0 + \tilde{V}y_0 = \alpha_1 x_0 \text{ and } Wx_0 - Zy_0 = 0,$$

hence  $\alpha_1$  is an eigenvalue for  $-\tilde{U} + \tilde{V}Z^{-1}W = \tilde{f}_1$ . An upper estimate for  $\varepsilon\|\tilde{f}_1\|$  can be obtained from Lemma 5: Choose the order  $\varepsilon$  eigenvalue with greatest absolute value, multiplied by some factor accounting for a coordinate change. Thus we see that  $\kappa$  is composed of the factor  $\|Z^{-1}W\|$  (which reflects the geometry of the slow manifold), the absolutely largest eigenvalue of order  $\varepsilon$  and some multiplicative constants from coordinate transformations. In our local setting, all the multiplicative constants mentioned above are of order one.

To summarize, the small parameter  $\varepsilon_L = \kappa/\gamma$  is determined by the ratio of the largest absolute eigenvalue of order  $\varepsilon$  to the smallest absolute real part of eigenvalues of order one. From this perspective, for slow manifolds of dimension one in particular, the relevance of the parameters  $\varepsilon^*$  and  $\mu^*$  is obvious. Their advantage lies in their (relative) computational accessibility. Likewise,  $\varepsilon^*$  is a both relevant and computationally accessible parameter for three-dimensional systems with two-dimensional slow manifolds.

<sup>19</sup>One may replace  $\sqrt{2}$  by any smaller constant which is  $> 1$ .

### 9.1.3 Remarks on steps 2 and 3

Lyapunov function arguments provide a small parameter  $\varepsilon_L$  which characterizes closeness of a solution of (89) to the slow manifold. This takes care of step 1 described in the Introduction, and clarifies the role of eigenvalues up to ( $\varepsilon$ -independent) factors due to coordinate changes.

For the ultimate goal of obtaining quantitative estimates for the discrepancy between the true solution and the singular perturbation approximation, one needs to go further. In step 2, an appropriate critical time for the onset of the slow dynamics, as well as an appropriate initial value for the reduced system, must be determined. As for step 3, by a continuity and compactness argument, the right hand sides of the full and the reduced equation differ by  $\varepsilon_L$  times some constant. With this, and an error estimate for the initial value for the reduced system, continuous dependence provides an estimate of the approximation error on compact time intervals. Further work may be required, since one is mostly interested in unbounded time intervals, so one cannot rely only on standard continuous dependence theorems.

In the present manuscript we generally did not address the determination of  $\varepsilon_L$  in examples and case studies. The only exception is irreversible Michaelis–Menten with slow product formation (see subsection 4.1), which also contains partial results for step 3. For the (more familiar and more relevant) irreversible Michaelis–Menten system with small enzyme concentration all three steps can be dealt with completely (even if some complications arise), as will be shown in a forthcoming paper. For any system of dimension  $> 2$ , even completing step 1 seems quite demanding.

## 9.2 A proof of Lemma 2

*Proof.* Part (a) is a special case of Lemma 7 below. To prove part (b), abbreviate  $\sigma_i^*(x) := \sigma_i(x, \hat{\pi})$  for  $x \in \tilde{Y} \cap K$ ,  $1 \leq i \leq n-1$ . Then the nonzero roots of the characteristic polynomial  $\chi$  are the roots of

$$\zeta(x, \tau) := \tau^{n-1} + \sigma_1^*(x)\tau^{n-2} + \cdots + \sigma_{n-1}^*(x).$$

By the blanket assumptions, the  $\sigma_i^*$  are bounded above and below by positive constants, hence the absolute values of all zeros of the  $\zeta(x, \cdot)$  are bounded above by some constant. Since  $\hat{\pi}$  is a TFPV, all zeros have negative real parts. Now assume that for every positive constant  $\delta$ , some  $\zeta(x, \tau)$  has a zero with real part  $\geq -\delta$ . Then there exist sequences  $(x_k)$  in  $\tilde{Y} \cap K$  and  $(\mu_k)$  in  $\mathbb{C}$  such that  $\zeta(x_k, \mu_k) = 0$  and  $\operatorname{Re} \mu_k \rightarrow 0$ . Due to boundedness of the sequence  $(\mu_k)$  and compactness of  $\tilde{Y} \cap K$  we may assume that the  $\mu_k$  converge to  $\mu^*$ ,  $\operatorname{Re} \mu^* = 0$ , and the  $x_k$  converge to  $x^* \in \tilde{Y} \cap K$ . By continuity  $\zeta(x^*, \mu^*) = 0$ ; a contradiction. Part (c) follows by continuity and compactness arguments.  $\square$

## 9.3 Parameter dependence of eigenvalues

Recall from (39) the definition

$$\tilde{\sigma}_i(x, \varepsilon) := \sigma_i(x, \hat{\pi} + \varepsilon\rho), \quad 1 \leq i \leq n, \quad \tilde{\sigma}_0 := 1.$$

We first prove (44), concerning the orders of the  $\tilde{\sigma}_i$  whenever  $s > 1$ .

**Lemma 6.** *Let  $\hat{\pi}$  be a TFPV for dimension  $s$ , with critical manifold  $\tilde{Y}$ . Then for all  $x \in \tilde{Y} \cap K$  one has*

$$\tilde{\sigma}_i(x, \varepsilon) = \varepsilon^{i-n+s} \hat{\sigma}_i(x, \varepsilon) \text{ for all } x \in \tilde{Y} \cap K, \quad n-s \leq i \leq n,$$

with polynomial  $\hat{\sigma}_i$ .

*Proof.* The arguments we will use are similar to those in the proof of Goeke et al. [21], Proposition 3. We set

$$\tilde{h}(x, \varepsilon) := h(x, \hat{\pi} + \varepsilon\rho) \text{ for } x \in \tilde{Y} \cap K.$$

There exists a local transformation of  $\tilde{h}$  into Tikhonov standard form; thus there exists a local analytic diffeomorphism  $\Phi$  and a vector field  $\tilde{q}$  such that

$$D\Phi(x)\tilde{h}(x, \varepsilon) = \tilde{q}(\Phi(x), \varepsilon)$$

and consequently

$$D\Phi(x)D\tilde{h}(x, \varepsilon) = D\tilde{q}(\Phi(x), \varepsilon)D\Phi(x), \quad x \in \tilde{Y} \cap K.$$

Therefore the Jacobian of  $\tilde{h}$  at  $x$  and the Jacobian of  $\tilde{q}$  at  $\Phi(x)$  are conjugate; in particular they have the same characteristic polynomial. Denoting by  $\tilde{\nu}_i(y)$  the coefficients of the characteristic polynomial of  $D\tilde{q}(y)$ , this means

$$\tilde{\sigma}_i(x, \varepsilon) = \tilde{\nu}_i(\Phi(x), \varepsilon) \text{ for all } x \in \tilde{Y} \cap K.$$

Since  $\tilde{q}$  is in Tikhonov standard form, we have

$$\tilde{q}(y, \varepsilon) = \begin{pmatrix} \varepsilon\tilde{q}_1(y, \varepsilon) \\ \tilde{q}_2(y, \varepsilon) \end{pmatrix},$$

with  $q_1$  having  $s$  entries, and

$$D\tilde{q}(y, \varepsilon) = \begin{pmatrix} \varepsilon D\tilde{q}_1(y, \varepsilon) \\ D\tilde{q}_2(y, \varepsilon) \end{pmatrix}.$$

Thus every entry of the first  $s$  rows of the Jacobian is a multiple of  $\varepsilon$ , and with the Laplace expansion of the determinant this implies

$$\tilde{\nu}_i(x, \varepsilon) = \varepsilon^{i-n+s} \hat{\nu}_i(x, \varepsilon), \quad n-s < i \leq n,$$

and finally (44). □

Now we turn to determining the orders of the eigenvalues.

**Lemma 7.** *With objects and notation as in Lemma 6, let (44) hold, and furthermore consider the nondegeneracy conditions:*

(i)  $\hat{\sigma}_{n-s}(x, 0) \neq 0$  and  $\hat{\sigma}_n(x, 0) \neq 0$  on  $\tilde{Y} \cap K$ .

(ii) *The polynomials*

$$\hat{\sigma}_{n-s}(x, 0)\tau^s + \hat{\sigma}_{n-s+1}(x, 0)\tau^{s-1} + \cdots + \hat{\sigma}_n(x, 0) \tag{94}$$

*admit only simple zeros, for all  $x \in \tilde{Y} \cap K$ .*

(a) *Whenever (i) holds then the zeros  $\lambda_i(x, \varepsilon)$  of the characteristic polynomial can be labeled such that*

$$\lambda_1(x, 0) \neq 0, \dots, \lambda_{n-s}(x, 0) \neq 0 \quad \text{on } \tilde{Y} \cap K,$$

*and*

$$\lambda_i(x, \varepsilon) = \varepsilon \hat{\lambda}_i(x, \varepsilon), \quad x \in \tilde{Y} \cap K, \quad i > n-s,$$

*with continuous  $\hat{\lambda}_i$  such that  $\hat{\lambda}_i(x, 0) \neq 0$  on  $\tilde{Y} \cap K$ ,  $n-s+1 \leq i \leq n$ .<sup>20</sup>*

(b) *Whenever (ii) holds in addition to (i) then all  $\hat{\lambda}_i$ ,  $n-s+1 \leq i \leq n$ , are analytic in  $(x, \varepsilon)$ .*

*Proof.* The proof rests on the Newton-Puiseux theorem and on Hensel's lemma; we refer specifically to Abhyankar [1], Lectures 12 and 13. According to Newton-Puiseux the equation  $\lambda^n + \sum \tilde{\sigma}_i \lambda^{n-i} = 0$  admits series solutions

$$\lambda = \alpha \varepsilon^\gamma + \cdots$$

in rational exponents of  $\varepsilon$ , with a positive rational number  $\gamma$  and  $\alpha \neq 0$ . For such an expansion to hold with some  $\gamma$  and  $\alpha \neq 0$ , cancellation of lowest order terms in (10) is necessary. The lowest orders of the terms in the monomials are

$$(n-i)\gamma \text{ for } 0 \leq i \leq s, \quad \text{and} \quad (n-j)\gamma + j - n + s \text{ for } s+1 \leq j \leq n,$$

---

<sup>20</sup>The  $\hat{\lambda}_i$  can be represented as convergent power series in  $(x, \varepsilon^{1/m})$  for some positive integer  $m$ .

and for cancellation one must have equality between two of these orders. Clearly two orders in the first block cannot be equal. Assuming that an order from the first block equals an order in the second block, we get

$$(n - i)\gamma = (n - j)\gamma + j - n + s \Rightarrow \gamma = \frac{j - (n - s)}{j - i} < 1 \text{ unless } i = n - s.$$

But in case  $\gamma < 1$  the lowest order equals  $s\gamma$ , with no cancellation; so only  $\gamma = 1$  remains. Finally, if two orders in the second block are equal then one directly sees  $\gamma = 1$ . This shows part (a).

Continuing the argument,  $\gamma = 1$  implies that precisely the monomials of degree  $\leq n - s$  contribute to the lowest order, and the ansatz yields

$$\widehat{\sigma}_{n-s}(x, 0)\alpha^s + \widehat{\sigma}_{n-s+1}(x, 0)\alpha^{s-1} + \cdots + \widehat{\sigma}_n(x, 0) = 0,$$

thus  $s$  distinct choices for  $\alpha$  by condition (ii), and  $\alpha \neq 0$ . By Hensel's lemma, each choice for  $\alpha$  yields a series  $\lambda = \alpha\varepsilon + \cdots$ , in positive integer powers of  $\varepsilon$ . This shows part (b).  $\square$

**Remark 6.** *In case  $s = 1$  the second condition is automatic. Therefore Lemma 2 (a) is also proven.*

## References

- [1] S.S. Abhyankar: *Algebraic geometry for scientists and engineers*. American Mathematical Society, Providence, RI (1990).
- [2] V.I. Arnold: *Ordinary differential equations*. Springer, Berlin (1992).
- [3] N. Berglund, B. Gentz: *Noise-induced phenomena in slow-fast dynamical systems. A sample-paths approach*. Springer, London (2006).
- [4] G. E. Briggs, J. B. S. Haldane: *A note on the kinetics of enzyme action*. *Biochem. J.*, **19**, 338 - 339 (1925).
- [5] M.S. Calder, D. Siegel: *Properties of the Michaelis–Menten mechanism in phase space*. *J. Math. Anal. Appl.* **339**, 1044–1064 (2008).
- [6] P.T. Cardin, M.A. Teixeira: *Fenichel theory for multiple time scale singular perturbation problems*. *SIAM J. Appl. Dyn. Sys.* **16**, 1452-1452 (2017)
- [7] C. Chicone: *Ordinary differential equations with applications*. Second edition. Springer, New York (2006).
- [8] B. Choi, G. A. Rempala, J. K. Kim: *Beyond the Michaelis–Menten equation: Accurate and efficient estimation of enzyme kinetic parameters*. *Sci. Rep.* **7**, 1-11 (2017).
- [9] J. Eilertsen, M.R. Roussel, S. Schnell, S. Walcher: *On the quasi-steady state approximation in an open Michaelis–Menten reaction mechanism*. *AIMS Math.* **6**, no. 7, 6781 – 6814 (2021).
- [10] J. Eilertsen, S. Schnell: *A kinetic analysis of coupled (or auxiliary) enzyme reactions*, *Bull. Math Biol.* **80**, 3154-3183 (2018).
- [11] J. Eilertsen, S. Schnell: *The quasi-steady-state approximations revisited: Timescales, small parameters, singularities, and normal forms in enzyme kinetics*, *Math. Biosci.* **325**, 108339 (2020).
- [12] J. Eilertsen, S. Schnell, S. Walcher: *On the anti-quasi-steady-state conditions of enzyme kinetics*. *Mathematical Biosciences* **350**, 108870 (2022).
- [13] J. Eilertsen, W. Stroberg, S. Schnell: *Phase-plane geometries in coupled enzyme assays*, *Math. Biosci.* **306**, 126-135 (2018).
- [14] J. Eilertsen, M.A. Tyczynska, S. Schnell: *Hunting  $\epsilon$ : The origin and validity of quasi-steady-state reductions in enzyme kinetics*. *SIAM J. Appl. Dyn. Syst.* **20**, 2450-2481 (2021).

- [15] L.C. Evans: *Partial Differential Equations, 2nd ed.* American Mathematical Society, Graduate Studies in Mathematics, v. 19 (2014).
- [16] P.A. Eyers, J.M. Murphy: *The evolving world of pseudoenzymes: Proteins, prejudice and zombies.* BMC Biol **14**, 98 (2016).
- [17] N. Fenichel: *Geometric singular perturbation theory for ordinary differential equations.* J. Differential Equations **31**(1), 53–98 (1979).
- [18] F.R. Gantmacher: *Applications of the theory of matrices.* Dover, Mineola (2005).
- [19] A. Goeke, S. Walcher: *Quasi-steady state: Searching for and utilizing small parameters*, In: A. Johann, H.-P. Kruse, F. Rupp, S. Schmitz (eds.): *Recent Trends in Dynamical Systems*, Springer-Verlag, New York, pp. 153 - 178 (2013).
- [20] A. Goeke, S. Walcher: *A constructive approach to quasi-steady state reduction.* J. Math. Chem. **52**, 2596 - 2626 (2014).
- [21] A. Goeke, S. Walcher, E. Zerz: *Determining “small parameters” for quasi-steady state.* J. Diff. Equations **259**, 1149–1180 (2015).
- [22] A. Goeke, S. Walcher, E. Zerz: *Classical quasi-steady state reduction – A mathematical characterization.* Physica D **345**, 11 - 26 (2017).
- [23] F.G. Heineken, H.M. Tsuchiya, R. Aris: *On the mathematical status of the pseudo-steady hypothesis of biochemical kinetics.* Math. Biosci. **1**, 95 - 113 (1967).
- [24] J. Keener, J. Sneyd: *Mathematical physiology I: Cellular physiology*, Second Ed. Springer-Verlag, New York (2009).
- [25] N. Kruff, S. Walcher: *Coordinate-independent singular perturbation reduction for systems with three time scales.* Math. Biosci. Eng. **16**, 5062 – 5091 (2019).
- [26] M. Krupa, P. Szmolyan: *Extending slow manifolds near transcritical and pitchfork singularities.* Nonlinearity **14**, 1473 – 1491 (2001).
- [27] S.H. Lam, D.A. Goussis: *The CSP method for simplifying kinetics.* Int. J. Chem. Kinet. **26**, 461 - 486 (1994)
- [28] L. Michaelis, M.L. Menten: *Die Kinetik der Invertinwirkung.* Biochem. Z. **49**, 333 - 369 (1913).
- [29] W. G. Miller, R. A. Alberty: *Kinetics of the reversible Michaelis–Menten mechanism and the applicability of the steady-state approximation.* J. Am. Chem. Soc. **80** 5146-5151 (1958).
- [30] J.M. Murphy, H. Farhan, P.A. Eyers: *Bio-Zombie: The rise of pseudoenzymes in biology.* Biochem. Soc. Trans. **45** 537-544 (2017).
- [31] L. Noethen, S. Walcher: *Quasi-steady state in the Michaelis–Menten system.* Nonlinear Anal. Real World Appl. **8**, 1512 - 1535 (2007).
- [32] L. Noethen, S. Walcher: *Tikhonov’s theorem and quasi-steady state.* Discrete Contin. Dyn. Syst. Ser. B **16**(3), 945–961 (2011).
- [33] B.O. Palsson, E.N. Lightfoot: *Mathematical modelling of dynamics and control in metabolic networks. I. On Michaelis–Menten kinetics.* J. Theor. Biol. **111**, 273 - 302 (1984).
- [34] D.G. Patsatzis, D.A. Goussis: *A new Michaelis–Menten equation valid everywhere multi-scale dynamics prevails.* Math. Biosci. **315**, 108220, 13 pp. (2019).
- [35] J.G. Reich, E.E. Selkov: *Mathematical analysis of metabolic networks.* FEBS Letters **40**, Suppl. 1, S119 - S127 (1974).

- [36] S. Schnell, P.K. Maini: *Enzyme kinetics at high enzyme concentration*. Bull. Math. Biol. **62**, 483–499 (2000).
- [37] S. Schnell: *Validity of the Michaelis–Menten equation–steady-state, or reactant stationary assumption: that is the question*. FEBS Journal **281**, 464–472 (2014).
- [38] L.A. Segel: *On the validity of the steady state assumption of enzyme kinetics*. Bull. Math. Biol. **50**, 579–593 (1988).
- [39] L.A. Segel, M. Slemrod: *The quasi-steady-state assumption: A case study in perturbation*. SIAM Review **31**, 446 - 477 (1989).
- [40] M. Seshadri, G. Fritzsche: *Analytical solutions of a simple enzyme kinetic problem by a perturbative procedure*. Biophys. Struct. Mech. **6**, 111 - 123 (1980).
- [41] W. Stroberg, S. Schnell: *On the estimation errors of  $K_M$  and  $V$  from time-course experiments using the Michaelis–Menten equation*. Biophys. Chem. **219**, 17-27 (2016).
- [42] A.R. Tzafriri: *Michaelis–Menten kinetics at high enzyme concentrations*. Bull. Math. Biol. **65**, 1111–1129 (2003).
- [43] A.N. Tikhonov: *Systems of differential equations containing a small parameter multiplying the derivative* (in Russian). Math. Sb. **31**, 575–586 (1952).
- [44] F. Verhulst: *Methods and applications of singular perturbations. Boundary layers and multiple timescale dynamics*, Springer, New York (2005).
- [45] W. Walter: *Ordinary differential equations*. Graduate Texts in Mathematics **182**. Springer, New York (1998).
- [46] F.Y.M. Wan: *Mathematical models and their analysis*. SIAM, Philadelphia (2018).
- [47] A. Zagaris, H.G. Kaper, T.J. Kaper: *Analysis of the computational singular perturbation reduction method for chemical kinetics*. J. Nonlinear Sci. **14**, 59–91 (2004).